1982

Inelastic analysis of steel multigirder highway bridges, August 1980, 195p.

J. C. Hall

C. N. Kostem

Commonwealth of Pennsylvania
Department of Transportation

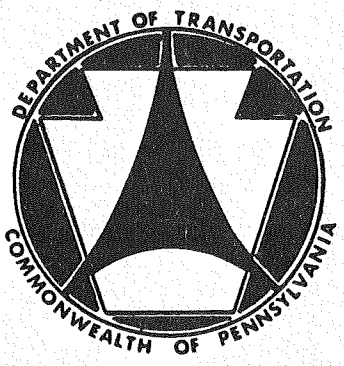

Office of Research and Special Studies

INELASTIC ANALYSIS OF STEEL MULTIGIRDER HIGHWAY BRIDGES

Jeffrey C. Hall
Celal N. Kostem

Research Project 77-1: Overloading Behavior of Steel Highway Bridges

Fritz Engineering Laboratory Report No. 435.1

LEHIGH UNIVERSITY
Fritz Engineering Laboratory

Technical Report Documentation Page

1. Report No.	2. Government Accession No.	3. Recipient's Catalog No.
FHWA-PA-RD-77-1-1		

4. Title and Subtitle	5. Report Date
INELASTIC ANALYSIS OF STEEL MULTIGIRDER HIGHWAY BRIDGES	August 1980
	6. Performing Organization Code
7. Author(s) Jeffrey C. Hall and Celal N. Kostem	8. Performing Organization Report No. Fritz Engineering Laboratory Report No. 435.1
9. Performing Organization Name and Address Fritz Engineering Laboratory, 13 Lehigh University Bethlehem, Pennsylvania 18015	10. Work Unit No. (TRAIS)
	11. Contract or Grant No. PennDOT Project 77-1
12. Sponsoring Agency Name and Address Pennsylvania Department of Transportation Harrisburg, Pennsylvania 17120	13. Type of Report and Period Covered Interim Report
	14. Sponsoring Agency Code

15. Supplementary Notes

Prepared in cooperation with the U.S. Department of Transportation, Federal Highway Administration

16. Abstract

The report presents a methodology developed to predict the elastic and inelastic response of highway bridge superstructures. Simple span or continuous multigirder bridges with steel girders and reinforced concrete deck are considered. Inelastic behavior of the bridge is modeled through the use of nonlinear stress-strain curves for concrete, reinforcing steel and structural steel. Initiation of the damage to the superstructure in the form of cracking or crushing of concrete and yielding of the steel is detected, progression of the damage is monitored, and load versus deformation, and damage to the bridge, is developed until the attainment of the collapse of the structure.

The developed method and the corresponding computer program BOVAS (Bridge OVerloading Analysis-Steel) are designed to predict the overload response of the types of bridges described above. The accuracy and applicability of the method is illustrated by applying the method to four bridge overload tests that had been conducted elsewhere and reported in the literature. Good agreement between the test results and analytical prediction is noted.

17. Key Words	18. Distribution Statement
Overloading of bridges, steel highway bridges, steel girders, reinforced concrete bridge deck, finite element method	

19. Security Classif. (of this report)	20. Security Classif. (of this page)	21. No. of Pages	22. Price
Unclassified	Unclassified	208	

Form DOT F 1700.7 (8-72) Reproduction of completed page authorized

COMMONWEALTH OF PENNSYLVANIA

Department of Transportation

Office of Research and Special Studies

Wade L. Gramling - Chief
Istvan Janauschek - Research Coordinator

Project 77-1: Overloading Behavior of Steel Highway Bridges

INELASTIC ANALYSIS OF STEEL MULTIGIRDER HIGHWAY BRIDGES

by

Jeffrey C. Hall
Celal N. Kostem

This work was sponsored by the Pennsylvania Department of Transportation and the U. S. Department of Transportation, Federal Highway Administration. The contents of this report reflect the view of the authors who are responsible for the facts and the accuracy of the data presented herein. The contents do not necessarily reflect the official views or policies of the Pennsylvania Department of Transportation or the Federal Highway Administration. This report does not constitute a standard, specification, or regulation.

LEHIGH UNIVERSITY

Office of Research

Bethlehem, Pennsylvania

August 1980

Fritz Engineering Laboratory Report No. 435.1

TABLE OF CONTENTS (continued)

TABLE OF CONTENTS

ABSTRACT

The report presents a methodology developed to predict the elastic and inelastic response of highway bridge superstructures. Simple span or continuous multigirder bridges with steel girders and reinforced concrete deck are considered. Inelastic behavior of the bridge is modeled through the use of nonlinear stress-strain curves for concrete, reinforcing steel and structural steel. Initiation of the damage to the superstructure in the form of cracking or crushing of concrete and yielding of the steel is detected, progression of the damage is monitored, and load versus deformation, and damage to the bridge, is developed until the attainment of the collapse of the structure.

The developed method and the corresponding computer program BOVAS (Bridge OVerloading Analysis-Steel) are designed to predict the overload response of the types of bridges described above. The accuracy and applicability of the method is illustrated by applying the method to four bridge overload tests that had been conducted elsewhere and reported in the literature. Good agreement between the test results and analytical prediction is noted.

FOREWORD

Prior to the study of the report, the reader should be informed of the contents of the report, the goals of the reported research, and the relations between the reported part of the research and the parent research project. The intent of the foreword is to inform the reader of these issues. Even though they have been included in various parts of the reports, they may not be easily recognizable by the reader.

The research project, "Overloading of Steel Highway Bridges," is aimed at the development of a computer based tool to be used to rate, to determine the overload response, and to determine the ultimate load carrying capacity of bridge superstructures and their main components. The bridges are steel multi-beam, or multi-girder, superstructures with reinforced concrete deck (or with monolithic deck with secondary details). Simple and continuous span bridges are considered. The research program consists of the following major phases: (1) mathematical model for beam-slab bridges of idealized materials, (2) overloading response of reinforced concrete slabs, (3) slip phenomena and its incorporation into the analysis scheme, (4) mathematical modeling of steel girder reinforced concrete deck bridges, (5) effects of web buckling, flange buckling, etc., (6) effects of design details, stiffeners, X-bracings, etc., on the overload response, (7) parametric studies on the overload of these bridges, and (8) development of guidelines for "overloading" and user's manual for the developed computer program.

Phases 1 and 2 have been completed within the framework of

another research project, and the findings have been reported. Phase 3 and part of phase 5 have also been completed and reported in two research reports. This report provides a summary of the work carried out in Phase 4. The reporting of this phase has been delayed in order to complete the pilot research in phases 5 and 6. The pilot research have indicated that the methodology employed in the reported research permits its extension to more complicated structural configurations.

The report briefly presents, even though it corresponds to about one quarter of the report, the research methodology of phases 1-3. The contained information should be sufficient for the reader, if the prime interest is on the overloading of steel multi-girder bridges. However, for in-depth study of this report a comprehensive understanding of the summarized research is needed. Thus, full use of the references provided in this report needs to be made.

Because of the highly theoretical nature of the analytical developments, efforts have been made to group together the parts of the formulae that will not be of any interest to bridge engineers or any researcher, but are essential for those who would like to follow the derivations. This material is included in the appendices. The reader could easily dispense with the study of these appendices, unless step-by-step checking of the theoretical derivations is required.

The developed methodology to predict the overload response of the steel bridges has been compared against available test data. The correlation between the analytical prediction and experimentally obtained results have been satisfactory. The report presents the results of two

full scale bridge tests, and two scale model tests, and the analytical predictions obtained via the developed method. Good correlation between the full scale bridges and corresponding analytical results was observed. The scale model tests and the corresponding analytical results have not been satisfactory. The reasons for these discrepancies have been postulated in the report. The authors have preferred to include both the good and the bad verification studies to inform the readers of the possible pitfalls that may occur when extrapolations are used.

The developed computer program is acronymed BOVAS (Bridge OVerload Analysis-Steel). BOVAS is under continual expansion and modification to include various factors associated with the overloading of the steel bridges. These activities are included in Phases 5 and 6 of the parent research program.

1. INTRODUCTION

1.1 Overview of Research

The report presents results of the research on the development of a computer based mathematical model to predict the overload response of highway bridge superstructures. The response considered includes the elastic and inelastic behavior of the superstructure, until its collapse. The reported research is a part of the overall research program on the "Overloading of Steel Highway Bridges" sponsored by the Pennsylvania Department of Transportation (Research Project 77-1). This report is an interim report of this research project.

The bridges considered in the research consist of steel beams, or girders, and composite reinforced concrete deck (Fig. 2). Henceforth, these bridges will be referred to as steel bridges.

In 1966 over 700,000 overweight permits were issued in the fourty-eight states (Ref. 24). Assuming no changes in regulations and load limits this total was expected to grow to approximately 1,250,000 by 1975. The fact that real factors of safety for bridges are not known is reflected in the widely varying levels of overload permitted by each individual state. Furthermore, recent information indicates that one in six bridges in the United States is structurally deficient (Ref. 15). Thus the purpose of the present research is twofold.

In the short term the methods will allow engineers to analytically assess any damage, e.g. cracking of concrete or yielding of steel, a bridge would undergo due to an overload vehicle. Over the long term, experience with the analytical results, parametric studies and field tests may permit

correction of any deficiencies in new design and retrofitting of existing bridges.

Theoretical work has already been completed on the inelastic analysis of highway bridge superstructures consisting of prestressed or reinforced concrete beams and a composite reinforced concrete deck (Ref. 29, 39 and 41). These structures will be referred to herein as concrete bridges. In addition, theoretical work has been completed on the linear elastic analysis of steel bridges, including the effects of shear lag of the deck, shear deformation of the girders, and slip between the slab and girder (Ref. 49). Wherever possible, use will be made of the previous works, even though the nonlinear behavior of steel bridges requires special considerations.

1.2 Purpose and Scope of Investigation

As stated earlier, the purpose of the overall research program is the development of a mathematical model and anaylsis technique to predict the overload response of steel highway bridge superstructures from initial dead loads, in elastic range, to complete collapse of the superstructure by the placement of vehicles with increasing gross weight. The main thrust of the reported research is the interfacing of the inelastic analysis for reinforced concrete slabs (Ref. 39) with the linearly elastic analysis for steel beams (with slip provisions) (Ref. 49), and development of a new analysis scheme which will model the initiation and spread of nonlinear behavior of the beams.

This report presents:

1. A summary of the analytical modeling of the reinforced concrete

slab and steel girder (Chapter 3).

2. A summary of the analytical modeling of the complete stress-strain behavior for the biaxially stressed concrete and uniaxially stressed steel, including cracking and crushing of concrete and yielding of steel (Chapter 2).
3. Analytic modeling of simply supported or continuous highway bridge superstructures (Chapter 3), and
4. Verification of the analytical model and solution technique by comparing to experimental tests (Chapter 4).

1.3 Previous Work

Much of the investigation into the behavior of composite beams started with two papers by Newmark (Refs. 38 and 45). In both papers the structures were limited to simply supported structures and the effects of shear lag were neglected. Although the second paper dealt with partial interaction of the beam and slab, it was applicable only to isolated T-beams. Terazkiewicz expanded on Newmark's second paper to incorporate an effective width (Ref. 47). Based upon an initial assumption for the effective width, an iterative process was used to converge to a particular effective width. Neither Newmark nor Terazkiewicz includes the effects of shear deformations of the beams in their analyses.

Gustafson and Wright presented a theory capable of analyzing multi-girder simply supported and continuous bridges using finite elements (Ref. 18). Wegmuller and Kostem rederived the basic formulations and showed favorable comparisons with field tests (Ref. 52). The theory, however,

while incorporating shear lag ignored the effects of slip and shear deformation of the beams. An attempt to incorporate slip into the theory was presented by du Plesis (Ref. 14).

Recent research has been aimed at extending the previous elastic theories to account for the effects of material nonlinearities. Newmark's differential equation has been rederived to account for non-uniform connector spacing, initial strains, and non-linear material properties. These approaches utilize an incremental approach.

Algorithms developed by Proctor, Baldwin, Henry and Sweeney at the University of Missouri (Ref. 4 and 43) and by Yam and Chapman at Imperial College (Ref. 56) handle the boundary value problem as an initial value problem where equations are solved by successive approximations. The schemes developed by Dai, Thiruvengadam and Seiss at University of Illinois (Ref. 12), Wu at Lehigh University (Ref. 55), and by Fu at the University of Maryland (Ref. 17) use finite differences. None of these works relieves all the basic inadequacies of shear lag, shear deformation, slip, and continuous structures.

The finite element formulations have been extended into the non-linear range in a multitude of ways. Kostem, Kulicki, Peterson, and Wegmuller have done considerable work at Lehigh University using J_2 theory and a new theory for reinforced concrete. The structures analyzed have had J_2 beams and deck (Ref. 53), concrete beams and J_2 deck (Ref. 32) and concrete beams and deck (Ref. 29, 39 and 41). They used both an incremental and incremental-iterative techniques but the basic elastic finite element

algorithm remains as derived by Wegmuller and Kostem.

A general finite element formulation, which can be used to perform elastic analysis of composite single or multibeam, simple or continuous bridge superstructures, has been presented by Tumminelli and Kostem at Lehigh University (Ref. 49). The formulation can include the effects of slip between the slab and the beams, shear deformation of the beams, and shear lag in the deck.

Several state of the art papers have discussed other aspects of composite beams and other theorectical work (Refs. 2, 27 and 50), but they indicate the lack in generally sophisticated enough methods to analyze steel bridges.

1.4 The Analytical Model

The behavior of the analytical model should adequately describe the behavior of the real structure. Thus, the developed model for steel highway bridge superstructures considers: (1) the flexural behavior of the superstructure, (2) shear deformations of the beams, (3) the composite action of the beam and the slab, (4) in-plane stresses in the beams and the slabs developed due to eccentricity of the beams, (5) slip between the beams and the slab, (6) the material nonlinearities, and (7) the coupling action of the in-plane and out-of-plane forces and deformations.

Since the material nonlinearities have a great effect on behavior of the superstructure, in particular, the structural stiffness, a realistic representation of the material behavior of the component parts

is essential. The biaxial stress-strain relationship and failure envelope for concrete slabs developed from experimental and analytical results (Refs. 33, 35, 36 and 37) and implemented in References 41 and 42 have also been used in the present model. In addition, the stress-strain relation for the slab reinforcement and the beam steel (Refs. 29, 30, 31 and 44) utilized in the research is similar to that employed in References 41 and 42 for mild steel. The variation of material properties through the depth of the beams and the slab is accounted for by dividing the finite elements into a series of layers through the depth. By defining the stress-strain relation on a layer by layer basis the progression of material failure in terms of cracking or crushing of concrete or yielding of steel can be monitored throughout the superstructure. Through the use of the layering technique excellent agreement has been obtained in previous investigations (Refs. 5, 19, 20, 29, 32, 34, 40, 53, 51 and 54).

Steel bridges present some special considerations not included in previous work on the inelastic analysis of concrete bridges. In the elastic analysis of composite steel bridges (Ref. 49) assumptions were made regarding which phenomena were considered of primary importance and which were of a secondary nature. Although these assmptions were based on a review of experimental results of composite beam tests and analytical studies of bridge superstructures, later research may alter some of the assumptions.

The following phenomena are considered to be of primary importance in the analysis of steel bridge superstructures:

1. Slip between the steel beam and concrete slab (Fig. 3a).
2. Shear deformations of the steel girders (Fig. 3b).
3. Shear lag of the concrete deck (Fig. 4).

The following phenomena are considered to be of secondary importance and are neglected:

1. Minor axis bending of the beams (Fig. 4).
2. Torsion of the beams (Fig. 4).
3. Interaction between the girders and wind bracing and diaphragms (Fig. 2).
4. Lateral torsional buckling of the beams.

Although these phenomena are ignored in the present analysis, the developed model does not preclude their inclusion during the later stages of the research program. In addition to these assumptions there are some other general assumptions:

1. Small deformations
2. Failure in a flexural mode
3. Constant slab thickness
4. Static loading

These are covered more in depth in Chapter 3. The shear punching of the deck is not considered.

2. MATERIAL BEHAVIOR

2.1 Introduction

This chapter presents the stress-strain relationships employed in the analysis scheme herein reported. The material stress-strain relations are defined for the steel reinforcing bars, the concrete, and the beam or girder steel. These relations are later used in establishing the stiffness properties of the bridge components.

The behavior of concrete is very much dependent upon the particular stress state, i.e. tension or compression, and whether the stress field is uniaxial, biaxial, or triaxial. A slab could be considered as a two dimensional structural element in which bending in both the longitudinal and the transverse directions produce a biaxial state of stress (Ref. 39). The inelastic biaxial stress-strain relations of concrete are analytically described by empirical formulae. These experimentally derived formulae are summarized in the following sections. The readers are refered to the previous work mentioned above for an in-depth treatment of the theory and the derivations.

A beam, whether composed of concrete or steel, may be idealized as a one dimensional structural element in which bending in the longitudinal direction produces a uniaxial state of stress (Ref. 29). The elastic-inelastic uniaxial stress-strain relations of steel can also be described analytically by an empirical formula. Once the analytic stress-strain equations are established, they are differentiated to obtain an expression

for the instantaneous slope, i.e. tangent modulus, of the stress-strain curve. The tangent modulus is then used to formulate the elasticity matrix,[D], which relates the stress increment to the strain increment.

$$\{\dot{\sigma}\} = [D]\{\dot{\varepsilon}\} \tag{2.1}$$

The elasticity matrix is utilized to establish the slab and beam finite element stiffness properties (see Chapter 3).

Throughout this report the stress-strain relationships discussed will involve both total stresses and strains and incremental stresses and strains. To differentiate between the two types, incremental quantities will be distinguished by the customary dot over the appropriate quantity, e.g. Eq. 2.1.

2.2 Biaxial Stress-Strain Relationships

The idealized biaxial stress-strain curves have basically two fundamental shapes: one nonlinear and one linear. In the region of biaxial stress where compression is dominant the nonlinear equation governs, while in the regions of biaxial stress where tension is dominate the linear expression controls. Figure 6 shows the approximate regions in the biaxial stress space where the nonlinear and linear equations are applicable. The peak slope of the stress-strain curve is designated by E_p in the figure.

2.2.1 Nonlinear Stress-Strain Equation for Concrete

The nonlinear stress-strain curve used for concrete has the form (Ref. 39);

$$\sigma = \frac{\varepsilon E_c}{(1-\nu\alpha)\ (1+C\varepsilon + D\varepsilon^2)} \qquad (2.2)$$

Where:

σ = the principal stress in the direction of interest

ε = the strain in direction of interest

ν = Poisson's ratio (taken to be 0.2)

α = the ratio of the principal stress in the orthogonal direction to the principal stress in the direction of interest, i.e.

$\alpha_1 = \sigma_2/\sigma_1$

E_c = Initial tangent modulus in uniaxial loading

A positive stress from equation 2.2 denotes compression, and correspondingly a positive strain denotes contraction.

The remaining parameters are:

$$C = \frac{E_c}{\sigma_p(1-\nu\alpha)} - \frac{2}{\varepsilon_p} + \frac{E_p E_c \varepsilon_p}{(1-\nu\alpha)\sigma_p^2}$$

$$D = \frac{1}{\varepsilon_p^2} - \frac{E_p E_c}{(1-\nu\alpha)\sigma_p^2} \qquad (2.3)$$

Where:

σ_p is the peak stress

ε_p is the strain at the peak stress and

E_p is the slope of the stress-strain curve at the peak stress

The instantaneous slope of the stress-strain curve is obtained by differentiating equation 2.2 which gives,

$$\frac{d\sigma}{d\varepsilon} = \frac{E_c\ (1-D\varepsilon^2)}{(1-\nu\alpha)(1+C\varepsilon + D\varepsilon^2)^2} \qquad (2.4)$$

When this equation is applied in the direction of the two principal stresses, the results are:

$$E_{1b} = \frac{d\sigma_1}{d\varepsilon_1} = \frac{E_c}{(1-\nu\alpha_1)} \quad \frac{(1-D_1\varepsilon_1^2)}{(1+C_1\varepsilon_1+D_1\varepsilon_1^2)^2} \tag{2.5a}$$

$$E_{2b} = \frac{d\sigma_2}{d\varepsilon_2} = \frac{E_c}{(1-\nu\alpha_2)} \quad \frac{(1-D_2\varepsilon_2^2)}{(1+C_2\varepsilon_2+D_2\varepsilon_2^2)^2} \tag{2.5b}$$

Where: E_1b and E_2b are the tangent moduli in the two principal directions 1 and 2 respectively.

$\alpha_1 = \sigma_2/\sigma_1$

$\alpha_2 = \sigma_1/\sigma_2$

$D_{1(2)}$ and $C_{1(2)}$ are the D and C curve parameters evaluated for the "1" ("2") principal direction using equation 2.3.

Thus, the incremental stress-incremental strain relation in matrix form can be defined as:

$$\begin{Bmatrix} \dot{\sigma}_1 \\ \dot{\sigma}_2 \end{Bmatrix} = \begin{bmatrix} E_{1b} & 0 \\ 0 & E_{2b} \end{bmatrix} \quad \begin{Bmatrix} \dot{\varepsilon}_1 \\ \dot{\varepsilon}_2 \end{Bmatrix} \tag{2.6}$$

The curve parameters C and D, which are presented in equation 2.3, can be determined if the following quantities are known: Ec, ν, α, σp, εp, and Ep. The first three quantities have already been defined, and the last three quantities will be defined in Sections 2.2.3, 2.2.4, and 2.2.5.

2.2.2 Linear Stress-Strain Equation for Concrete

The linear stress-strain curve used for concrete has the form:

$$\sigma = \frac{\sigma_p}{\varepsilon_p} \quad \varepsilon \tag{2.7}$$

Where the tangent modulus, which is constant, is obtained by differentiating the stress-strain equation:

$$\frac{d\sigma_1}{d\varepsilon_1} = \frac{\sigma_p}{\varepsilon_p}$$

The incremental stress-incremental strain relationship follows from equation 2.8 as:

$$\begin{Bmatrix} \dot{\sigma}_1 \\ \dot{\sigma}_2 \end{Bmatrix} = \begin{bmatrix} E_{1b} & 0 \\ 0 & E_{2b} \end{bmatrix} \begin{Bmatrix} \dot{\varepsilon}_1 \\ \dot{\varepsilon}_2 \end{Bmatrix} \tag{2.9}$$

Where:

$$E_{1b} = \frac{d\sigma_1}{d\varepsilon_1} = \frac{\sigma_{p1}}{\varepsilon_{p1}} \tag{2.10}$$

$$E_{2b} = \frac{d\sigma_2}{d\varepsilon_2} = \frac{\sigma_{p2}}{\varepsilon_{p1}}$$

σ_{p1} (ε_{p1}) and σ_{p2} (ε_{p2}) denote the peak stress (strain) for the "1" and "2" principal directions, respectively. Thus, the linear stress-strain curve can be established once the peak stress and peak strain values are known.

2.2.3 Biaxial Failure Envelope - Definition of σ_p

Nondimensional experimental peak stress envelopes for various concrete strengths (Ref. 5, 33 and 39) indicate that the fundamental shape of the failure envelope is essentially invariant and that only the size of the envelope will change with concrete strength. The true failure surface can be idealized as a series of straight lines as shown in Figure 7. The characteristic points used to define the idealized peak stress envelope are shown in Figure 8 and the corresponding coordinates and equations defining

the straight line segments, which are expressed in terms of the characteristic points and the stress ratio, α, are given in Refs. 5 and 39.

2.2.4 Peak Strain Envelope - Definition ε_p

The nondimensional peak strain envelope, shown in Figure 9 , is approximated by a series of straight lines passing through or close to, the experimental peak strain points indicated in the figure (Ref. 33 and 35). The characteristic points used to define the peak strain envelope are shown in Fig. 10 and the corresponding coordinates and equations defining the straight line segments, which are expressed in terms of the characteristic points and the stress ratio, α, are given in Refs. 5 and 39.

2.2.5 Peak Slope - Definition of E_p

The peak slope is defined as the tangent of the non-linear stress-strain curve evaluated at the peak stress. Experimental evidence indicates that this peak slope has a value of zero in the compression-compression region (Refs. 33, 35 and 37). In the tension-compression region experiments show that the value of peak slope can vary from a value of zero for stress states near uniaxial compression to a value equal to σ_p/ε_p for stress states near uniaxial tension. The idealization used assumes the ratio of the peak slope to the initial slope varies linearly with respect to the stress ratio. This ratio has a value of zero near uniaxial compression state and a value of 1.00 near uniaxial tension state. An in depth descrip-

tion of this relationship and the resulting equations defining the straight line segments are given in Ref. 5 and 39.

2.2.6 Biaxial Constitutive Relationships for Concrete

The incremental stress-stress relationship for concrete in terms of the principal stresses is:

$$\begin{Bmatrix} \dot{\sigma}_1 \\ \dot{\sigma}_2 \\ \dot{\sigma}_{12} \end{Bmatrix} = [\bar{D}] \begin{Bmatrix} \dot{\varepsilon}_1 \\ \dot{\varepsilon}_2 \\ \dot{\gamma}_{12} \end{Bmatrix} \tag{2.11}$$

Where the subscripts 1 and 2 identify the principal stress directions and the dots indicate incremental quantities.

Even though the shear stress increment, $\dot{\tau}_{12}$, will be zero, its inclusion is needed in the principal stress vector so as to include the contribution of shearing stiffness term in the [D] matrix. This is necessary so that when transforming the [D] matrix from the principal axes to the global x-y axes the correct elasticity relationships are obtained. The $[\bar{D}]$ matrix can be expressed by (Ref. 35).

$$[\bar{D}] = \begin{bmatrix} \dfrac{E'_{1b}}{1-\nu_1\nu_2} & \dfrac{\nu_2 E'_{1b}}{1-\nu_1\nu_2} & 0 \\ \dfrac{\nu_1 E'_{2b}}{1-\nu_1\nu_2} & \dfrac{E'_{2b}}{1-\nu_1\nu_2} & 0 \\ 0 & 0 & \dfrac{E'_{1b}\,E'_{2b}}{E'_{1b}+E'_{2b}+2\nu_1 E'_{2b}} \end{bmatrix} \tag{2.13}$$

E'_{1b} and E'_{2b} are the tangent moduli on the first and second principal stress

directions, respectively and ν_1 and ν_2 are the Poisson's ratios in the same directions. In the euqation above it is assumed that $\nu_1/E'_{1b} = \nu_2/E'_{2b}$.

The analytic stress-strain curves of Sections 2.2.1 and 2.2.2 relate the stress in a particular principal direction to the strain in the same direction only. Thus, the following relationships were formed:

$$\begin{aligned} \dot{\sigma}_1 &= E_{1b}\,\dot{\varepsilon}_1 \\ \dot{\sigma}_2 &= E_{2b}\,\dot{\varepsilon}_2 \end{aligned} \tag{2.13}$$

Where E_{1b} and E_{2b} are the effective tangent moduli for the principal stress space. A relationship must now be established between the known moduli, E_{1b} and E_{2b}, and the unknown quantities of the $[\bar{D}]$ matric E'_{1b}, E'_{2b}, ν_1, and ν_2.

Solving Eq. 2.11 for $\dot{\varepsilon}_1$ and $\dot{\varepsilon}_2$ and noting that $\dot{\sigma}_1 = \dot{\sigma}_2\dot{\alpha}_2$ and $\dot{\alpha}_2 = \dot{\sigma}_2\dot{\alpha}_1$, leads to:

$$\dot{\varepsilon}_1 = \dot{\sigma}_1 \left(\frac{1}{E'_{1b}} - \frac{\nu_2 \alpha_1}{E'_{2b}} \right) \tag{2.14a}$$

$$\dot{\varepsilon}_2 = \dot{\sigma}_2 \left(\frac{1}{E'_{2b}} - \frac{\nu_1 \alpha_2}{E'_{1b}} \right) \tag{2.14b}$$

Then by noting that $\nu_2/E'_{2b} = \nu_1/E'_{1b}$ and rearranging yield:

$$\dot{\sigma}_1 = \left(\frac{E'_{1b}}{1 - \nu_1 \alpha_2} \right) \dot{\varepsilon}_1 \tag{2.15a}$$

$$\dot{\sigma}_2 = \left(\frac{E'_{2b}}{1 - \nu_2 \alpha_2} \right) \dot{\varepsilon}_2 \tag{2.15b}$$

Comparison of Eq. 2.15 and Eq. 2.13 shows the relationship between the effective tangent moduli and the actual tangent moduli and Poisson's ratios.

After some rearranging this gives:

$$E'_{1b} = E_{1b} (1 - \nu_1 \alpha_1) \tag{2.16a}$$

$$E'_{2b} = E_{2b} (1 - \nu_2 \alpha_2) \tag{2.16b}$$

E_{1b} and E_{2b} are defined in Eq. 2.5 for the nonlinear case and Eq. 2.10 for the linear case. E_{1b}, E_{2b}, and the α's are computed using the current total stress state. The curve parameters C and D in the aforementioned expressions are given by Eq. 2.3.

ν_1 and ν_2 in Eq. 2.12 must still be obtained. Again noting the relation $\nu_2/E'_{2\,b} - \nu_1/E'_{1b}$ the following equations are formulated:

$$\nu_A = \nu \tag{2.17a}$$

$$\nu_B = \frac{1}{\frac{E_{Ab}(1 - \nu_A \alpha_A)}{E_{Bb} \alpha_B} + \alpha_B} \tag{2.17b}$$

where the subscripts (A,B) correspond to directions (1,2) or (2,1) which ever is applicable. The value for ν_A is chosen as 0.2 and ν_B is limited to positive values. Bases upon the various combinations of cylinder strength, stress ratios and stress levels, ν_B has been found to range from 0.80 to 1.20 times the value of ν_A.

Thus all the terms of Eq. 2.12 can be defined, and the resulting $[\bar{D}]$ matrix is the constitutive relationship for a particular layer expressed in the principal stress directions. Before computing the contribution of this layer to the element stiffness matrix, the $[\bar{D}]$ matrix must be transformed into an elasticity matrix [D], relating the stress and strain in the x-y coordinate system of the element.

$$\begin{Bmatrix} \dot{\sigma}_x \\ \dot{\sigma}_y \\ \dot{\tau}_{xy} \end{Bmatrix} = [D] \begin{Bmatrix} \dot{\varepsilon}_x \\ \dot{\varepsilon}_y \\ \dot{\gamma}_{xy} \end{Bmatrix} \tag{2.18}$$

where (Ref. L, M, N)

$$[D] = [T] [D] [T]^T \tag{2.19}$$

and T is defined by:

$$[T] = \begin{bmatrix} \cos^2\theta & \sin^2\theta & \mp 2\cos\theta\sin\theta \\ \sin^2\theta & \cos^2\theta & 2\cos\theta\sin\theta \\ \cos\theta\sin\theta & -\cos\theta\sin\theta & \cos^2\theta - \sin^2\theta \end{bmatrix} \tag{2.20}$$

The angle θ is defined as the angle between the x direction and the "1" direction, and is positive when measured clockwise from the positive x axes.

2.27 Concrete Failure Mode

Concrete exhibits different types of failure modes which are dependent upon the applied stress ratio as shown in Figure 12a. The four physically distinct failure modes are described on (Ref. 5 and 39). The idealized failure modes used in this report are depicted on Fig. 12b. A cracking mode failure is assumed to occur from the tension-tension region to a stress ratio of -1/15. The direction of the crack(s) is assumed to be perpendicular to the largest tensile stress and to the free surface of the specimen. From the compression-compression region to the stress ratio -1/15, a crushing failure mode is assumed to occur. The direction of crushing is assumed to be perpendicular to the largest compressive stress and perpendicular to the free surface of the specimen.

The method presented here defines cracked regions and not individual cracks which may occur. The validity of this method has already been proven in (Ref. 5 and 39). In addition the effects of cracking or crushing of concrete on the element stiffness and the stiffness of the rest of the superstructure is approximated.

2.2.8 Cracked or Crushed Concrete

Cracking or crushing of the concrete is deemed to occur when the principal stress has exceeded the idealized peak stress as defined on Fig. 8. The concrete layer is assumed to have stiffness only in the uncracked or uncrushed direction. For example, the constitutive stress-strain relation for a concrete layer which has experienced a failure caused by the stress in "2" would be:

$$\begin{Bmatrix} \dot{\sigma}_1 \\ \dot{\sigma}_2 \\ \dot{\tau}_2 \end{Bmatrix} = \begin{bmatrix} E'_{1b} & 0 & 0 \\ 0 & 0 & 0 \\ 0 & 0 & 0 \end{bmatrix} \begin{Bmatrix} \dot{\varepsilon}_1 \\ \dot{\varepsilon}_2 \\ \dot{\gamma}_{12} \end{Bmatrix} \tag{2.21}$$

The first principal direction is still effective in contributing stiffness the the element.

After cracking or crushing of the concrete layer, the layer will be incapable of sustaining the stress that caused the failure. This stress must be reduced to zero within the layer while maintaining equilibrium between external forces and internal stresses. This unloading of stress requires a redistribution of the unloaded stress to other layers. This redistribution is accomplished through the use of a fictitious force matrix

which is statically equivalent to the amount of stress to be redistributed. Including these fictitious forces in the solution of the stiffness equations will produce the desired adjustments.

Experimental evidience indicates that after attainment of the peak concrete strength, compression or tension, the stress-strain curve exhibits a downward leg (Res. 5, 25, 26, 33, 35, 42 and 46). For this research the unloading portion of the stress strain curve has been assumed to be a straight line. (Refs. 5 and 29) Thus, unloading of the element will occur with a gradual transfer of stress from the failed concrete layer to the steel reinforcing bars (Ref. 34).

2.3 Uniaxial Stress-Strain Relationships

The beam steel and steel reinforcing bars are considered to be in a state of uniaxial stress. The uniaxial stress-strain curve is assumed to follow the Ramberg-Osgood formulation (Refs. 29, 32 and 44) given by:

$$C = \frac{\sigma}{E_i} + \left(\frac{1-m}{m}\right) \frac{\sigma s}{E_i} \left(\frac{\sigma}{\sigma s}\right)^n \qquad (2.22)$$

Where:

σ = stress

ε = strain

E_i = initial modulus of elasticity

σ_s = secant yield strangth equal to the ordinate of the intersection of the stress-strain curve and a line of slope (m) (E_i)

m = dimensionless constant defining a line of slope (m) (E_i) on the stress-strain curve

n = a dimensionless constant

The tangent modulus can be found by differentiating the stress-strain equation as follows:

$$\frac{d\sigma_1}{d\varepsilon_1} = \frac{E_i}{1+n\left(\frac{1-m}{m}\right)\left(\frac{\sigma_1}{\sigma s}\right)^{n-1}} \tag{2.23}$$

The constitutive relations between the stress and strain increments are:

$$\begin{Bmatrix} \dot{\sigma}_1 \\ \dot{\sigma}_2 \\ \dot{\tau}_{12} \end{Bmatrix} = \begin{bmatrix} \bar{D}_{11} & 0 & 0 \\ 0 & 0 & 0 \\ 0 & 0 & 0 \end{bmatrix} \begin{Bmatrix} \dot{\varepsilon}_1 \\ \dot{\varepsilon}_2 \\ \dot{\gamma}_{12} \end{Bmatrix} \tag{2.24}$$

Where $\bar{D}_{11} = d\sigma_1 / d\varepsilon_1$, as in Eq. 2.23 and the subscript "1" refers to the principal stress direction.

2.31 Beam Steel and Slab Reinforcement

The complete stress-strain curve for typical beam steel on uniaxial tension or compression is approximated with Ramberg-Osgood curves. (Eq. 2.22). The curve parameters for typical bridge steel are as follows:

σ_s = fy, yield strength of steel

E_i = E_s, Young's modulus for steel which may be taken as equal to 29,000 ksi

n = 300

m = 0.67

Since the Ramberg-Osgood formula provides a continuous stress-strain curve a mathematical distinction between yielded and non-yielded steel is not required.

The proper selection of the curve parameters can provide an almost perfectly plastic plateau in the case for mild steels. This plateau will have a small finite slope but its value will be so small that for all practical purposes its effect on the structural behavior will be negligible.

The stress-strain relation for mild steel reinforcing would have the following Ramberg-Osgood parameters:

$$\sigma_s = fy$$

$$E_i = 29000 \text{ ksi}$$

$$n = 100$$

$$m = 0.7$$

The slight difference in the values of n and m from those of the beam steel represents a more rounded knee for the reinforcing bar.

Special consideration must be made when the slab reinforcement is placed at an angle with respect to the longitudinal x-axis of the bridge. In this case, the "1" direction does not coincide with the x-direction, and the $\bar{D}$ matrix of Eq. 2.24 must be transformed to the x-y axes by the T matrix.

3. FINITE ELEMENT ANALYSIS

3.1 Introduction

The analytical technique employed in this research is based on the finite element method. Only a brief review of the finite element method is presented, and for an in-depth treatment of the method the reader can refer to numerous text on the subject (e.g. Refs. 48 and 57). The underlying assumptions that were made and their implications with regards to the finite element model are discussed. In addition the basic equations and notations used throughout the remainder of the report are provided.

3.2 Assumptions

The general assumptions made in the development of the analytical model and any associated implications are discussed in the following paragraphs.

1. Geometry Restrictions:

   At the present time the bridge superstructures to be analyzed are limited to those which are rectangular in plan, e.g., right bridges.

2. Assumptions Regarding Strain Distributions:

   Kirchoff's assumption that plane sections normal to the plate before deformation remain plane and normal after beam theory is employed, where the plane section

assumption for beam bending is used but in addition the effects of shearing deformation are also included. It is also assumed that the slab behaves as a thin plate, and that the slab and the beam do not change thickness.

A. These restrictions allow the stresses and strain normal to the slab to be neglected, and thus reduce the three dimensional continuum problem to a two dimensional plate bending problem, and a one dimensional beam bending problem.

B. In addition, the restrictions permit the strain at any depth to be computed from the displacements at the reference plane.

3. Small Deformations:

The in-plane and bending displacements are assumed small with respect to the dimensions of the slab, thereby, allowing all calculations to be computed based upon the undeformed position of the structure.

4. Small Strains:

The reinforced concrete slab and highway bridge superstructures are assumed to be subjected to small strains, therefore, linear strain-displacement relations can be employed.

5. Layering:

Due to the material nonlinearities, such as nonlinear stress-strain relations, cracking and crushing of concrete and yielding of steel, the finite element stiffness

properties will vary with the depth of the slab or beam element. To facilitate the computation of the element stiffness, the finite element will be divided into a series of layers through the depth (Figs. 5, 11). The total stiffness of the element is then obtained by summation of the stiffness properties of each individual layer. The stresses within a particular layer will be assumed to be constant throughout the layer for the purposes of computing element stiffnesses. Thus, the stress field on the beam or slab will vary in a step-like manner. By increasing the number of layers the representation of the stress field could be improved, and this leads to increased accuracy.

3.3 The Finite Element Method

The analytical technique employed to establish global, equilibrium is the displacement-based finite element method, which leads directly to the familiar set of equilibrium equations (Ref. 57):

$$\{F\} = [K]\ \{\delta\} \tag{3.1}$$

where

$\{F\}$ = vector of applied forces at the nodes

$[K]$ = stiffness matric of the structure

$\{\delta\}$ = vector of displacements at the nodes

The structural stiffness matrix is obtained by stacking the element stiffness matrices at each node point for each degree of freedom:

$$[K] = \Sigma [k]_i^e \tag{3.2}$$

where the summation is overall the elements on the structure and $[k]_i^e$ is the element stiffness matrix for element-i.

The displacement based method presented in Eqs. 3.1 and 3.2 is the most prevalent finite element scheme employed today, and it has repeatedly shown its reliability as an analytical instrument in previous research (Refs. 5, 29, 39, 41, 49, 52 and 53).

The primary concern of the analysis technique is the development of the element stiffness matrix in the equilibrium equations:

$$\{F\}^e = [k]^e \{\delta\}^e \tag{3.3}$$

where

$\{F\}^e$ = vector of applied forces at the element nodes

$\{\delta\}^e$ = vector of displacements at the element nodes.

The procedure employed to formulate the generalized coordinate finite elements can be separated into two parts. The first part is the derivation of the shape functions from the assumed displacement fields; and the second is the derivation of the element stiffness matrix from the shape functions. The second part, although generally available in the literature, is reviewed in this section to define terminology. The first part is presented in the following section, which details the methods used to derive shape functions from displacement fields.

Zienkiewicy outlined the following formulation, which begins with shape functions for the displacement fields within the element as a function of the element node displacements (Ref. 57):

$$\{f\} = [N] \{\delta\}^e \tag{3.4}$$

where

$\{f\}$ = displacement field of the element

$[N]$ = shape functions.

Customarily the shape functions take the form of polynomials, but the theory is not restricted to their use.

By differentiation of the displacement field given in Eq. (3.4) the internal strains are determined.

$$\{\varepsilon\} = [B] \{\delta\}^e \tag{3.5}$$

where

$\{\varepsilon\}$ = vector of element strains

$[B]$ = strain-displacement matrix.

Assuming no initial strains or stresses, the stresses can be obtained from the appropriate constitutive relations:

$$\{\sigma\} = [D] \{\varepsilon\} \tag{3.6}$$

where

$\{\sigma\}$ = vector of element stresses

$[D]$ = stress-strain (elasticity) matrix.

Applying a small virtual displacement to the element and equating internal and external work (i.e. the principle of virtual work) results

in the formulation of the element stiffness matrix:

$$[k]^e = \int_v [B]^T [D] [B] \, dv \tag{3.7}$$

The successful element formulation is the one that uses the appropriate shape function to model the desired phenomena and considers all the internal work terms consistent with the shape functions.

3.4 Shape Functions

The shape functions are derived from assumed displacement fields. In order to preserve generality and increase computational efficiency, the displacement field of the element and the node displacements are written at a reference plane which is parallel to, but at an arbitrary distance from, the centroidal axis of the element. This technique is valid so long as the strain-displacement matrix relates the displacements at the reference plane to the strains within the element. In the reported research the displacement fields at the reference plane are taken as polynomials. The following procedure is adapted from material presented by Peterson and Kostem (Ref.39) and Tumminelli and Kostem (Ref. 49) and begins with the assumed displacement fields:

$$\{f\} = [P(x,y)] \{\alpha\} \tag{3.8}$$

where

$[P(x,y)]$ = functions of x and y used to describe the shape of the displacement fields

$\{\alpha\}$ = vector of the coefficients of the displacement functions.

Enforcing compatibility at the element nodes between the internal displacement function and the external node displacement defines the coefficients of the polynomial. Usually in this type of formulation the number of coefficients and node displacements (degrees of freedom) are equal, thereby allowing all coefficients to be determined exactly by the compatibility equations.

In the present formulation for the beam element the number of coefficients exceeds the number of element degrees of freedom, so additional equations must be established. One conventional approach to obtain additional equations is to introduce internal node(s) which have a sufficient degree of freedom to completely determine all the coefficients. Then through static condensation techniques the added degrees of freedom are removed from the resulting stiffness matrix. An uncommon approach, which is applied in this case, is to relate the polynomials directly to one another via equilibrium and/or compatibility equations without introducing new degrees of freedom. Thus evaluating and partitioning of Eq. 3.8 yields

$$\begin{Bmatrix} \{\delta\} \\ \{o\} \end{Bmatrix} = \begin{bmatrix} C \end{bmatrix} \{\alpha\} = \begin{bmatrix} C1 \\ \hline C2 \end{bmatrix} \{\alpha\} \tag{3.9}$$

where

$\{o\}$ = vector of zeros representing left hand side of equilibrium and/or compatibility equations.

$[C1]$ = matrix consisting of $P(x)$, evaluated at the appropriate nodes

[C2] = coefficients of the equilibrium and/or compatibility equations.

Inverting [C] to solve for $\{\alpha\}$:

$$\{\alpha\} = [C]^{-1} \begin{Bmatrix} \{\delta^e\} \\ \\ \{o\} \end{Bmatrix} \tag{3.10}$$

and

$$\{\alpha\} = [CC]\ \{\delta^e\} \tag{3.11}$$

where

[CC] = coefficient displacement matrix consisting of the first n columns of $[C]^{-1}$ where n is the number of displacements in the vector $\{\delta\}^e$.

Therefore, the shape function is defined:

$$\{f\} = [P(x,y)]\ \{\alpha\} = [P(x,y)]\ [CC]\ \{\delta\}^e = [N]\ \{\delta\}^e \tag{3.12}$$

When performing the detailed derivations, the shape functions are not explicitly formed because they are cumbersome. Since the [CC] matrix is not a function of x, all derivatives of the shape functions need be performed on [P(x,y)] only. All of the strains are functions of x only, thus only [P(x,y)] will be differentiated. The operator necessary to define the strains derived from the displacement fields will be called [Γ], hence:

$$\{\varepsilon\} = [\Gamma]\ \{f\} = [\Gamma]\ [P(x,y)]\ \{\alpha\} = [Q]\ \{\alpha\} \tag{3.13a}$$

and now substituting for $\{\alpha\}$

$$\{\varepsilon\} = [Q]\ [CC]\ \{\delta\}^e = [B]\ \{\delta^e\} \tag{3.13b}$$

This strain-displacement matrix and the stress-strain matrix can be substituted into Eq. 3.7 to formulate the element stiffness matrix.

3.5 The Layered Slab Model

In sections 3.3 and 3.4 the general steps required to obtain the element stiffness matrix were discussed. These steps with regards to the nonlinear analysis of reinforced concrete slabs will now be presented in detail. Explicit expressions for matrices used in the layered slab model can be found in Appendix A.

3.5.1 Plate Bending and Inplane Displacement Functions

The purpose of this section is to present the displacement functions and to describe the displacement field, $\{\Delta\ (x,y)\}$.

The bending deformation of a plate can be completely described by the vertical displacement of the middle plane of the plate via the Kuchoff's assumption. The bending deformation will consist of a vertical displacement, W, the rotation about the x-axis, θ_x, and the rotation about the y axis, θ_y. These rotations can be obtained by differentiation of the vertical displacement. Expressed in vector form this gives:

$$\begin{Bmatrix} W \\ \theta_x \\ \theta_y \end{Bmatrix} = \begin{Bmatrix} W \\ \frac{\partial w}{\partial y} \\ \frac{\partial w}{\partial y} \end{Bmatrix} \tag{3.14}$$

The ACM plate bending element originally proposed by Adini, Clough and Melosh (Ref. 13) and a plane stress element originally proposed by Clough (Ref. 11) are used in this research. As noted by Tumminelli and Kostem (Ref. 49) as long as the reference plane of the slab is at the midheight, the beam and plate element stiffnesses are uncoupled and, in addition, the finite element model is conforming and complete. These requirements are needed to insure convergence and an upper-bound solution. This element has been successfully used in previous research and has shown itself to be both accurate and reliable (Refs. 5, 39, 41, 52 and 53). The ACM vertical displacement field (W) is given by a twelve term polynomial (Refs. 49 and 52).

$$W = a_1 + a_2x + a_3y + a_4x^2 + a_3xy + a_6y^2 + a_7x^3 + a_8x^2y$$

$$a_9xy^2 + a_{10}y^3 + a_{11}x^3y + a_{12}xy^3 \tag{3.15}$$

The plate-in-plane displacement fields are given as (Refs. 49 and 52)

$$U = b_1 + b_2x + b_3y + b_4xy \tag{3.16a}$$

$$V = b_5 + b_6 + b_7y + b_8xy \tag{3.16b}$$

The coefficients, a_i's and b_i's, of these equations correspond to the constant coefficients of the displacement fields, $\{\alpha\}$, used in Eq. 3.8.

The nodal points of the plate element, labeled as I, J, K and L, as indicated in Fig. 11, are located in the middle of the plate reference plane and in the four corners of the rectangular finite element. The element displacement vector, $\{\delta\}^e$, consists of five deformation components per node or a total of twenty components per element.

The displacement functions, W, U and V are used to define the element displacement function for any location given by the coordinates (x,y):

$$\{\delta\}_i^{eT} = \{U\ V\ W\ \theta_x\ \theta_y\}^T = \{U\ V\ W\ \partial w/\partial y\ -\ \partial w/\partial x\}^T \qquad (3.17)$$

where

$\{\delta\}_i^e$ = node i displacements of element e.

Thus Eq. 3.8 can be established once the displacement functions have been chosen. For added computational efficiency the displacement field is partitioned into those involving only in-plane displacements and those involving only bending displacements. For the entire plate element we have:

$$\{\delta\}^e = [P(x,y)]\ \{\alpha\} \qquad (3.18)$$

and by partitioning we get:

$$\begin{Bmatrix} \delta_u \\ \\ \delta_\phi \end{Bmatrix}^e = \left[\begin{array}{c|c} P_u(x,y) & 0 \\ \hline 0 & P_\phi(x,y) \end{array}\right] \begin{Bmatrix} \alpha_u \\ \\ \alpha_\phi \end{Bmatrix} \tag{3.19}$$

The subscripts u and ϕ refer to the in-plane and bending displacements respectively.

3.5.2 Strain-Displacement Relations

Based upon the assumptions of thin plate small-deflection theory the strain displacement relationships for a point at a distance z from the reference plane are:

$$\begin{aligned} (\varepsilon_x)_z &= \frac{U_z}{dx} \\ (\varepsilon_y)_z &= \frac{V_z}{dy} \\ (\varepsilon_{xy})_z &= \frac{U_z}{dy} + \frac{V_z}{dx} \end{aligned} \tag{3.20}$$

where

z = distance of point under consideration from the reference plane

U_z = displacement in the x-direction at depth z

V_z = displacement in the y-direction at depth z

$(\varepsilon_x)_z$ = strain in x-direction at depth z

$(\varepsilon_y)_z$ = strain in y-direction at depth z

$(\gamma_{xy})_z$ = shear strain at depth z

Using Kirchoff's assumption the displacements U_z and V_z can be expressed in terms of the middle surface in-plane displacements and the rotation of the middle plane times the distance to the point under consideration from the middle plane.

$$\begin{aligned} U_z &= U - z\frac{\partial W}{\partial x} \\ V_z &= U - z\frac{\partial W}{\partial y} \end{aligned} \tag{3.21}$$

Substituting Eq. 3.21 into Eq. 3.20 leads to

$$\{\varepsilon\}_z = \begin{Bmatrix} \varepsilon_x \\ \varepsilon_y \\ \gamma_{xy} \end{Bmatrix}_z = \begin{Bmatrix} \frac{\partial U}{\partial x} \\ \frac{\partial V}{\partial y} \\ \frac{\partial U}{\partial y} + \frac{V}{x} \end{Bmatrix} + Z \begin{Bmatrix} -\frac{\partial^2 W}{\partial x^2} \\ -\frac{\partial^2 W}{\partial y^2} \\ -\frac{\partial^2 W}{\partial x \partial y} \end{Bmatrix} \tag{3.22}$$

where $\{\varepsilon\}_z$ represents the strain at depth z. Performing the operations outlined in section 3.4 and partitioning the following strain-displacement relation is obtained (Ref. 5).

$$\{\varepsilon\}_z = [Q_u][Cl_u]^{-1} \{\delta_u\}^e - z\,[Q_\phi][Cl_\phi]^{-1} \{\delta_\phi\}^e \qquad (3.23)$$

where

$$[Q_u] = [\Gamma_u]\,[P_u(x,y)]$$

$$[Q_\phi] = [\Gamma_\phi]\,[P_\phi(x,y)]$$

$[Cl_u]$ = $[P_u(xn, yn)]$ evaluated at xn, yn.

$[Cl\ ]$ = $[P_\phi(xn, yn)]$ evaluated at xn, yn

Using the notation of section 3.4 this reduces to:

$$\{\varepsilon\}_z = [B_u]\,\{\delta u\}^e + z\,[B_\phi]\,\{\delta_\phi\}^e \qquad (3.24)$$

3.5.3 Layering

Bending of the slab about both the longitudinal and transverse directions produces a continuously varying biaxial stress state with the concrete. Since the elasticity matrix, [D], is dependent upon the stress state, it too will vary throughout the finite element. To determine the plate element stiffness matrix as given in Eq. 3.7, integration must be performed over the volume of the element. Because of the complexities in explicitly defining the elasticity matrix for reinforced concrete under biaxial stress, the stiffness matrix is evaluated by performing numerical integration.

A slab finite element can be subdivided into a series of layers as shown in Fig. 11. Each layer can have its own elasticity matrix,

$[D_i]$, which depends upon the state of stress in the layer, $\{\bar{\sigma}_i\}$. This implies that each layer is in a constant state of assumed plane stress and stiffness, and that there is a step-like variation in the plane stress and stiffness through the depth of the finite element.

The state of stress for each layer is represented by the weighted average stress at the middle depth of the layer, which is defined as being a distance $\bar{z}_i$ from the reference plane of the slab. This average stress is calculated by multiplying the layer elasticity matrix times the integrated average strain vector at that depth:

$$\{\bar{\sigma}_i\} = [D_i]\ \{\bar{\varepsilon}_i\}_{zi} \tag{3.25}$$

The integrated average strain is found using Eq. 3.24 and integrating over the area of the element:

$$\{\bar{\varepsilon}\}_{zi} = \frac{1}{4ab}\left(\int\int [B_u]dx\ dy\ \{\delta_u\}^e + \iint Z_i\ [B_\phi]\ dx\ dy\ \{\delta_\phi\}^e\right) \tag{3.26}$$

where

$\frac{1}{4ab}$ = area of element in x,y plane.

Combining Eqs. 3.25 and 3.26 yield:

$$\{\bar{\sigma}_i\} = \frac{[D_i]}{4ab}\left(\int\int [B_u]\ dx\ dy\ \{\delta_u\}^e + Z_i\int\int [B_\phi]\ dx\ dy\ \{\delta_\phi\}^e\right) \tag{3.27}$$

Because the elasticity matrix, $[D_i]$, is dependent upon the stress, $\{\bar{\sigma}_i\}$, and visa versa an iterative solution technique is required, as discussed in Section 3.8.

The steel reinforcing bars are idealized as a layer of steel of equivalent thickness with uniaxial stiffness properties, and these layers are included in the integration processes in the same manner as the concrete layers. The direction in which the uniaxial stiffness acts is specific with respect to the angle it makes with respect to the x axis. The steel layer is located at the center of gravity of the reinforcement, and the equivalent thickness is calculated by:

$$t_s = \frac{A_s}{b_s} \tag{3.28}$$

where A_s indicates the area of a bar and b_s is the bar spacing.

The progression of cracking and crushing of concrete and yielding of steel through the depth of the slab can be monitored by maintaining a stress history of each layer. The angle of crushing or cracking of any one layer is in no way predefined by previous cracking and crushing of another layer, and thus the pattern can vary from one layer to the next throughout the depth of the slab.

3.5.4 Element Stiffness Matrix

The element stiffness matrix was previously defined as

$$[k]^e \int_v [B]^T [D] [B] \, dv \tag{3.7}$$

in which the matrix [B] relates the strains to the displacements. If the

matrix [B] is partitioned as in Eq. 3.23, then the element stiffness can be rewritten as:

$$[k]^e = \int_v \begin{bmatrix} [B_u]^T \\ \\ Z[B_\phi]^T \end{bmatrix} [D] \quad \left[[B_u] \; Z \; [B_\phi] \right] \quad dv \tag{3.29a}$$

or multiplying out

$$[k]^e = \int_v \left[\begin{array}{c|c} [B_u]^T [D] [B_u] & Z [B_u]^T [D] [B_\phi] \\ \hline Z[B_\phi]^T [D] [B_u] & Z^2 [B_\phi]^T [D] [B_\phi] \end{array}\right] dv \tag{3.29b}$$

For simplicity the following definitions are made:

$$[k_{uu}]^e = \int_v [B_u]^T [D] [B_u] \, dv$$

$$[k_{u\phi}]^e = [K_{\phi u}]^{e^T} = \int_v Z [B_u]^T [D] [B_\phi] \, dv \tag{3.30a}$$

$$[k_{\phi\phi}]^e = \int_v Z^2 [B_\phi]^T [D] [B_\phi] \, dv$$

Therefore the element stiffness matrix can be written as:

$$[k]^e = \left[\begin{array}{c|c} [k_{uu}]^e & [k_{u\phi}]^e \\ \hline [k_{u\phi}]^{eT} & [k_{\phi\phi}]^e \end{array}\right] \tag{3.31}$$

Where $[k_{uu}]^e$ is the in-plane stiffness matrix, which relates in-plane forces and displacements. $[k_{\phi\phi}]^e$ is the bending stiffness matrix which relates bending forces and displacements. The $[k_{u\phi}]^e$ and $[k_{\phi u}]^e$ are the coupling stiffness matrices which inter-relate bending and in-plane action (Ref. 40).

Noting from earlier discussions that the elasticity matrix [D] is dependent only on z and the matrices $[B_u]$ and $[B_\phi]$ are dependent only on x and y, Eqs. 3.30 can be rewritten as:

$$[k_{uu}]^e = \int_x \int_y [B_u]^T \left(\int_z [D]dz \right) [B_u]\, dx\, dy$$

$$[k_{u\phi}]^e = \int_x \int_y [B_u]^T \left(\int_z Z\,[D]dz \right) [B_\phi]\, dx\, dy \tag{3.30b}$$

$$[k_{\phi\phi}]^e = \int_x \int_y [B_{\phi\phi}]^T \left(\int_z Z^2[D]dz \right) [B_\phi]\, dx\, dy$$

Performing numerical integration of the quantities in parenthesis gives:

$$[D_{uu}] = \int_z [D]dz = \sum_{i+1}^{L} [D_i] (Z_{i+1} - Z_i)$$

$$[D_{u\phi}] = \int_z Z[D]dz = \sum_{i+1}^{L} [D_i] (Z_{i+1} - Z_i)^2 \qquad (3.32)$$

$$[D_{\phi\phi}] = \int_z Z^2[D]dz = \sum_{i+1}^{L} [D_i] (Z_{i+1} - Z_i)^3$$

Where the sumation is over all of the layers, and Z_{i+1} and Z_i are the Z distances to the top and bottom of layer i.

Substituting Eqs. 3.32 into Eqs. 3.31 yields:

$$[k_{uu}]^e = \int_x \int_y [B_u]^T [D_{uu}] [B_u] \, dx \, dy$$

$$[k_{u\phi}]^e = \int_x \int_y [E_u]^T [D_{u\phi}] [B_\phi] \, dx \, dy \qquad (3.33)$$

$$[k_{\phi\phi}]^e = \int_x \int_y [B_\phi]^T [D_{\phi\phi}] [B_\phi] \, dx \, dy$$

Thus, performing the integration over the element area will give the slab element stiffness matrix.

In Appendix A of Ref. 5 the slab element stiffness matrix formulation is presented in detail, with all components of each matrix leading up to Eq. 3.33 and all integrations were performed. However, the submatrices in Eqs. 3.33 are left as a series of matrix operations to be performed by the computer. To reduce computation costs, time and increase efficiency considerable effort has been made to perform all those matrix multiplications by hand, so that in the end the formation of the slab element matrix requires only direct substitution of the parameters. In Appendix A of this report the resulting 20 by 20 stiffness matrix is presented. A comparison of the previous matrix multiplication method and the present method show a reduction in element formulation time of 1/100, and since element formulation is a large percentage of the total computation time, the value of this new formulation becomes immediately apparent.

3.6 Layered Beam Element

The theoretical development for an elastic composite finite element hereafter referred to as the Tumminelli-Kostem element, consisting of a concrete slab on top and a steel beam on the bottom, is presented in detail in Ref. 5. This sophisticated element can include the effects of slip between the bridge deck and the beam, shear deformations in the beam and shear lag in the deck. Since the goal of the present research is to develop a model to predict the inelastic behavior of highway bridges, some alterations and refinements of the Tumminelli-Kostem element must be made to model inelastic behavior.

Since the displacement fields defining the elastic plate portion of the Tumminelli-Kostem element are identical to those already presented to describe the inelastic layered slab element, the element stiffness matrices just developed to model inelastic slab behavior can replace the Tumminelli-Kostem plate element without any complications. Therefore, the major thrust of the discussions to follow is concerned with the beam portion of the Tumminelli-Kostem element. Figure 13 shows the typical arrangement of beam and plate nodes, and Fig. 14 defines the node deformations and sign conventions. It should be noted that the vertical displacement field for the beam and plate is the same, but that the respective axial displacement and rotation fields are different.

All deformations are written at the reference planes of the slab and beam.

3.6.1 Composite Displacement Fields

The Tumminelli-Kostem element was derived considering the combined action of the beam and slab as a unit. After establishing the coefficient displacement matrix, however, the element development was divided into four separate components by partitioning the coefficient-displacement matrix. As will be shown this allows for the separate consideration of the beam and plate stiffness matrices.

The vertical displacement field (W) used, following the assumptions of Section 3.2, is:

$$W = \bar{a}_1 + \bar{a}_2 x + \bar{a}_3 x^2 + \bar{a}_4 x^3 \qquad (3.34)$$

This is simply Eq. 3.15 with y held constant. The vertical displacement for the slab and the beam is assumed to be the same. In order to permit slip to occur between the beam and the slab the axial deformation for each must be different.

$$U_A = b_1 + b_2x + b_3x^2 \tag{3.35a}$$

$$U_B = c_1 + c_2x + c_3x^2 \tag{3.35b}$$

The first equation for the axial deformation of the slab is simply Eq. 3.16a with y held constant. To include the effects of shear deformation, a separated rotation field for the beam and slab must exist because the slope of the deformed beam ($\frac{dw}{dx}$) is not equal to the rotation (θ) (Ref. 5). The rotation of the slab will be given by the differentiation of the vertical displacement Eq. 3.34 with respect to x, and the rotation of the beam will be given by:

$$\theta_B = d_1 + d_2x + d_3x^2 \tag{3.35c}$$

Enforcing compatibility between the node displacements and the displacement fields and noting the $\theta = -\frac{dw}{dx}$ generates the [C1] matrix of Eq. 3.9:

$$\{\delta\}^e = [C1]\ \{\alpha\}$$

or

$$
\begin{Bmatrix} U_{LA} \\ U_{LB} \\ W_L \\ \theta_{LA} \\ \theta_{LB} \\ U_{MA} \\ U_{MB} \\ W_M \\ \theta_{MA} \\ \theta_{MB} \end{Bmatrix} =
\begin{bmatrix}
1 & 0 & 0 & 0 & 0 & 0 & 0 & 0 & 0 & 0 & 0 & 0 & 0 \\
0 & 0 & 0 & 1 & 0 & 0 & 0 & 0 & 0 & 0 & 0 & 0 & 0 \\
0 & 0 & 0 & 0 & 0 & 0 & 1 & 0 & 0 & 0 & 0 & 0 & 0 \\
0 & 0 & 0 & 0 & 0 & 0 & 0 & -1 & 0 & 0 & 0 & 0 & 0 \\
0 & 0 & 0 & 0 & 0 & 0 & 0 & 0 & 0 & 0 & -1 & 0 & 0 \\
1 & L & L^2 & 0 & 0 & 0 & 0 & 0 & 0 & 0 & 0 & 0 & 0 \\
0 & 0 & 0 & 1 & L & L^2 & 0 & 0 & 0 & 0 & 0 & 0 & 0 \\
0 & 0 & 0 & 0 & 0 & 0 & 1 & L & L^2 & L^3 & 0 & 0 & 0 \\
0 & 0 & 0 & 0 & 0 & 0 & 0 & -1 & -2L^2 & -3L^2 & 0 & 0 & 0 \\
0 & 0 & 0 & 0 & 0 & 0 & 0 & 0 & 0 & 0 & -1 & -L & -L^2
\end{bmatrix}
\begin{Bmatrix} b_1 \\ b_2 \\ b_3 \\ c_1 \\ c_2 \\ c_3 \\ a_1 \\ a_2 \\ a_3 \\ a_4 \\ d_1 \\ d_2 \\ d_3 \end{Bmatrix}
\tag{3.36}
$$

The sign conventions for node displacements and internal displacement fields are shown in Fig. 14.

There are ten node displacements and thirteen coefficients, therefore, three more equations must be established. Considering the equilibrium of the axial forces and the interface shear flow results in the equations (Fig. 15).

$$\frac{dN_A}{dx} = + s \tag{3.37a}$$

and

$$\frac{dN_B}{dx} = - s \tag{3.37b}$$

where

N_A = axial force in plate

N_B = axial force in beam

s = interface shear flow.

The axial force N_A can be found by integrating the axial stress over the area of plate:

$$N_A = \int_A \sigma_{xA}\, dA = \int_A \varepsilon_{xA}\, E_A\, dA = \int_A E_A \left(\frac{dU_A}{dx^2} - Z \frac{d^2W}{dx^2} \right) dA \tag{3.38}$$

Substituting for U_A and W interms of the polynomial and differentiating N_A with respect to x yields:

$$\frac{dN_A}{dx} = E_A \int_A \left(\frac{d^2U_A}{dx^2} - Z \frac{d^3W}{dx^3} \right) dA = E_A \int_A (2\, \bar{b}_3 - Z\, 6\, \bar{a}_4)\, dA \tag{3.39}$$

Performing the required integration:

$$\frac{dN_A}{dx} = 2\, EA_A\, \bar{b}_3 - 6\, ES_A\, \bar{a}_4 \tag{3.40a}$$

where

$$EA_A = E_A \times \text{area plate}$$

and

$$ES_A = E_A \times \text{first moment of inertia of plate with respect to reference plane}$$

$$= 0 \text{ since reference plane is at mid-height}$$

Performing similar operations for the beam, but noting that the axial strain is computed using θ_B and not $\frac{dW}{dx}$ gives:

$$\frac{dN_B}{dx} = 2\ E\ A_B\ c_3 - 2\ E\ S_B\ d_3 \tag{3.40b}$$

Setting Eqs. 3.40 equal to zero provides the first two of the three required equations. Even though the interface shear has been set to zero, no accuracy is lost in the final solution because the restrictions are made at the lowest level of element formulation. The interconnection between the beam and slab is accounted for later via the slip stiffness matrix (Ref. 5).

The last constraining equation is obtained by enforcing compatibility between the rotational fields. First, the shearing strain in the beam must be expressed in terms of the polynomial coefficients. Consider the equilibrium of an element of the beam (Fig. 16). In order to maintain generality, the interface shear flow (s) will not be set to zero until after equilibrium is established.

Summing the moments about point 0 (Fig. 16):

$$0 = S\ Z_{iB} + V_B\ dx + dM_B \tag{3.41a}$$

Substituting for s Eq. 3.37b and dividing through by dx yields the shear in the beam

$$V_B = \frac{d\ M_B}{dx} - Z_{iB}\ \frac{dN_B}{dx} \tag{3.41b}$$

The average shear strain can be expressed as

$$\gamma_B = \frac{V_B}{A_{SB}\ G_B} \tag{3.42}$$

where

A_{SB} = shear area of beam

G_B = shearing modulus of beam.

Now letting $\frac{dN_B}{dx}$ equal zero (i.e. s = 0) and finding the polynomial expression for:

$$\frac{dM_B}{dx} = \frac{d}{dx}\left(EI\ \frac{d\theta_B}{dx}\right) = EI_B\ (2d_3) \tag{3.43}$$

gives the shear strain in terms of the polynomial coefficients:

$$\gamma_B = \frac{2\ EI_B}{A_{SB}\ G_B}\ d_3 \tag{3.44}$$

where

EI_B = E_B x second moment of inertia of the beam about the reference plane of ence plane of beam.

Compatibility between the vert ical displacement field and the rotation field requires:

$$0 = -\frac{dW}{dx} + \theta_B + \gamma_B \tag{3.45a}$$

or, in terms of polynomial coefficients:

$$0 = -\bar{a}_2 - 2\bar{a}_3 - 3\bar{a}_4 x^2 + d_1 + d_2 x + d_3 x^2 - \frac{2\ EI_B}{A_{SB}\ G_B}\ d_3 \tag{3.45b}$$

Enforcing Eq. 3.45b for all possible values of x would yield too many constraining equations, but previous research shows that sufficient accuracy is obtained by enforcing compatibility at z = L/2 only:

$$0 = -\bar{a}_2 - L\bar{a}_3 - \frac{3}{4} L^2 \bar{a}_4 + d_1 + \frac{L}{2} d_2 + \left(\frac{L^2}{4} - \frac{2\ EI_B}{A_{SB}\ G_B}\right) d_3 \tag{3.46}$$

Combining the three constraining equations into matrix form yields the [C2] matrix of Eq. 3.9:

$$\begin{Bmatrix} 0 \\ 0 \\ 0 \end{Bmatrix} = \begin{bmatrix} 0 & 0 & 2EA_A & 0 & 0 & 0 & 0 & 0 & 0 & 0 & 0 & 0 & 0 & 0 \\ 0 & 0 & 0 & 0 & 0 & 2EA_B & 0 & 0 & 0 & 0 & 0 & 0 & 0 & -2ES_B \\ 0 & 0 & 0 & 0 & 0 & 0 & 0 & -1 & -L & -\frac{3L^2}{4} & 1 & \frac{L}{2} & \left(\frac{L^2}{4} - \frac{2EI_B}{A_{SB}\ G_B}\right) & \end{bmatrix} \{\alpha\} \tag{3.47}$$

Combining Eq. 3.36 and Eq. 3.37 gives the [C] matrix of Eq. 3.9 which is solved to give the [CC] matrix indicated in Eq. 3.11 where [CC] consists of the first ten columns of $[C]^{-1}$:

$$
\begin{Bmatrix} \bar{b}_1 \\ \bar{b}_2 \\ \bar{b}_3 \\ c_1 \\ c_2 \\ c_3 \\ \bar{a}_1 \\ \bar{a}_2 \\ \bar{a}_3 \\ \bar{a}_4 \\ d_1 \\ d_2 \\ d_3 \end{Bmatrix} =
\begin{bmatrix}
1 & 0 & 0 & 0 & 0 & 0 & 0 & 0 & 0 & 0 \\
-\frac{1}{L} & 0 & 0 & 0 & 0 & \frac{1}{L} & 0 & 0 & 0 & 0 \\
0 & 0 & 0 & 0 & 0 & 0 & 0 & 0 & 0 & 0 \\
0 & 1 & 0 & 0 & 0 & 0 & 0 & 0 & 0 & 0 \\
0 & -\frac{1}{L} & -\frac{3\bar{Z}_B J1}{2} & \frac{\bar{Z}_B J1L}{4} & \frac{\bar{Z}_B J1L}{2} & 0 & \frac{1}{L} & \frac{3\bar{Z}_B J1}{2} & \frac{\bar{Z}_B J1L}{4} & \frac{\bar{Z}_B J1L}{2} \\
0 & 0 & \frac{3\bar{Z}_B J1}{2L} & -\frac{\bar{Z}_B J1}{4} & -\frac{\bar{Z}_B J1}{2} & 0 & 0 & -\frac{3\bar{Z}_B J1}{2L} & -\frac{\bar{Z}_B J1}{4} & -\frac{\bar{Z}\ J1}{2} \\
0 & 0 & 1 & 0 & 0 & 0 & 0 & 0 & 0 & 0 \\
0 & 0 & 0 & -1 & 0 & 0 & 0 & 0 & 0 & 0 \\
0 & 0 & -\frac{3}{L^2} & \frac{2}{L} & 0 & 0 & 0 & \frac{3}{L^2} & \frac{1}{L} & 0 \\
0 & 0 & \frac{2}{L^3} & -\frac{1}{L^2} & 0 & 0 & 0 & -\frac{2}{L^3} & -\frac{1}{L^2} & 0 \\
0 & 0 & 0 & 0 & -1 & 0 & 0 & 0 & 0 & 0 \\
0 & 0 & -\frac{3J1}{2} & \frac{J1L}{4} & (\frac{1}{L}+\frac{J1L}{2}) & 0 & 0 & \frac{3J1}{2} & \frac{J1L}{4} & (-\frac{1}{L}+\frac{J1L}{2}) \\
0 & 0 & \frac{3J1}{2L} & \frac{J1}{4} & \frac{J1}{2} & 0 & 0 & -\frac{3J1}{2L} & -\frac{J1}{4} & -\frac{J1}{2}
\end{bmatrix}
\begin{Bmatrix} U_{LA} \\ U_{LB} \\ W_L \\ \theta_{LA} \\ \theta_{LB} \\ U_{MA} \\ U_{MB} \\ W_M \\ \theta_{MA} \\ \theta_{MB} \end{Bmatrix}
\tag{3.48}
$$

where

$$J1 = \frac{4A_{SB}\ G_B}{L^2\ A_{SB}\ G_B + 8EI_B}$$

The [CC] matrix is then partitioned to handle the displacement fields separately:

$$[CC] = \begin{bmatrix} CA \\ --- \\ CB \\ --- \\ CW \\ --- \\ CD \end{bmatrix} \tag{3.49}$$

where [CA], [CB], [CW] and [CD] are coefficient-displacement matrices for the U_A, U_B, W and θ_B fields respectively.

The internal work of the element consists of four separate and uncoupled components. The first two are the work due to axial stresses and strains of the plate and the beam, the third is the work due to shear stresses and strains in the beam, and the fourth is the work due to the shear flow and slip at the interface. Therefore, the element stiffness matrix can be formed as:

$$[k]^e = [k_A]_b + [k_B]_b + [k_B]_s + [k]_d \tag{3.50}$$

where $[k_A]_b$, $[k_B]_b$, $[k_B]_s$, and $[k]_d$ are the portions of the element stiffness matrix resulting from the consideration of the internal work due to axial stresses and strains in the plate, axial stresses and strains

in the beam, shear stresses and strains in the beam, and shear flow and slip at the interface.

Up to this point in the derivation we have ignored the contribution of the strain (ε_y) in the y direction of the plate and the shearing strain (γ_{xy}) in the plate. However, as pointed out by Tumminelli and Kostem, using the plate element presented in Section 3.5, the beam and plate elements are of compatible displacement fields, and thus these added degrees of freedom do not alter the relations just developed. Thus, the plate element stiffness matrix developed in Section 3.5 with twenty degrees of freedom, will take the place of the $[k_A]_b$ matrix.

Performing the required operations on the displacement fields indicated by $[\Gamma]$ in Eq. 3.13a and substituting the coefficient-displacement matrices for $\{\alpha\}$ as in Eq. 3.13b results in the remaining strain-displacement matrices. Axial strain in the beam:

$$\varepsilon_{xB} = \frac{dU_B}{dx} - Z \frac{d\theta_B}{dx} \tag{3.51a}$$

therefore

$$\varepsilon_{xB} = [[0\ 1\ 2x]\ [CB] - Z\ [0\ 1\ 2x]\ [CD]]\ \{\delta\}^e \tag{3.51b}$$

or

$$\varepsilon_{xB} = [B_B]_b\ \{\delta\}^e \tag{3.51c}$$

Shear strain in the beam

$$\gamma_B = \frac{dW}{dx} - \theta_B \tag{3.52a}$$

therefore

$$\gamma_B = [[0\ 1\ 2x\ 3x^2]\ [CW] - [1\ x\ x^2]\ [CD]]\ \{\delta\}^e \qquad (3.52b)$$

or

$$\gamma_B = [B_B]_S\ \{\delta\}^e \qquad (3.52c)$$

Slip at the interface

$$\delta U = (U_A - Z_{iA}\frac{dW}{dx}) - (U_B - Z_{iB}\ \theta_B) \qquad (3.53a)$$

therefore

$$\delta U = [1\ x\ x^2 - 1 - x - x^2\ 0 - Z_{iA} - 2Z_{iA}\ x$$

$$- 3Z_{iA}\ x^2 \quad Z_{iB} \quad Z_{iB}x \quad Z_{iB}x^2]\ [CC]\ \{\delta\}^e \qquad (3.53b)$$

or

$$\delta_U = [xU]\ [CC]\ \{\delta\}^e = [B]_d\ \{\delta\}^e \qquad (3.53c)$$

Forming the expressions for the internal work as in Eq. 3.7a results in the component stiffness matrices of Eq. 3.50:

$$[k_B]_b = \int_v [B_B]_b^T\ [E_B]\ [B_B]_b\ dV \qquad (3.54)$$

$$[k_B]_s = \int_v [B_B]_s^T\ [G_B]\ [B_B]_s\ dV \qquad (3.55)$$

$$[k]_d = \int_L [B]_d^T\ [k_{sc}]\ [B]_d\ dx \qquad (3.56)$$

where

k_{sc} = the stiffness of the uniform connection used to mathematically describe the shear connectors.

It should be noted that k_{sc} values have not been as yet directly related to the number shear connector or their arrangement, but that there does exist an upper bound to k_{sc} to insure composite action.

$$k_{max} = \frac{10}{L^2} \left\{ EA_A \, (C_E^2) + EA_B \, (1 - 2C_E + C_E^2) \right\} \qquad (3.57)$$

where

$$C_E = \frac{1}{EA_A/EA_B + 1}$$

L = length of element

The matrices developed above are presented explicitly in Appendix B. The $[k_B]_b$, $[k_B]_s$ and $[k]_d$ matrices are added together to form the beam stiffness matrix, and this in turn would be added to the plate stiffness matrices according to Eq. 3.2 to result in a total structural stiffness matrix for the solution of Eq. 3.1.

3.6.2 Layering

As with the slab finite element, the beam finite element is subdivided into a series of layers as shown in Fig. 5. Each layer will have its own elasticity $[E]_i$, which depends upon the state of stress in the layer, $(\sigma_x)_i$. For the beam, each layer is assumed to be in a state of

uniform uniaxial stress, and thus there exists a step-like variation in stress through the depth of the element. The state of stress for each layer is represented by the stress at the mid-depth of the layer.

Referring to the element stiffness matrices present in Appendix B, there exist four terms which are related to the elasticity of the element: EA_B, ES_B, EI_B and GA_{SB}. First it is assumed that the shearing modulus, G, is related to E by:

$$G = \frac{E}{2\ (1 + \nu)} \tag{3.58}$$

The four terms above are then calculated in the following manner:

$$EA_B = \sum_{i=1}^{n} E_i\ A_i \tag{3.59a}$$

$$ES_B = \sum_{i=1}^{n} E_i\ A_i\ Z_i \tag{3.59b}$$

$$EI_B = \sum_{i=1}^{n} E_i\ (I_i + A_i\ Z_i^2) \tag{3.59c}$$

$$GA_{SB} = \frac{1}{2\ (1 + \nu)} \sum_{i=1}^{n} E_i\ A_{SBi} \tag{3.59d}$$

where

E_i = the instantaneous slope of stress-strain curve of layer i

A_i = the area of layer i

Z_i = the distance from reference plane to layer i centroid

I_i = the moment of inertia of layer i about its centroid

A_{SBi} = the shear area of layer i.

Thus, once the rigidity, E_i, of the layer is established the element and, ultimately, the layer stress can be calculated. However, since the elasticity, E_i, is dependent upon the stress level, an iterative process is required.

3.7 Unloading of Cracked or Crushed Concrete

As was noted in Section 2.2.8 when a concrete layer has cracked or crushed, the layer will be incapable of maintaining the stress that caused the failure. The stress within the layer in a direction perpendicular to the crack will be reduced to zero, and the overall internal stress field will be adjusted accordingly. In order to maintain equilibrium, however, a statically equivalent fictitious force vector must be applied to the structure to redistribute to stress loss due to failure. In Ref. 41 the equations for computing the required fictitious force vector are presented in detail; the reader need only be aware of the necessity of and not the specifics of the fictitious force vector to understand its contribution to the solution process.

3.8 Solution Scheme

The solution process consists of four main phases:

I Problem Definition

II Dead Load Solution

III Scaling Procedure

IV Overload Solution Procedure

A cursory explanation of each of the phases enumerated above is presented in the following paragraphs:

I Problem Definition - In this phase the particular problem to be solved is defined by supplying the following data:

A. Bridge Superstructure Geometry - The bridge is discretized into layered beam and slab finite elements.

B. Material Properties - All the beam and slab material properties and stress-strain parameters are defined.

C. Loading - The dead loads and live loads are specified.

D. Boundary Conditions - The appropriate displacement boundary conditions for the node points must be used to model the actual structure, employing where needed any lines of symmetry in this consideration.

II Dead Load Solution - Due to the nonlinear behavior of the overload problem, the initial stress state due to dead loads cannot be superimposed on a separate overload solution. The dead load solution must be performed first to obtain an initial stress state to which the stresses due to the overload are then applied, as would be the actual case. The initial dead load solution, reflecting the dead weight of the slab and beams, is performed assuming only the beams to be acting. If, after the concrete is hardened, additional dead loads due to parapets or curbs are added to the structure, a second dead load solution is performed on the composite structure.

III Scaling Procedure - The scaling procedure modifies the initial live load solution so as to increase load to load level just below which the first crushing or cracking of concrete or yielding of steel occurs. This technique eliminates any excessive number of live load solutions in the elastic range. At the same time if the initial live load is above the first material failure load, the solution scheme begins at a live load of zero.

IV Overload Procedure - The structural response to an overload vehicle is obtained by solving the set of equilibrium equations presented by:

$$\{F\} = [K]\ \{\delta\} \tag{3.1}$$

However, because the behavior to be analyzed is nonlinear in nature, a piecewise or increment approach must be employed. Expressing Eq. 3.1 in incremental form yields:

$$\{\dot{F}\} = [K\ (\sigma + \dot{\sigma})]\ \{\dot{\delta}\} \tag{3.60}$$

where [K] is dependent upon the current total stress and an unknown stress increment. In addition, $\{\dot{F}\}$ is the applied force increment and $\{\dot{\delta}\}$ is the resulting displacement increment. Because the unknown stress increment is dependent upon the stiffness and the stiffness is dependent upon the stress increment, conventional linear elastic solution techniques cannot be employed.

Using a tangent stiffness approach to the solution of the overload problem, the system of equations given by Eq. 3.60 is assumed to be linear in a given load increment. Then at the beginning of each load increment or step, the tangent to the stress-strain curve, based on the current stress level, is used for each layer in computing the element stiffness and ultimately the global stiffness matrix. Equation 3.60 is then solved for the node point displacements, and using the strain-displacement and stress-strain relations, the incremental stresses are calculated. New stiffness matrices are recomputed using the new increments of stress and the procedure is repeated to obtain a second set of node point displacements. Since nonlinear behavior in the form of cracking or crushing of concrete and yielding of steel will be taking place in each load step, the initial displacement and second set of

displacements will not match. Thus the entire process must be repeated until the difference between the displacements of any two cycles converges to within a certain tolerance. When this iteration scheme is employed, the analytical technique is labeled as the "incremental-iterative" method. As an approximation the iterative process could be eliminated leaving simply an "incremental" method, but because at the end of the first load cycle some error exists due to the failure to update the stiffness matrix, any succeeding load will only compound the error. Thus, the "incremental" method generally will produce unreliable results.

Flow charts descibing the basic operations for both the incremental and incremental-iterative solution techniques, as well as in-depth descriptions of each of the key steps of the two methods, are presented in Ref. 41.

4. Experimental Correlation

4.1 Introduction

In order to verify the validity of the analysis technique and the finite element model comparisons must be made between analytically produced results and data obtained from experimental testing. A total of four concrete slab and steel beam structures, which were previously subjected to overload testing and reported on in the available literature, were analyzed by the nonlinear finite element method presented in this report. Two of the tests were conducted on full scale bridge superstructures, while the remaining tests were performed on scale models. This report is concerned with the comparison of the overall elastic and inelastic behavior of the above mentioned highway bridge structures or models. The development and verification of the layered slab model and the Tumminelli-Kostem elastic composite element have been presented elsewhere (Refs. 39 and 49).

4.2 Steel Beam and Concrete Slab Highway Bridge Superstructures

A comparison of experimental and analytical results for four test cases listed below has been made:

No. 1: A simply supported right bridge with a span length of 50' and a width of 15' having three W18 x 60 steel beams with partial length coverplates (Bridge 3B of Refs. 22 and 23)

No. 2: A four span continuous right bridge with span length of 70', 90', 90' and 70' and a width of 34'-6" and having four

W36 x 170 steel beams with W36 x 160 with coverplates over the piers. (Bridge 1, Test - 1300 of Refs.10 and 13)

No. 3: A two span continuous right bridge model with two span lengths of 9' and a width of 5'-3", with three S6 x 12.5 steel beams and partial length coverplates. (Two span model of Refs.8, 17 and 21)

No. 4: A three span continuous right bridge model with three span lengths of 6' and a width of 5'-3" with three S5 x 10 steel beams and partial length coverplates. (Three span model of Refs. 8, 17 and 21)

4.2.1 Example No. 1

This bridge was constructed as part of the AASHTO Road Test conducted in the early 1960's (Refs. 22 and 23). The testing consisted of three phases: (1) a regular test traffic program of 500,000 trips, (2) dynamic load tests, and (3) increasing load tests, i.e. overload tests. Bridge 3B was designed as a simply supported composite slab and steel girder bridge with a span length of 50 ft. center-to-center of bearing. The deck slab for the bridge had an average measured depth of 6.45 in. and was 15 ft. wide. Three W18 x 60 steel beams were placed 5 ft. apart and 7/16 in. by 6 in. coverplates extended over 18'-6" of the middle of the span. Figs. 17 and 18 show the shape of the cross section including dimensions and reinforcement details.

The loads were applied to the superstructure by moving overload

vehicles. For the testing of Bridge 3B three different overload vehicles were used (vehicles 97, 98 and 99 as shown in Fig. 19). The loading procedure consisted of placing weights on the overload vehicle which would then travel across the bridge, usually thirty times. During the loading process the midspan deflections of each beam were monitored and recorded. The load was then increased and another set of runs made. The procedure was continued until the bridge superstructure collapsed onto the safety crib below the bridge superstructure.

Because the loads were not applied in a static manner but by moving vehicles, the moment envelope produced by the passage of the overload vehicle is of interest. Since the finite element program requires a static loading pattern which will then be incremented, some equivalent static loading pattern would correspond to a realistic simulation. In addition, because three different overload vehicles were used, three different moment envelopes must be simulated by one constant loading pattern. Based upon previous experience and numerical computations, the moment envelope could be best simulated by a line load (Ref. 42).

Figure 20 shows the superstructure discretized into a series of finite elements. The node points, element numbering, and element dimensions are indicated in the figure. Since the structure was assumed to be symmetric in geometry and loading, only one-quarter of the structure need be analyzed. A total of eighteen slab elements and twelve beam elements were used. It should be noted that because a line of symmetry lies along the axis of the interior beam, only one-half of the interior beam cross-section is included in the model. The line load was simulated by a series of

concentrated loads indicated by the cross-hatched squares.

The layered slab and beam models are shown in Fig. 21. A total of six layers of concrete and four layers of steel reinforcement were used in the slab finite element. The direction of action of the reinforcement is indicated by the cross-hatched area and is given along with the thickness, and bar size/spacing in Table 1A. The beam finite element consists of a total of ten layers as indicated. The cross-hatched layer, which represents the coverplate, has two sets of material properties. In the region where there is no coverplate in the actual structure, the material properties are set to artificially low values to simulate the "nonexistence" of the coverplate. In the area where there is a coverplate the properties of steel were used.

In Table 2 are presented the material properties of the steel and concrete used in Bridge 3B, and the corresponding material properties used in the finite element simulation. The Ramberg-Osgood curve parameters are also specified for each material.

At the end of the regular test traffic program one of the three beams of Bridge 3B was discovered to have a fatigue crack at the end of the coverplate. Even so, it was determined that the small permanent set of the bridge at that stage was due to cracking and crushing of the concrete slab, and the fatigue crack had no effect on the stiffness of the bridge. During the overload procedure the fatigue crack was repaired with a butt weld in order to prevent premature failure.

The bridge failed in a flexure mode and in Ref. 23 the overload behavior of the bridge is presented in terms of a plot of the maximum static

moment in midspan caused by the overload vehicle versus the average displacement at midspan of the three beams. Figure 22 shows the midspan moment displacement history of the bridge. The analytical results of program BOVAS and the test results are represented by the (□) and (○) symbols as noted. As can be observed from the plots, the results produced by the two methods agree relatively well, especially at the beginning, and from a deflection of 4 inches (1/150 deflection to span ratio) to about 10 inches (1/60 deflection to span ratio). The main discrepancies between test results and the calculated response occur within two regions: first, from approximately 1.3 inches to 4.0 inches deflection, and secondly, from about 10 inches in deflection to the termination of the test.

Some difference between test results and computed results is to be expected because the loads were applied to the test structure by three different overload vehicles in motion and the finite element program applied an approximate equivalent static loading pattern in an incremental fashion. In addition, as with any finite element model, there exists the effect of the size of the discretization used. However, in the second region of disagreement the difference in maximum loads is only around seven percent and thus within acceptable modelling limits. A considerable improvement can be made in the modelling scheme if the effects of residual stresses in the steel beams are included. Residual stress measurements in the beams were made and reported on in Ref. 22. Assuming a parabolic distribution of residual stresses in both the flanges and the web, an average value of residual stress in each of these parts of the cross section is calculated. Using these values of residual stress as initial stress values in the beams and

repeating the finite element analysis, much better agreement with test results is obtained, as indicated on Fig. 22.

A qualitative description of the extent of damage at different load levels, as reported in Ref. 23, is compared to damage as predicted by program BOVAS in Table 3. In general the damage record shows that the method of failure and the loads at which different types of structural damage occurred can be predicted by program BOVAS.

4.2.2 Example No. 2

This bridge was one of four bridges which were to be inundated as part of a reservoir in Tennessee (Ref. 10). Bridge 1, referred to as such by the experimental researchers, was a four span continuous composite structure with span lengths of 70', 90', 90', and 70'. It was constructed in 1963 and designed for HS-20 loading. The deck slab was 7 inches deep and was 34'-6" wide, including the curb (Fig. 23). For the finite element analysis the curb portion of the superstructure was considered to be in the same plane and of the same thickness as the slab. A total of four W36 x 170 steel beams was used to support the deck with 8'-4" spacing center-to-center between the beam. In the negative moment regions there were W36 x 160 steel beams with 10½" by 1" coverplates. A plan view of the superstructure and the location of the applied loads and points where readings were taken are shown in Fig. 24.

The loads were applied to the bridge deck by 200 kip center hole jacks resting on bearing grills. The bearing grills were constructed from two W14 x 30 steel beams 46 in. long and 30 in. center-to-center, and resting on

concrete pads poured directly on the bridge deck. The location of the grills is shown in Fig. 25 by cross-hatched areas.

Due to the symmetry of the loads only one half the structure needs to be discretized. The node points, element numbering, and element dimensions of the discretized structure are indicated in Fig. 25. The cross hatched areas represent the location of the patch loads that must be applied to the idealized structure. A total of 42 slab finite elements and 28 beam elements were used, resulting in 90 nodes and 360 degrees of freedom. The area of main structural interest was that portion of the bridge near the midspan of the loaded span; therefore, the element discretization is finer in this region and much coarser in other spans. While the coarse discretization of the unloaded spans will be sufficient to model accurately the stiffness of the bridge, deflections and stresses in these regions will not be reliable because of the element size.

The layered slab and beam finite elements are shown in Fig. 26. A total of six layers of concrete and four layers of steel reinforcement were used. The direction of action of the slab reinforcement is perpendicular to the cross-hatched area and is specified, along with the thickness and bar size/spacing, in Table 1B. The exact reinforcement and pattern in the slab were not specified in Ref. 10, so a reinforcement distribution based upon the existing design practices was choosen. The beam finite element consists of ten layers as indicated. Because the length of the cover-plated sections was not specified, the same beam element was used throughout.

In Table IV the actual material properties of the steel and concrete used in Bridge 1 and the material properties and parameters assumed for the

finite element analysis are listed.

Bridge 1 was described as being "structurally sound" prior to the beginning of the experimental tests (Refs. 10 and 13). The bridge had been in service for approximately five years and prior to the testing the average daily traffic was 600 vehicles per day. Before the ultimate load test was conducted, other load tests involving lateral load distribution studies and dynamic response studies to rolling and vibratory loading were carried out. References 10 and 13 contain all the information concerning the results of these other tests.

A plot of the load and corresponding average deflection at the midspan of the loaded span is presented in Fig. 27 for both the analytical (+) and experimental (*) results. In general, the two curves are in close agreement except in the range of about five inches (1/216 deflection to span ratio) to thirteen inches (1/83 deflection to span ratio) deflection. However, even in this range the maximum difference in load is only five percent.

Qualitative bridge damage, as reported in Refs. 10 and 13, is compared to damage as predicted by program BOVAS in Table 5. As can be seen, considerable difference can be observed between the first cracking loads for the experiment and the analytical predictions. This noteable difference is not all that distrubing if one evaluates all the facts. First, the real structure had coverplated sections over the piers, making the composite section in that area more resistant to cracking. Second, and most important, the finite element discretization in the region near the support piers is extremely coarse. This leads to poor element stress distribution and

therefore damage predictions. As mentioned before, however, the coarse discretization still produces reliable stiffness properties (i.e. overall load versus deflection results). Lastly, the visual observation of cracking in the slab does not give any quantitative information on the extent of cracking through the slab. The reported cracking thus may be either "surface deep" or halfway through the depth of the slab. Looking at other recorded damage the observation of first yield in the beams differs by only ten percent, and considering the qualitative nature of the observation, this is within acceptable limits.

As reported in Refs. 10 and 13, at a load just above first yielding the bridge "lifted off" the abutment nearest the load. The present version of the finite element model is not capable of simulating this behavior, but as indicated in Fig. 27 the experimental and analytical results are not very different. This is in part due to the fact that when the "lift off" occurred, the moment capacity of the composite section over the first pier had reached much of its capacity. Considering coarseness of the discretization, the leaving out of the coverplated sections, and the lifting off of the bridge from the abutment, the BOVAS results are remarkably good.

4.2.3 Examples No. 3 and No. 4

The testing of these two multispan concrete slab-steel beam highway bridge scale models was conducted at the University of Maryland as part of a research project in conjunction with the Maryland State Highway Administration and the Federal Highway Administration to ascertain

(1) distribution factors and (2) effective widths of composite bridges at ultimate load. The concrete slab used in both models measured 216 inches in length, 63 inches in width, and was 3 inches in thickness. Wire mesh reinforcement was placed at mid-depth in both slabs. The two span model consisted of three twenty-foot long S6 x 12.5 beams composed of A-36 steel and spaced 21 inches apart center-to-center. Over the interior support 5" x 3/8" x 5' coverplates were welded to the top and bottom flanges to provide negative moment resistance. The three span model consisted of three twenty-foot long S5 x 10 beams of A36 steel and spaced 21 inches apart center-to-center. Coverplates measuring 5" x 3/8" x 3' were welded on to the top and bottom flanges over the interior supports. In both models, headed, 1/2" x 2" shear studs were used in pairs spaced at six inches to insure full composite action. The total length of each of the models was eighteen feet. This means the two-span model had two nine foot span lengths and the three-span model had three six foot span lengths. Typical cross-sectional and elevation views of the two models are presented in Figures 28 and 29.

The loads were applied with a fifty ton hydraulic jack acting through a strain gage actuated load cell. For the two span model the load was centered directly over the interior girder and at mid-span of one of these spans (Fig. 29). In the ultimate load test for the three span model the load mechanism was centered directly over the middle beam and at mid-span of one of these spans (Fig. 29). Prior to the ultimate load test each of the models was loaded and unloaded several times in the elastic range to check out

the test set up and equipment. The load increment to failure in the ultimate load test was 2.5 kips and 5.0 kips for two span and three span models respectively.

Figures 30 and 32 show the respective finite element discretizations for the two span and three span models. The node point and element numbering and the element dimensions are indicated in each figure. Because of the inherent symmetry in these structures and their loading only one half of the two span and one quarter of the three span are required for the finite element analysis as shown. The two span model uses fifty-seven slab elements and thirty-eight beam elements with a total of 120 node points. The three span model has thirty slab elements and twenty beam elements with a total of 66 node points. The loaded area is indicated by the cross-hatched area (Figs. 30 and 32). As has been noted earlier, since the longitudinal axis of the center beam lies along a line of symmetry, only one half of the interior beam cross sectional properties is included in each model.

The layered slab and beam finite elements for the two span and three span models are shown in Figures 31 and 33 respectively. A total of six layers of concrete and two layers of wire mesh reinforcement were used in each slab finite element. The size of the actual reinforcement was 3" x 3" -6/8 for the two span model and 4" x 4" -4/4 for the three span model. The direction of action of the reinforcement is perpendicular to the cross-hatched area (Figs. 31 and 33), and this direction along with the layer thickness, wire size and spacing is given in Tables 4A and 4B. The beam finite elements consists of eleven layers as indicated (Figs. 31 and 33). The cross hatched layer corresponds to the coverplate; however, since the coverplate does

not run the full length of the beam, the material stiffness of the coverplate, in the regions in the actual structure where no plate exists, is set to an artificially low value to simulate this "nonexistence" of the coverplate. In all other regions the normal coverplate material stiffness properties were used.

In Table 7 the material properties of the steel and concrete in two-span and three-span models are reported (Ref. 8) and the corresponding material properties used in the finite element analysis. The Ramberg-Osgood parameters are also specified for each material.

The load versus deflection at midspan of the loaded span of the two span model is plotted for both the analytical and test results in Figure 34. Unlike similar plots for Examples 1 and 2, here there exists considerable differences in analytical and experimental results, even in the elastic range. The unexpected deviation in the elastic range is considerably unsettling in that in this range the previous results (Figs. 22 and 27) show excellent agreement in the elastic region with a maximum absolute difference of 3% between analytical and test results. For the two span model, however, the maximum absolute difference in this region is around 39% for the center beam. After a careful review of Reference 8, it was discovered that firstly, during the elastic loading and unloading of the two span model the deflection gages recorded a noticeable amount, about 0.007 inches of permanent set; thus, if this fact is not reflected in the ultimate load test results the deflections reported will all be shifted to the right. This is quite possible considering the noticeable kink in the test curve at 10 kips load. However, shifting the test curve to the left to account for the initial perman-

ent set would give an improvement of only 5% between the two curves. Secondly, it was noted in Reference 8 that "...noticeable support movement occurred at high loadings...". These support movements were measured and the reported deflections were "adjusted" to account for this occurence. However, past experience has indicated that in the conduct of a test, if the test frame and the loading devices move, even a minute amount, during the conduct of a test the establishment of an exact reference plane free of all movements cannot be easily undertaken without the inclusion of errors of unknown magnitude (Ref. 39). In this light if one looks carefully at the interior beam deflection curves starting at around a load of 10 kips and up to a load of around 40 kips, the two curves are almost parallel. In fact, moving the deflection at 10 kips for both the interior and exterior beam test results to agree with the analyticals shows very good agreement from 10 kips to 35 kips as seen in Fig. 35. Starting at around 35 kips load, however, the apparent failure of the exterior beam to take any more load in that there is no further deflection could account for the separation of the two curves for the interior beam. The behavior of the exterior beam would suggest that slab was completely cracked in the longitudinal direction and that the reinforcement was no longer capable of transmitting additional load. Because wire mesh reinforcement would have little bending stiffness once the slab was cracked, the excessive differential deflection between the two beams would cause the wire mesh to be subjected to bending in addition to just axial force effectively violating the assumptions of the finite element analysis. This additional bending stress would cause premature attainment of the ultimate load transmitted between the beams. The center and outside beams would then deviate from

expected as indicated by the test results. The ultimate load obtained during the test was 65 kips while BOVAS predicted an ultimate load of 57.9 kips. The fact that the experimental ultimate strength exceeded the program predicted would seem to contradict the statement just made concerning the dropping off of the experimental load versus deflection curve; however, BOVAS does not yet include the effects of strain hardening and this additional capacity might be attributed to this effect.

One other comparison was made with regards to the two span model. Based upon information provided by Tall and Beedle (Ref. 7) an estimation of the residual stresses present in the beams was made. Then the assumed parabolic distribution in the flanges and web was approximated by uniform average stresses in the flanges of 9.05 ksi and in the web of -18.66 ksi. The effect of the assumed residual stresses on the load versus deflection diagram of the interior beam is shown in Fig. 36. As can be seen, while the effect is clearly evident, no significant improvement in the results is obtained.

The load versus deflection diagram of the three span model is presented in Fig. 37. As with the two span model, there exists substantial differences between the analytical results and test results, even in the elastic range. While no unloading curves were presented for the three span model in Ref. 8, it would be logical to assume some small amount of permanent set occurred during the initial loadings. Support movements were again noted to have occurred and the reported results were "adjusted" to account for the support movements.

Thus, as with the two span model, there exists some question concerning the establishment of the true reference plane. Proceeding as with

the two span model, but setting, in this case, the test results at 20 kips equal to the analytical results and shifting the interior and exterior test curves left, gives Fig. 38. As can be observed, the analytical and test results are in very good agreement up to 55 kips for the exterior beam and up to about 50 kips for the interior beam. The deviation between the test results and BOVAS results starting at around 50 kips could again be attributed in part to the possible bending action of the mesh reinforcement. The ultimate test load obtained was 80 kips while BOVAS predicted a maximum load of 60.9 kips. More than likely the effects of strain hardening could not account for all of the difference between these maximum loads, but certainly it would account for some of the discrepency. Additional ultimate strength above that predicted by the finite element analysis and not due to strain hardening effect might be attributed to the conditions at the exterior supports of the unloaded spans. At these supports the girders were clamped to the supports to prevent uplift. Thus, the actual end condition might reflect a partially fixed support instead of a simple support, and obviously this type of support would create a larger ultimate load.

As with the two span model, an estimate of possible residual stresses was made. The analysis was reconducted with the residual stresses. This has resulted in a dip, or kink, in the inelastic curve similar to that in Fig. 22. However, as shown in Figs. 35 and 38, the results without assumed residual stresses are in good agreement with test results, thus one could assume the actual residual stresses are probably small and thus have little effect.

In view of the results presented above, and in particular in Figs. 35 and 38, sufficient evidence exists to indicate that the test results

and BOVAS results do in fact agree quite well up to about 60% of the ultimate test load for both the two span and three span models. Beyond that point possible reasons for the difference in the two results are presented above.

These reasons may or may not be totally correct. Since BOVAS performed quite well in the actual bridge tests of Examples 1 and 2, there exists sufficient reason to assume that the computer program is reliable in the inelastic range. Beyond 60% of the maximum test load, the behavior of the models probably does not reflect the actual behavior of real life loading conditions and real size bridge structures.

5. Summary, Conclusions and Other Considerations

5.1 Summary and Conclusions

This report presents a method for analyzing composite beam-slab type highway bridge superstructures subjected to overloads. The analytical technique employs a finite element method of structural analysis. The concrete slab and steel beams are discretized into a series of layered finite elements. The elements, and particularly the layers, provide a means to monitor the spread of cracking and crushing of concrete and yielding of steel throughout the bridge superstructure. In addition, the layering technique allows for the inclusion of inherent nonlinearities in material stress-strain curves and for the variation in material properties through the depth of the element.

The nonlinear and linear stress-strain behavior of the slab concrete is analytically described by empirically formulated biaxial stress-strain laws in terms of principal stresses and directions. In addition, the establishment of biaxial failure envelopes in terms of peak stress, peak strain, and peak modulus allows for the determination of the initiation of the failure of concrete by cracking and/or crushing of concrete. Elastic-plastic stress-strain behavior of slab reinforcement and of the beam steel is incorporated into the analysis scheme via nonlinear and linear uniaxial Ramsberg-Osgood stress-strain formulation.

The analysis technique utilized a linear tangent stiffness approach in which the solution corresponding to a particular load level is obtained by summing up the individual solutions obtained from a series of previous

load increments. Two different tangent stiffness methods of analysis have been presented: an incremental-iterative method and an incremental method. The incremental-iterative technique, which performs iterations and updates the tangent stiffness matrix within each load step, is the only method actually used in experimental comparisons because of its more reliable solutions. In the incremental method, no updating or iterations are performed in each load increment.

A total of four composite bridge type structures were investigated by comparing experimentally produced data and analytically produced results from the developed finite element model. In general, the layered finite element program was shown to be capable of reliably predicting the linearly elastic and inelastic behavior of simply supported or continuous composite slab-beam highway superstructures. In particular the analytical load (or moment) versus deformation diagrams were, for each case, in close agreement with the experimental results after all factors involved were included or accounted for. In addition, the progression of cracking and crushing of concrete and yielding of steel was dependably forecast by the developed analytical model.

The importance of including residual stresses in the beams is clearly evident in Example No. 1 and to a lesser extent in Examples No. 3 and 4. While limit data exists for predicting residual stresses without actually testing for them, even this limited data can produce results which show the importance of residual stresses in the ultimate strength behavior of beam-slab bridges. Also of essential importance, as was evident in Examples No. 3 and No. 4, is the need for taking the utmost care in the

conducting of any test so that there can be no question as to the reliability of the experimental results. While not the focus of this report, experimental data which is questionable even to the slightest degree, minimizes greatly its value.

In particular, while very close agreement was obtained from the load versus deflection diagrams for the latter examples simply by shifting the reference point for the experimental results, the question of the reliability of either analytical and/or especially experimental results is somewhat in doubt. However, in light of the information presented previously, the reliability of the finite element program stands up reasonably well even without including Examples No. 3 and No. 4, but they are still included as part of good research practice. As has been demonstrated, the analytical method even shows good agreement with the two-span and three-span models after considering all factors.

While in three of the tests the structures were loaded statically, in the remaining test the loads were produced by moving vehicles. However, by creating a loading pattern which approximates the actual moment envelope, the analytical model produced very satisfactory results. In addition, in each case the beams were subjected to the dead load of the structure. If this had not been done the ultimate load, as well as the nonlinear behavior, would have been entirely different because the dead load solution produces initial stresses in the beams. Finally, the finite element program produced reliable predictions of the ultimate capacity of each bridge superstructure.

The analytical method thus gives a solution for the flexural response of the structure in terms of displacements, strains, stresses, and regions of

cracking and crushing of the concrete and yielding of the steel. Serviceability criteria can then be evaluated at various load levels up to the flexural collapse of the bridge superstructure.

5.2 Other Considerations

5.2.1 AASHTO Overload Provision

The 1977 AASHTO specifications have an overload provision to allow for the possibilityof infrequent heavy loads. The provision applies to all loadings except H20 and HS20 loadings. The design truck load is to be applied to a single lane, increased by 100 percent, and without any concurrent loading in any other lane. The combined dead, live and impact stresses resulting from such loading are not to exceed 150% of the allowable design stresses. The question arises as to how does this provision relate to an actual overload analysis such as those presented in this report.

In the first example Bridge 3B of the AASHTO test, the allowable design stress in the steel beams was 27 ksi, which is greater than the present AASHTO allowable tension stress for A-36 steel of 20 ksi. The critical section for bridge 3B occurred at the ends of the coverplated section where the maximum stress was calculated to be 26.9 ksi by assuming an impact factor of 10% and a distribution factor of 33%. However, after measuring dead load stresses and recording the maximum live load stresses due to the regular test traffic the actual maximum stresses in the three beams were 26.0, 28.8 and 31.0 ksi at the ends of the coverplated sections of 97, 107, and 115 percent

of the design load. The actual computed moment distributions of the three beams were 33.8, 33.4 and 32.8 percent confirming the 33% distribution factor, but the measured impact factor was an average of 18.9%. Thus, part of the difference between the design stresses and the actual stresses can be attributed to excess dead load and excess impact factor. In an attempt to apply the overload provision the stresses at the critical section will be factored down to a maximum stress of 20 ksi while maintaining the same ratio of dead load to live load. By then doubling the live load plus impact stress in accordance with the overload provision the total maximum average stress becomes 28.9 ksi or 145% of the design stress. Thus, according to the overload provision the bridge would be sufficient as designed. However, in the process of performing the necessary steps to get these results a number of important factors are overlooked in this simplified overload provision.

Firstly, as was evident, the actual design stress was exceeded even in this carefully controlled test; thus, an actual multigirder, multi-lane bridge superstructure will also have a possibility of design stresses being exceeded with normal live loads. Thus, if an overload is to occur it would be possible that although the bridge met the specifications, the actual stresses could be greater than calculated by simplified means. Secondly, the arbitrary nature of the overload provision does not allow for a vehicle by vehicle analysis nor does it allow for any quantitative or qualitative analysis of the bridge subjected to the overload. For example, if the vehicle weight limits were to be increased, how does one then apply

the code and is it possible that even if the 150% limit is exceeded will the structure behave reliably.

With program BOVAS such questions and others can easily be answered because the engineer will have a grasp on what is happening at each particular load level and any loading condition. From the damage record for Bridge 3B with residual stress effect in Table 3, it can be seen that localized yielding begins at 762 kip-ft. but that the load deformation curve remained linear up to 1059 kip-ft. However, when the residual stress effect is not included then yielding does not begin until 1167 kip-ft. Thus, the importance of including the residual stress effect which is ignored in conventional analysis becomes extremely important. At the same time both the test results and BOVAS clearly show that the bridge could successfully take a design load of 27 ksi without any detrimental effect. Since the stress calculation is so dependent upon the ratio of the live load to dead load, the distribution factor, the impact factor and residual stresses, all of which are complex and variable factors, the use of a simplified overload provision becomes questionable. For the overload calculation, which arrived at a maximum stress of 28.9 ksi, this corresponds to a maximum static moment of 815 kip-ft. Depending on how one views this value in light of the damage record, it could be considered as a conservative value or as an unsafe value. However, in light of the fact that in the actual test results it was noted that even at loads much in excess of first yielding the bridge had only a small permanent set. The 815 kip-ft. limit would appear to be conservative.

5.2.2 Fatigue

While program BOVAS cannot account directly for the effects of fatigue, the results from the finite element analysis can be used to establish an estimate of the fatigue life of the component parts. By simply recording all element layer stresses in the vicinity of each particular type of detail and corresponding to a particular overload, a stress range can be calculated for the detail. Then using published S-N curves established for each category of detail, the estimated cycle life can be found. If the bridge has had many years of service an approximation of the number cycles already made and the corresponding stress range can be used in conjunction with the above information to perform a root-mean-square summation of the stress range effects to arrive at a fatigue life prediction.

5.2.3 Local Instability

In addition to failure by yielding or by fatigue, there exists the possibility of failure due to local instability or localized or general buckling of the steel member or a component of the steel member. This could amount to buckling of the compression flange, lateral torsional buckling, or buckling of the web due to shear. At the present time an analysis similar to the one performed for the fatigue analysis could be made where a stress check is made of the element layers and then compared to critical buckling values. Determining when this type of failure would occur would be extremely important in any overload analysis, because if the member component buckled at some given load, but the analysis did not

reflect this fact, then the performance of the structure beyond the buckling load would be unreliable. While the compression flange in the positive moment region is unlikely to buckle due to the restraining effect of the concrete slab, the compression flange of beams over interior supports in continuous bridges in negative moment regions could buckle because there is no such restraint. However, to perform a correct flange buckling analysis an appropriate critical buckling formula must be established, such as

$$\sigma_{cr} = k^* \left(\pi E / \left(12\ (1-\nu)^2\ \ (b/t)^2 \right) \right)$$

from Ref. 28. BOVAS could then be modified to flag the occurrance of such stresses, and although the post buckling performance would not reflect the buckling phenomena, the engineer would know when buckling occurred. Similarly, a critical stress could be established for lateral torsional buckling of the entire beam section in the negative moment region, such as:

$$\sigma_{CR} = \frac{C_1 \pi^2 E I_{yh}}{2 S_x (KL)^2} \left(\sqrt{1 + C_2^2 + \frac{(KL)^2 GJ}{\pi^2 E C_w}} \pm C_2 \right)$$

from Ref. 28. L, K, C_1, C_2 are constants depending upon boundary and loading conditions and span length. However, since the above equation is for doubly symmetric sections, only some adjustment would have to be made. As far as web buckling due to shear is concerned, experiments and theory show, unlike the first two local instability effects, a considerable amount of post buckling strength. However, the major task in investigating web and post buckling strength remains in determining which of the many web

shear buckling models can be used in analysis and they can reliably predict post buckling behavoir. Thus a major effort remains to determine the significance of these features and to what extent they can be included in the finite element analysis.

5.2.4 Details and Floor Systems

The effects of secondary details of the main girder, such as transverse stiffeners, longitudinal stiffeners, and cross bracing on the behavior of the bridge superstructure, is not accounted for by program BOVAS at this time. In general, transverse stiffeners are used to control the shear in thin webbed plate girders, and their effect on the behavior of the bridge in the elastic range is minimal, but due to the possibility of web shear buckling, they could become important. However, the effect of these vertical stiffeners can be accounted for in connection with the web shear problem above. Longitudinal stiffeners could be accounted for by using an element layer to simulate their effect while ignoring any possible beneficial effect on shear capacity. Cross-bracing would be difficult to include in the analysis without increasing the degrees of freedom of the finite element model, and such a manuveur might not be warranted in light of its secondary nature. However, some type of back subsituation involving relative displacement of slab and girders in transverse and vertical direction might allow for the calculation of approximate cross-bracing stresses.

As far as changing the program to model floor systems composed of a deck slab, longitudinal stringers, transverse floor beams and longitu-

dinal main girders, some approximations could be made. However, considerable effort should be made via parametric studies to insure exactly what effect these members have on each other. For example, when the stringer is attached to the floor beams twisting moments are introduced to the floor beams, and as of the present time, the beam finite element does not include the effects of torsion. In addition, the beams will run transversely as well as longitudinally and care must be taken not to violate any assumptions already made concerning slab-beam interaction. Thus, while BOVAS can handle many typical bridge superstructures, some further refinements are necessary to insure a wider range of applicability. However, some features may or may not be realistically included in the analysis scheme without major changes.

TABLES

TABLE 1A

REINFORCEMENT EXAMPLE 1

Centroidal Distance from Midheight (Positive Downward) (inches)	θ_x (degrees)	Thickness (inches)	Size/Spacing
-1.435	-90	0.0620	5 @ 5"
-0.935	0	0.0550	3 @ 20"
0.935	0	0.0550	3 @ 20"
1.435	-90	0.0620	5 @ 5"

TABLE 1B

REINFORCEMENT EXAMPLE 2

Centroidal Distance from Midheight (Positive Downward) (inches)	θ_x (degrees)	Thickness (inches)	Size/Spacing
-1.6875	-90	0.05636	5 @ 5.5"
-1.0625	0	0.03875	5 @ 8"
1.0625	0	0.03875	5 @ 8"
1.5625	-90	0.05636	5 @ 5.5"

TABLE 2

MATERIAL PROPERTIES

EXAMPLE NO. 1

Concrete Slab

	Actual	Finite Element Model
Compressive Strength, f_c'	5.74 ksi	5.74 ksi
Tensile Strength, f_t	--	.4592 ksi
Initial Modulus, E_c	5,200 ksi	5,200 ksi
Unload Modulus comp., E_{d_c}	--	1,000 ksi
Unload Modulus tension, E_{d_t}	--	800 ksi
Ramberg-Osgood m	--	0.77
Ramberg-Osgood n	--	9.0

Reinforcing Steel

	Actual	Finite Element
Yield Strength, f_y	61.2 ksi	61.2 ksi
Modulus, E_s	28,800 ksi	28,800 ksi
Ramberg-Osgood m	--	0.70
Ramberg-Osgood n	--	100.0

Steel Beam

	Actual	Finite Element
Yield Strength, flange, f_y	35.1 ksi	25.1 ksi
Yield Strength, web, f_y	39.9 ksi	39.9 ksi
Yield Strength, coverplate, f_y	38.9 ksi	38.4 ksi
Modulus E_s	30,000 ksi	30,000 ksi
Ramberg-Osgood m	--	0.67
Ramberg-Osgood n	--	300

TABLE 3

LOAD VS DAMAGE RECORD - EXAMPLE NO. 1

Load (kip-ft)	Damage - Test	Load (kip-ft)	Damage - BOVAS
		762	Yielding of exterior beam bottom flange @ mid span
		906	Yielding of interior beam bottom flange @ mid span
		1059	Yielding of coverplate of exterior beam @ mid span
		1156	Yielding of exterior & interior beam bottom flange at end of coverplate
1333	Yielding of bottom flange near ends of coverplate	1364	Complete yielding of exterior beam coverplate. 85% of exterior beam bottom flange has yielded
1493	Almost complete yielding of bottom flange except near supports, extensive coverplate yielding	1455	Complete yielding of interior beam coverplate. 85% of interior beam bottom flange has yielded
		1662	Bottom layer of slab has a transverse crack all the way across at mid span
		1883	The web of exterior beam has yielded over 70% of its depth
2000	Web yielding is clearly evident	1919	The web of interior beam has yielded over 70% of its depth
2277	Extensive web yielding and tension cracks in slab halfway through depth in coverplated section	2296	The slab has a transverse crack through 50% of its depth at mid span and 33% through depth in coverplated section. The web has yielded through 86% of depth at midspan

TABLE 4

MATERIAL PROPERTIES

EXAMPLE NO. 2

Concrete Slab

	Actual	Finite Element Model
Compressive Strength, f_c'	6.87 ksi	6.87 ksi
Tensile Strength, f_t	----	0.4898 ksi
Initial Modulus, E_c	----	4,776 ksi
Unload Modulus comp., E_{d_c}	----	1,000 ksi
Unload Modulus tension, E_{d_t}	----	800 ksi
Ramberg-Osgood m	----	0.77
Ramberg-Osgood n	----	9.0

Reinforcing Steel

	Actual	Finite Element
Yield Strength, f_y	40 ksi	40 ksi
Modulus, E_s	29,000 ksi	29,000 ksi
Ramberg-Osgood m	----	0.7
Ramberg-Osgood n	----	100.0

Beam Steel

	Actual	Finite Element
Yield Strength, f_y	40 ksi	40 ksi
Modulus, E_s	30,750 ksi	30.750 ksi
Ramberg-Osgood m	----	0.67
Ramberg-Osgood n	----	300

TABLE 5

LOAD VS DAMAGE RECORD - EXAMPLE NO. 2

Load (kip-ft)	Damage - Test	Load (kip-ft)	Damage - BOVAS
		259.5	Up to this point there has only been longitudinal cracking of the slab in the bottom layers at the center line of the bridge under or near the 1 load
		402.5	The first transverse cracks appear in the top layer of the slab near first pier
		446.7	Transverse cracks appear in the top of slab near the second pier
		556.4	First yielding begins in bottom flange of interior beams in area under the load
		590.9	First yielding begins in bottom of web of interior beams in area under the load.
620	First yielding of steel appears to occur at this load - shortly after yielding started the bridge "lifted off" the abutment nearest the load	625.5	The transverse crack over the first pier is now through 50% of the slab depth
650	Tension cracks visible in deck slab over first pier		
700	Tension cracks which extend across the slab and through the curb at second pier	710.4	The first transverse crack in the bottom of the slab in the area under the load now appears
		757.5	The slab over first pier is now completely cracked longitudinally through the complete depth, however, the reinforcement is still functional

TABLE 5--Continued

Load (kip-ft)	Damage - Test	Load (kip-ft)	Damage - BOVAS
		767.8	The slab over second pier is now cracked completely through the depth in the longitudinal direction
		819.3	Yielding of the bottom flange of the exterior beams in the area of the load has started
		851.6	The slab between the interior and exterior beam at the second pier is now also cracked through 60% of its depth in the longitudinal direction
		925.4	The bottom transverse reinforcement in the slab in the area of the load has now yielded in tension
		991.6	Yielding in compression of the bottom flange of interior beam at first pier
		1029.2	The transverse crack in the bottom of the slab under the load is now halfway through the slab depth in the area near the center of the bridge
		1072.6	The web of interior beam under the load is now fully yielded
		1119.9	First crushing of slab at load point
		1202.3	Yielding in compression of top transverse slab reinforcement in area under load. Yielding in tension of top longitudinal slab reinforcement near the first pier. Yielding on tension of bottom longitudinal slab reinforcement in area under the load.

TABLE 5--Continued

Load (kip-ft)	Damage - Test	Load (kip-ft)	Damage - BOVAS
		1221.2	The interior beam in the area under the load has now fully yielded forming a plastic hinge in the beam
		1254.7	The web of exterior beam under point of loading has now fully yielded
1265	Maximum load reached. Compression failure of curb section.		

TABLE 6A

REINFORCEMENT EXAMPLE 3

Centroidal Distance from Midheight (Positive Downward) (Inches)	θ_x (Degrees)	Thickness (Inches)	Size/Spacing
0.00	-90	0.02667	W8 @ 3"
0.00	0	0.0200	W6 @ 3"

TABLE 6B

REINFORCEMENT EXAMPLE 4

Centroidal Distance from Midheight (Positive Downward) (Inches)	θ_x (Degrees)	Thickness (Inches)	Size/Spacing
0.00	-90	0.0100	W4 @ 4"
0.00	0	0.0100	W4 @ 4"

TABLE 7

MATERIAL PROPERTIES - EXAMPLE NO. 1 AND EXAMPLE NO. 2

Concrete Slab

	TWO SPAN		THREE SPAN	
	Actual	F.E.M.	Actual	F.E.M.
Compressive Strength, f_c'	4.83 ksi	4.83 ksi	3.99 ksi	3.99 ksi
Tensile Strength, f_t	--	0.3946 ksi	--	0.3591 ksi
Initial Modulus, E_c	3600 ksi*	4044 ksi	3900 ksi*	3640 ksi
Unload Modulus Comp., E_{d_c}	--	1000 ksi	--	1000 ksi
Unload Modulus Tension, E_{d_t}	--	800 ksi	--	800 ksi
Ramberg-Osgood m	--	0.77	--	0.77
Ramberg-Osgood n	--	9.0		9.0

* Secant Modulus

Reinforcement Steel

	TWO SPAN		THREE SPAN	
	Actual	F.E.M.	Actual	F.E.M.
Yield Strength, f_y	High Strength	64 ksi	High Strength	64 ksi
Modulus, E_s	29000 ksi*	29000 ksi	29000 ksi*	29000 ksi
Ramberg-Osgood m	--	0.7	--	0.7
Ramberg-Osgood n	00	200	--	200

* As given by manufacturer

Beam Steel

	TWO SPAN		THREE SPAN	
	Actual	F.E.M.	Actual	F.E.M.
Yield Strength, f_y	40 ksi	40 ksi	40 ksi	40 ksi
Modulus, E_s	30000 ksi	30000 ksi	30000 ksi	30000 ksi
Ramberg-Osgood m	--	0.67	--	0.67
Ramberg-Osgood n	--	300	--	300

FIGURES

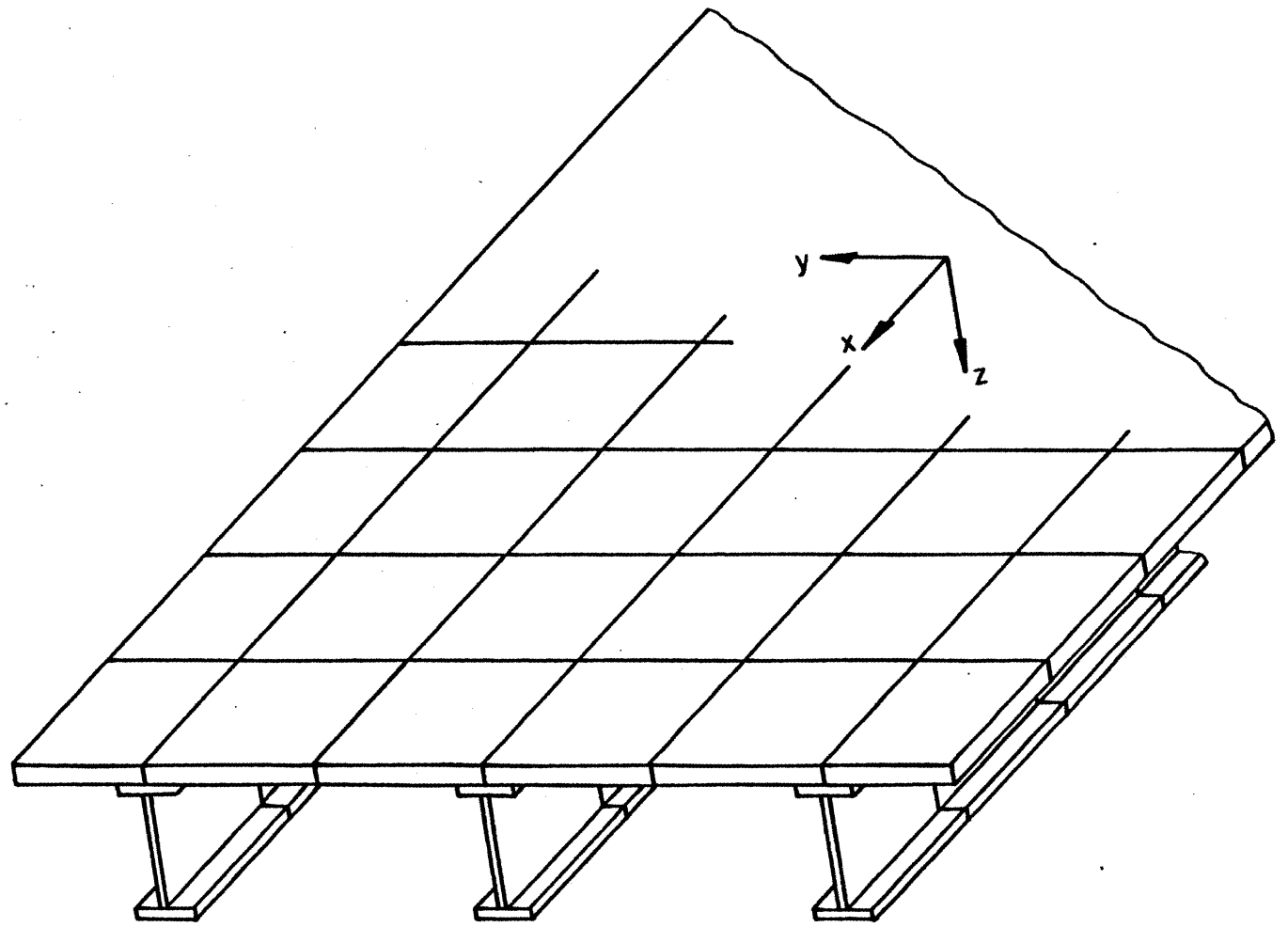

Fig. 1 Typical Slab-Girder Highway Bridge Finite Element Discretization

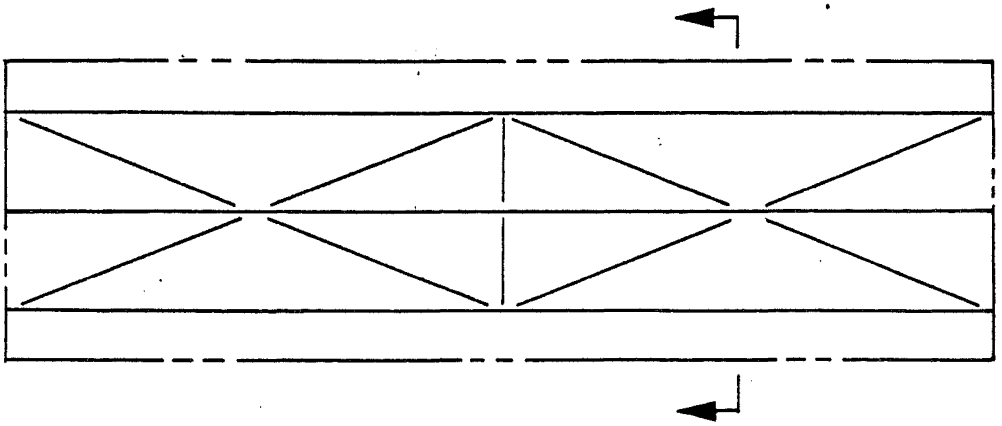

PLAN (BELOW DECK)

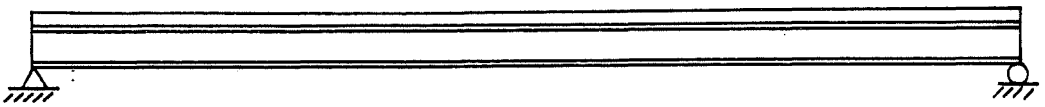

ELEVATION

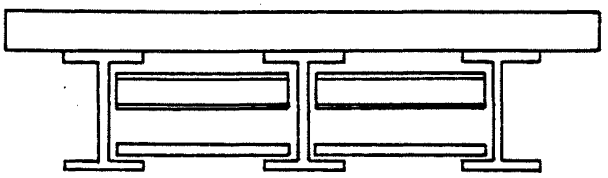

SECTION

Fig. 2 Steel Bridge Superstructure

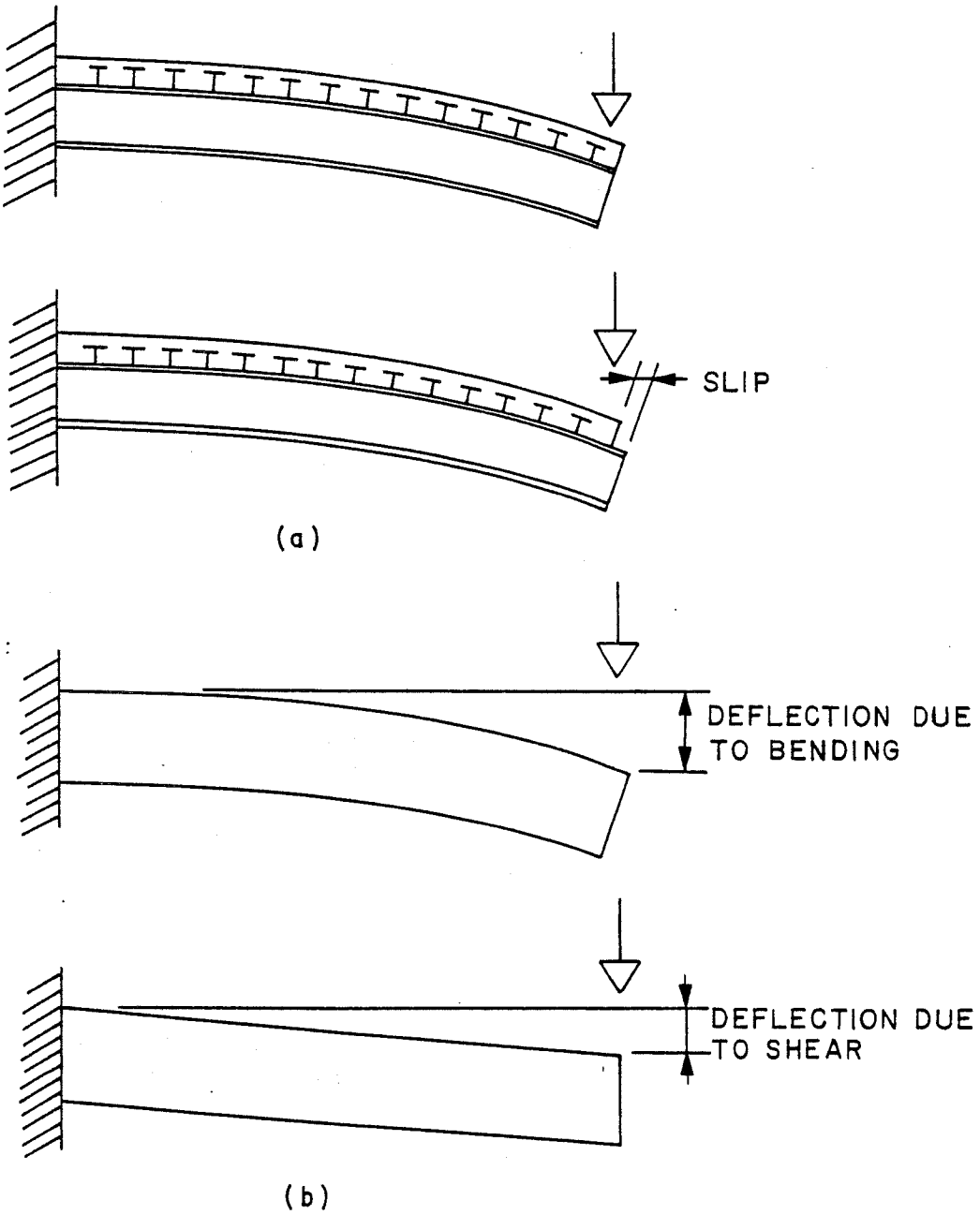

Fig. 3 (a) Composite Beam With and Without Slip
(b) Deflections Due to Bending and Shear

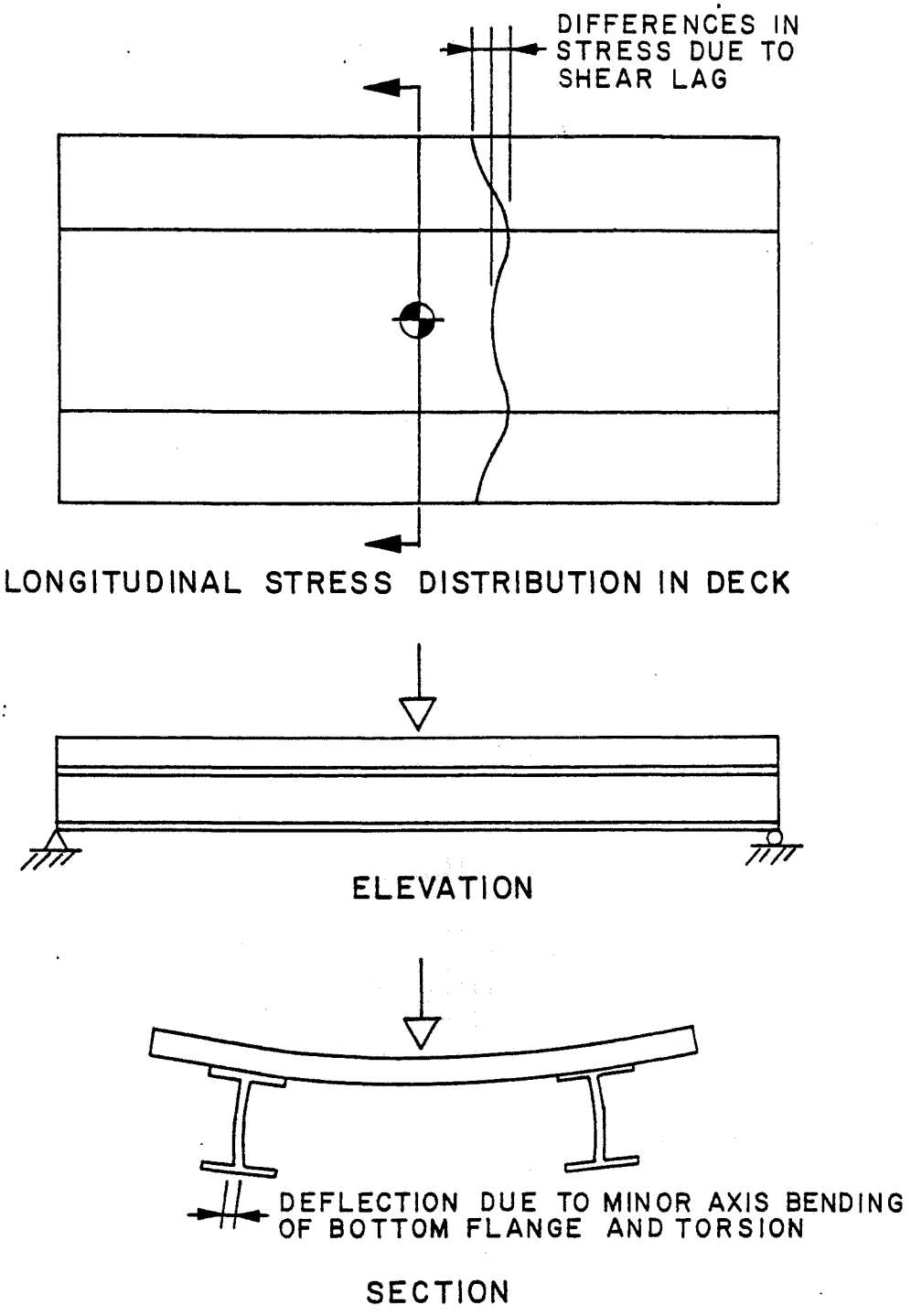

Fig. 4 Longitudinal Stress Distribution in Deck and Traverse Deflection of Beams

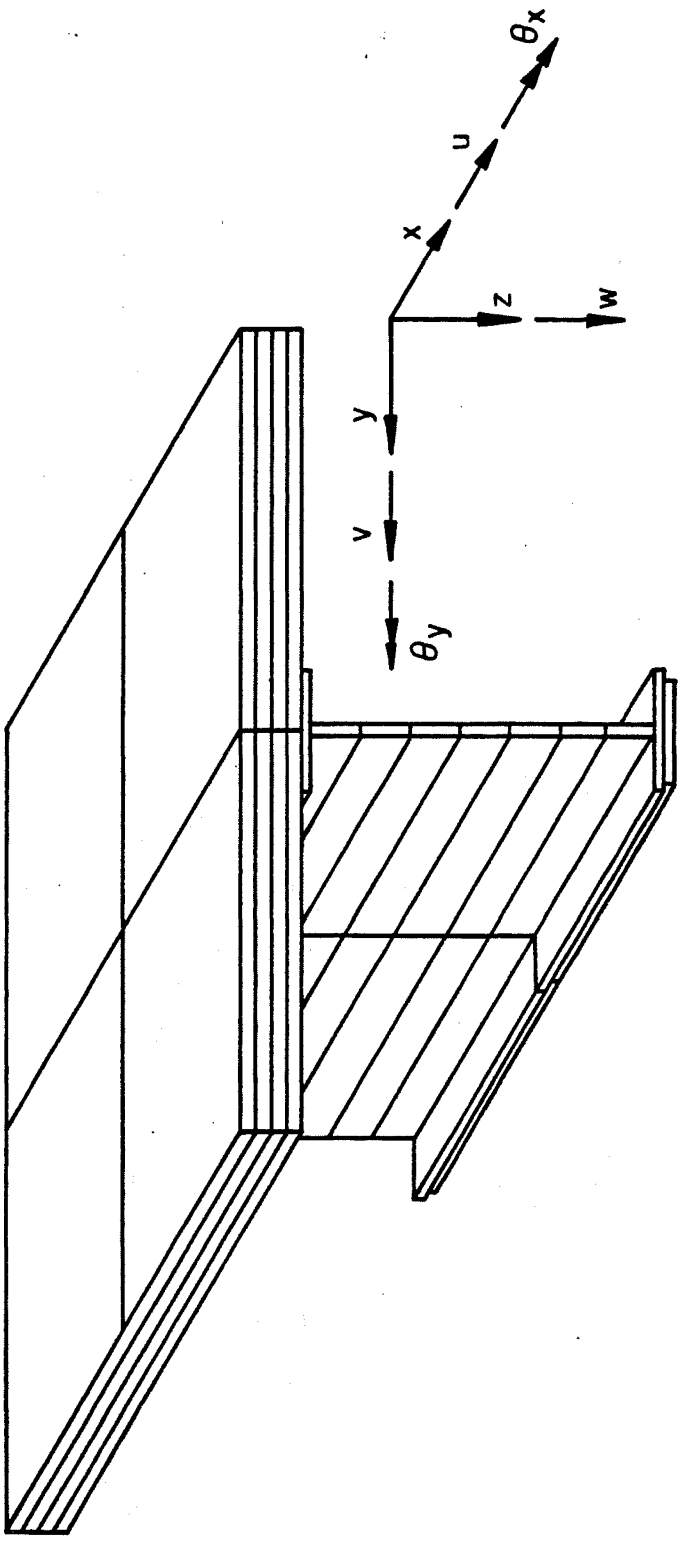

Fig. 5 Slab and Girder Layering

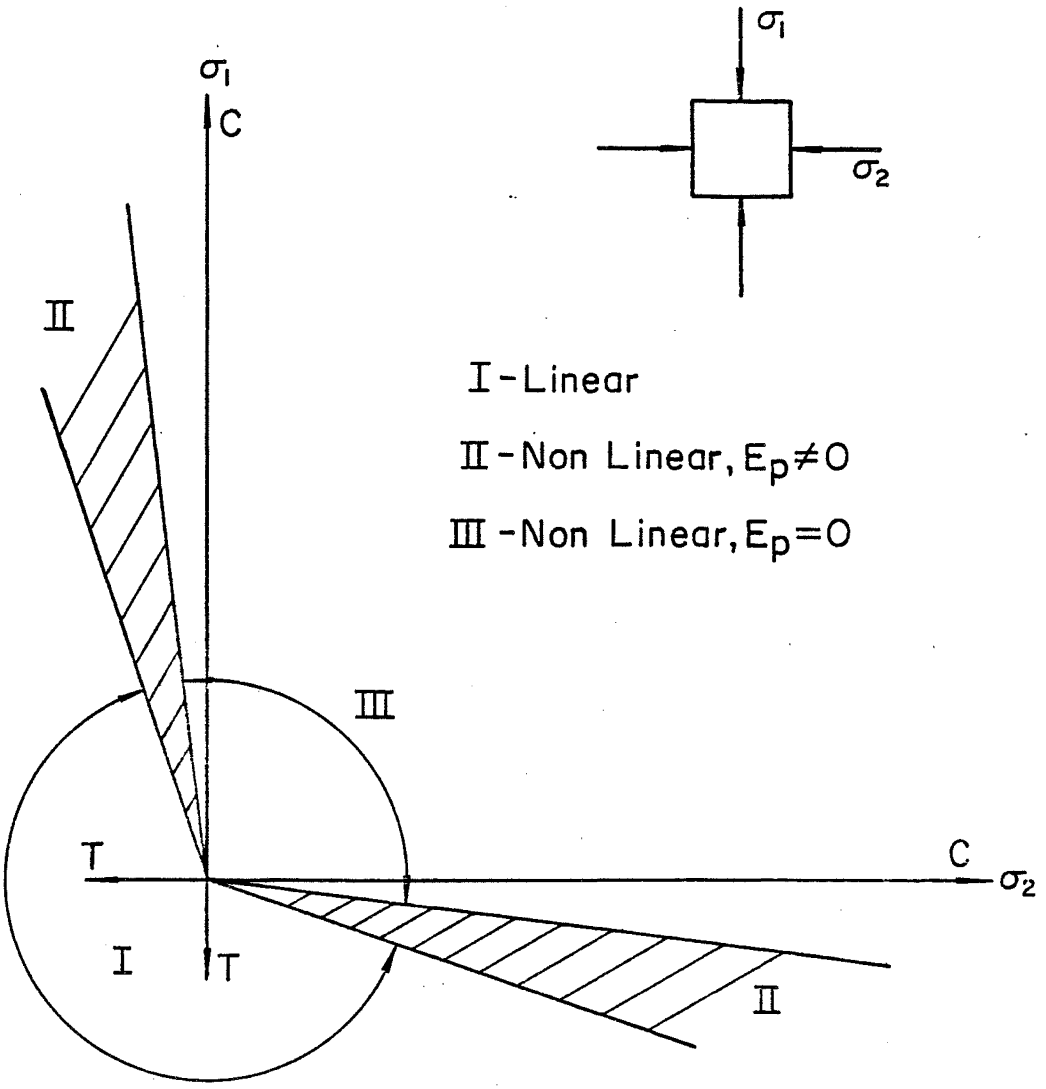

Fig. 6 Linear and Nonlinear Concrete Stress-Strain Curve Regions

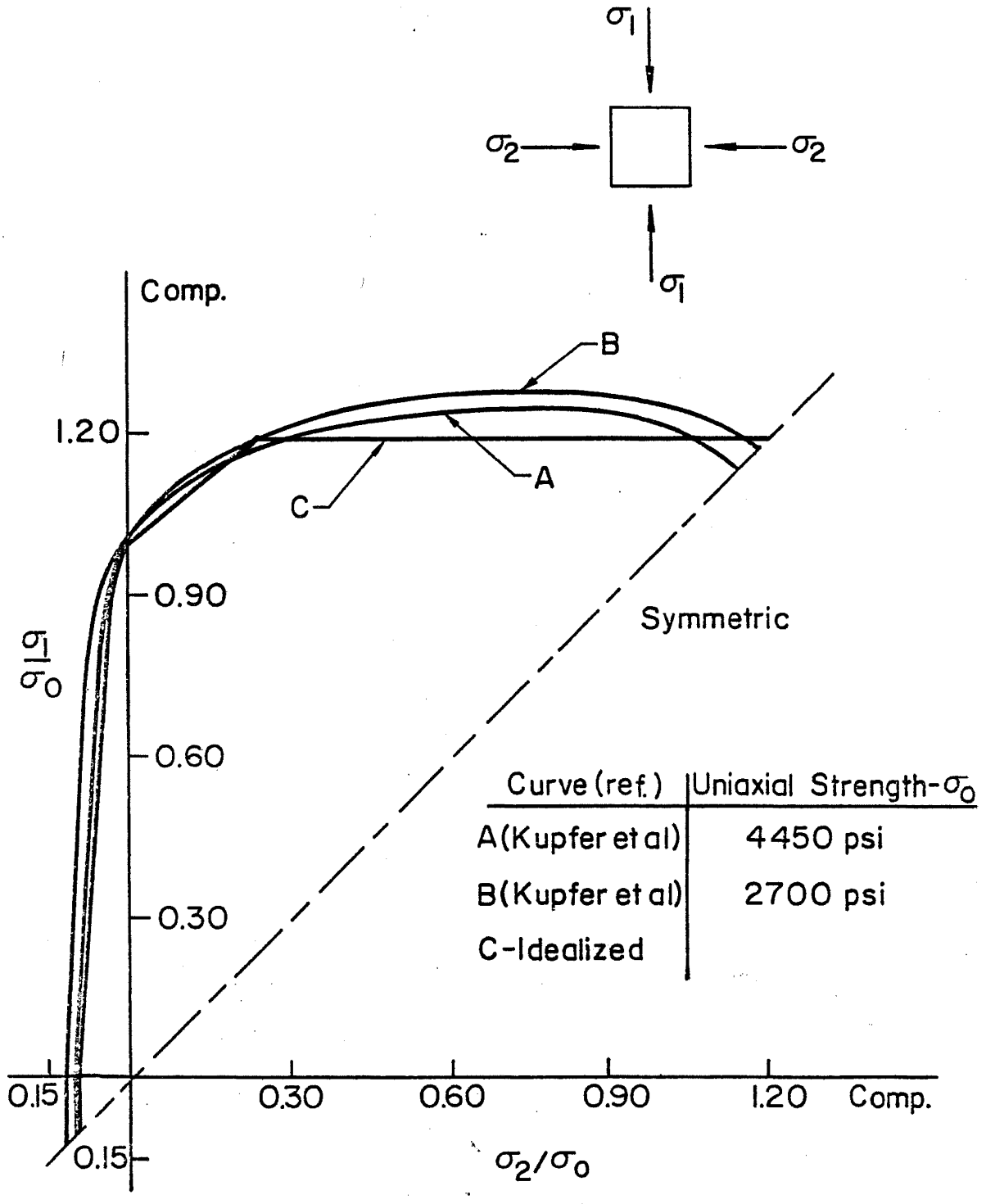

Fig. 7 Actual and Idealized Concrete Failure Envelopes for the Biaxial Stress Space

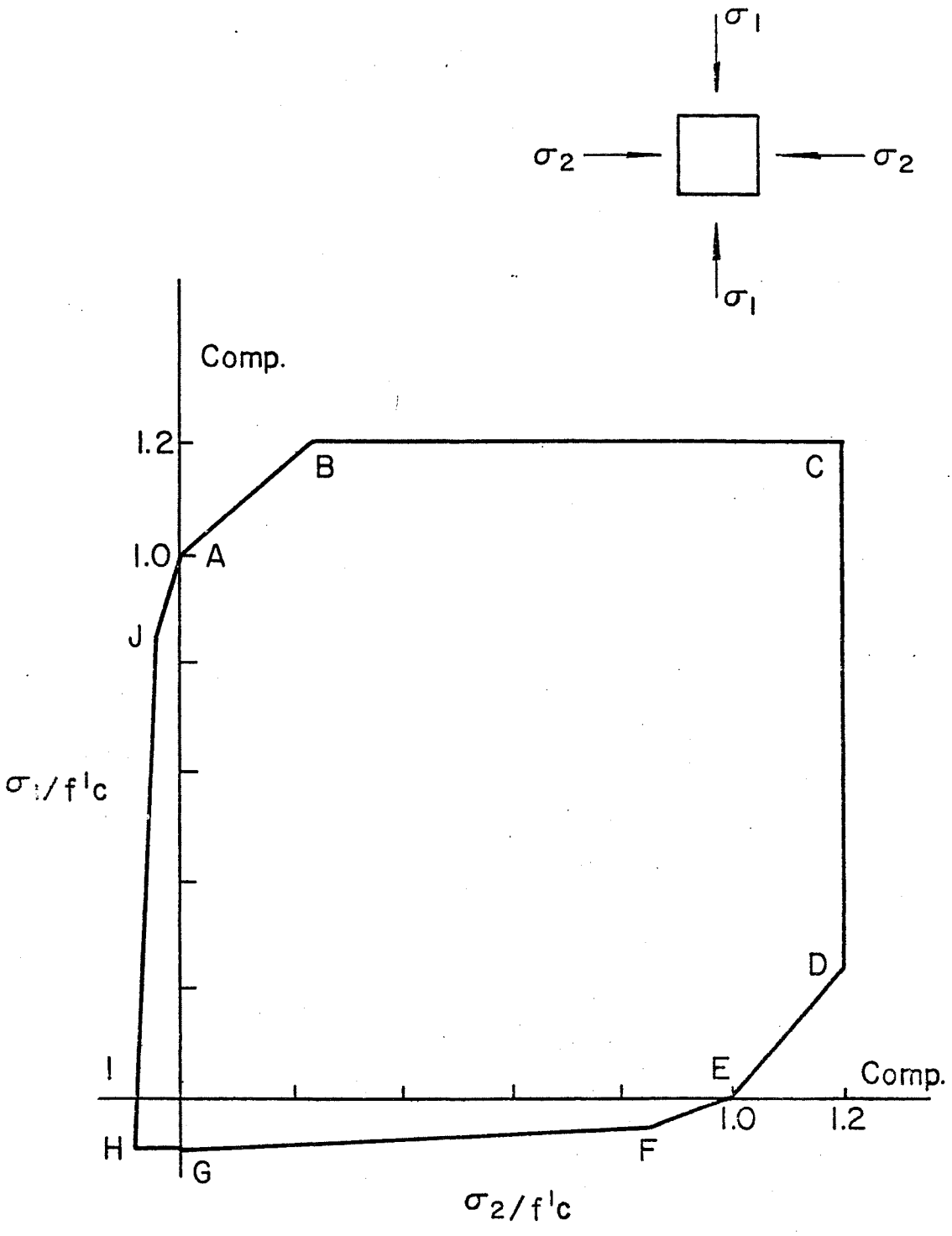

Fig. 8 Idealized Biaxial Failure Envelope with Characteristic Points

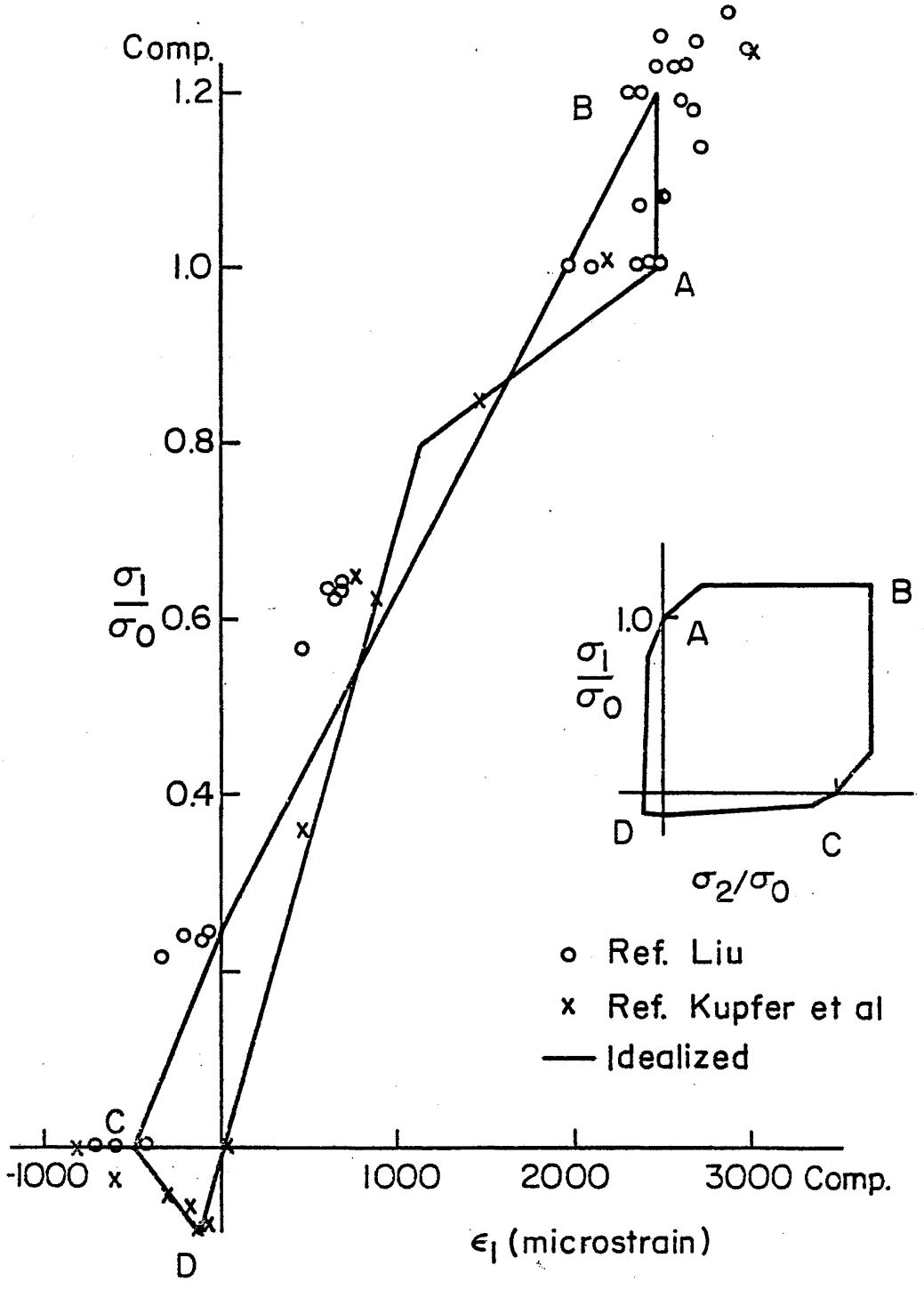

Fig. 9 Peak Strain Envelope

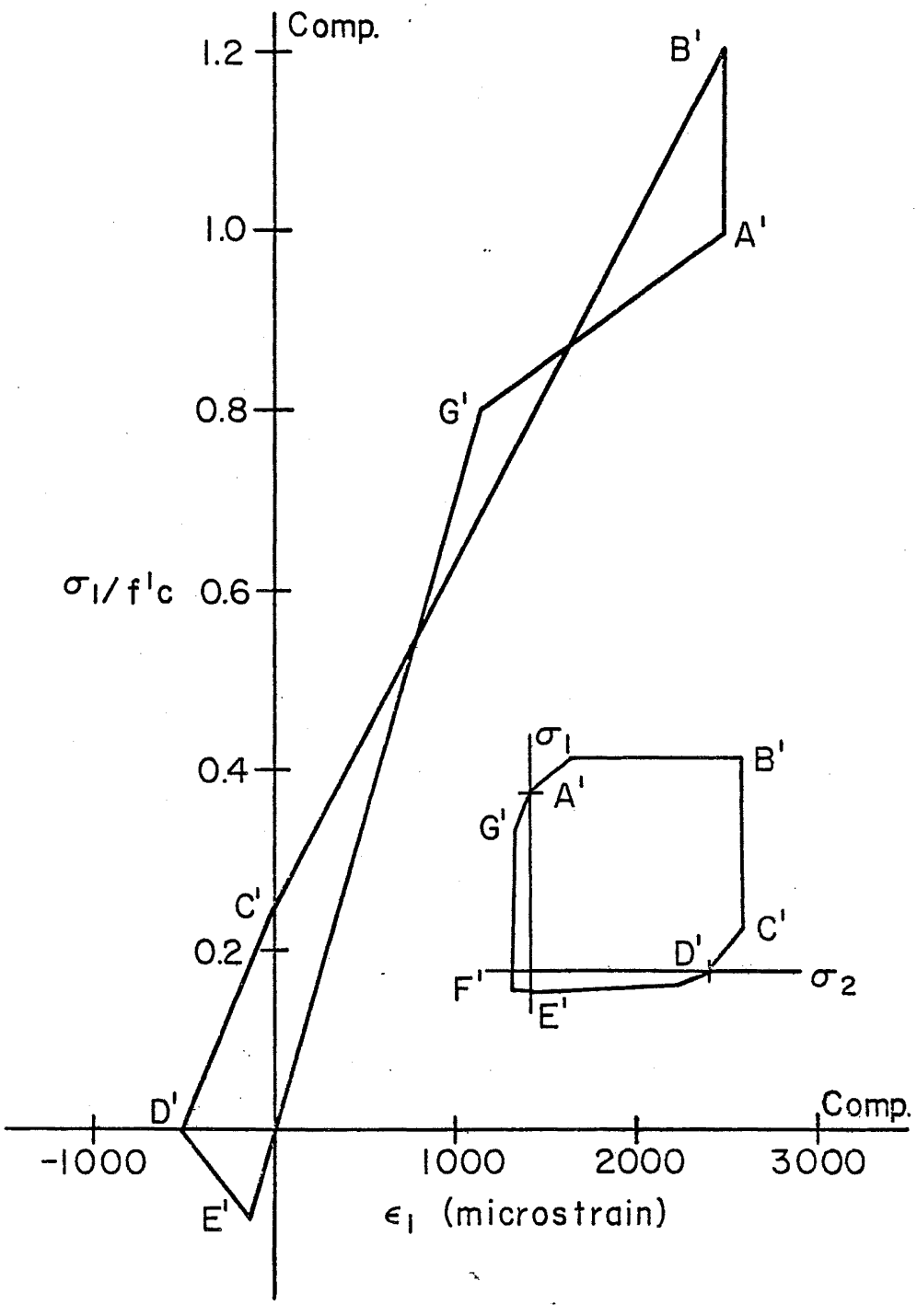

Fig. 10 Peak Strain Envelope with Characteristic Points

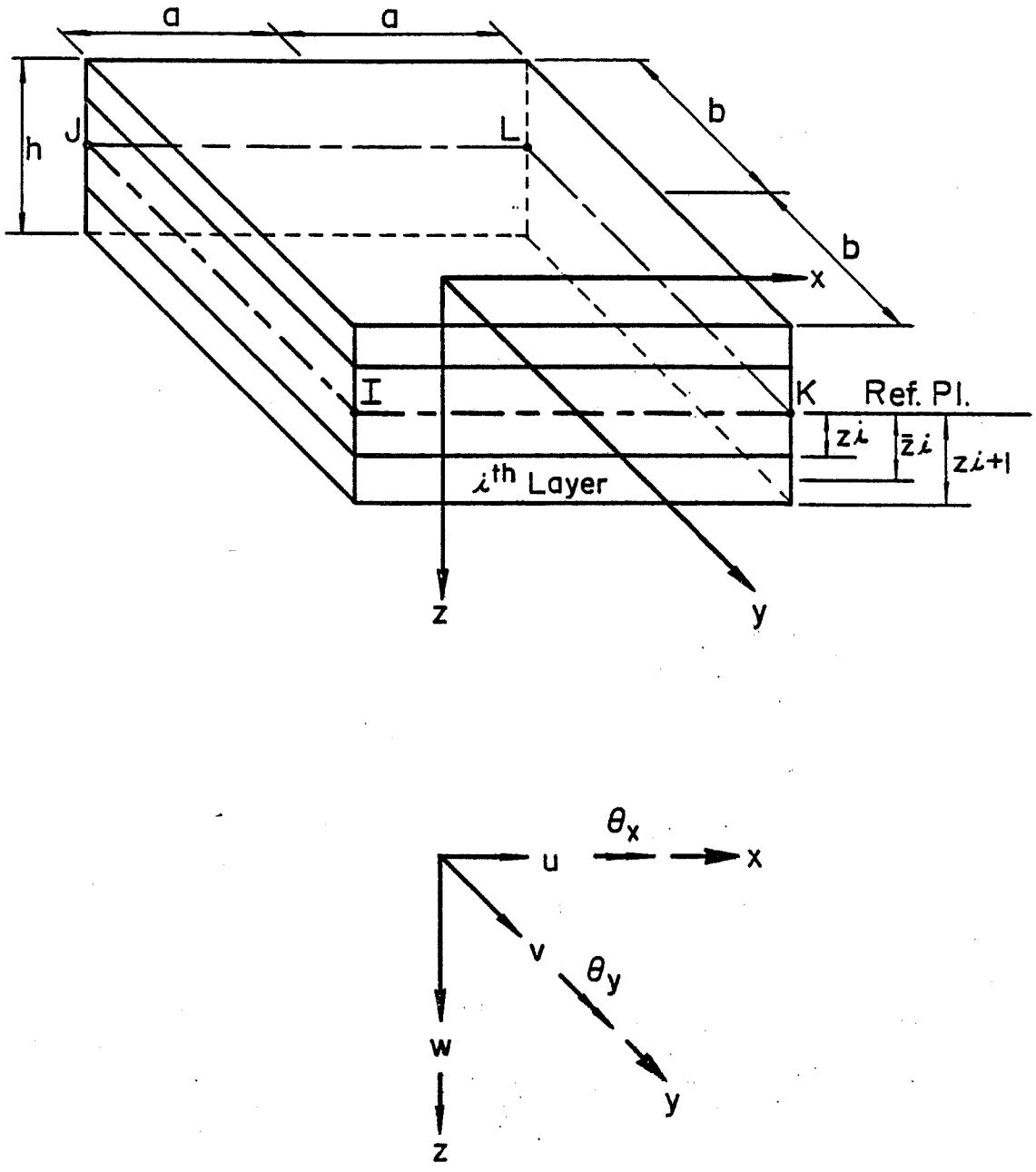

Fig. 11 Rectangular Slab Finite Element:
Layering and Coordinate System

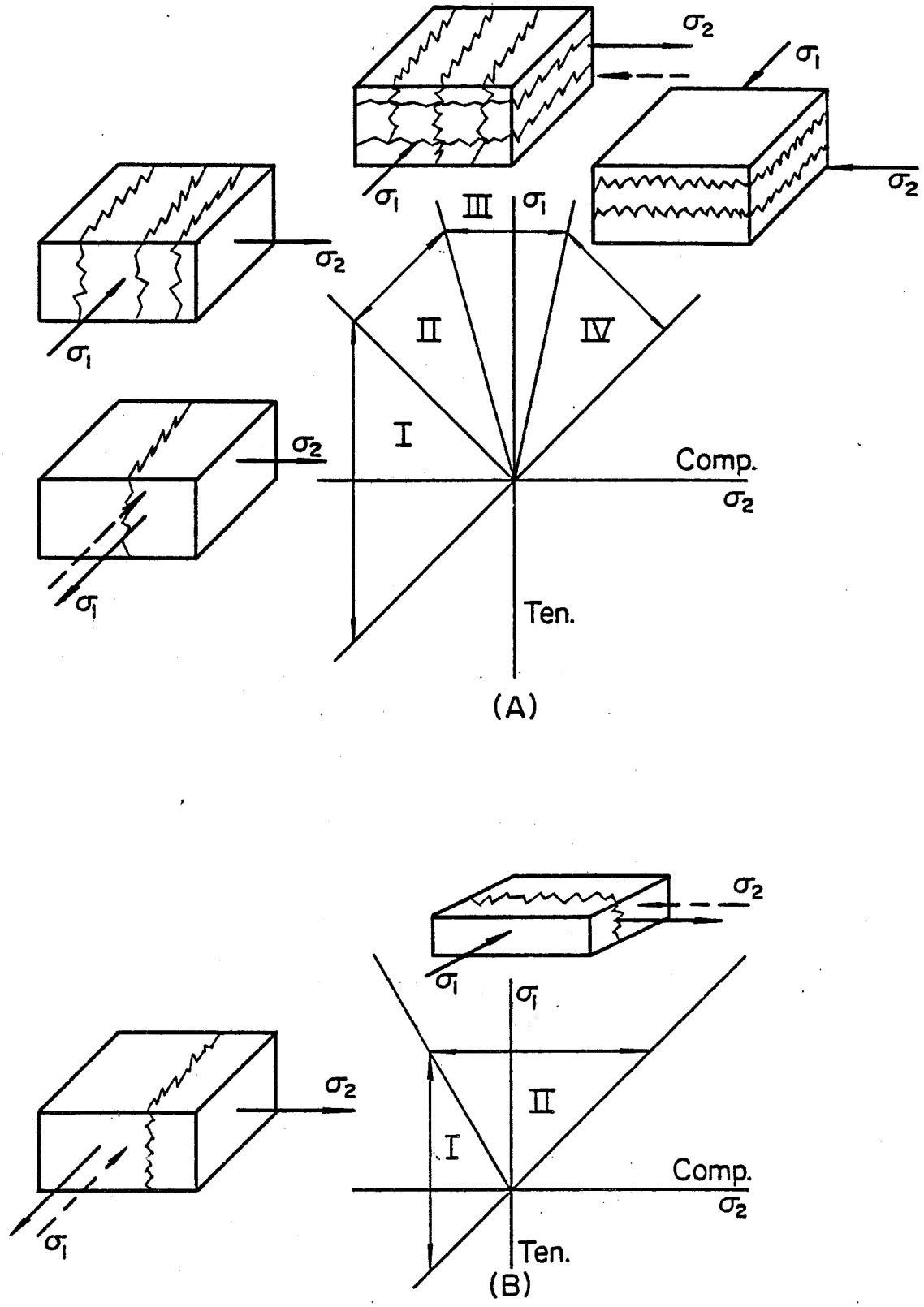

Fig. 12 Actual (A) and Idealized (B) Concrete Failure Modes

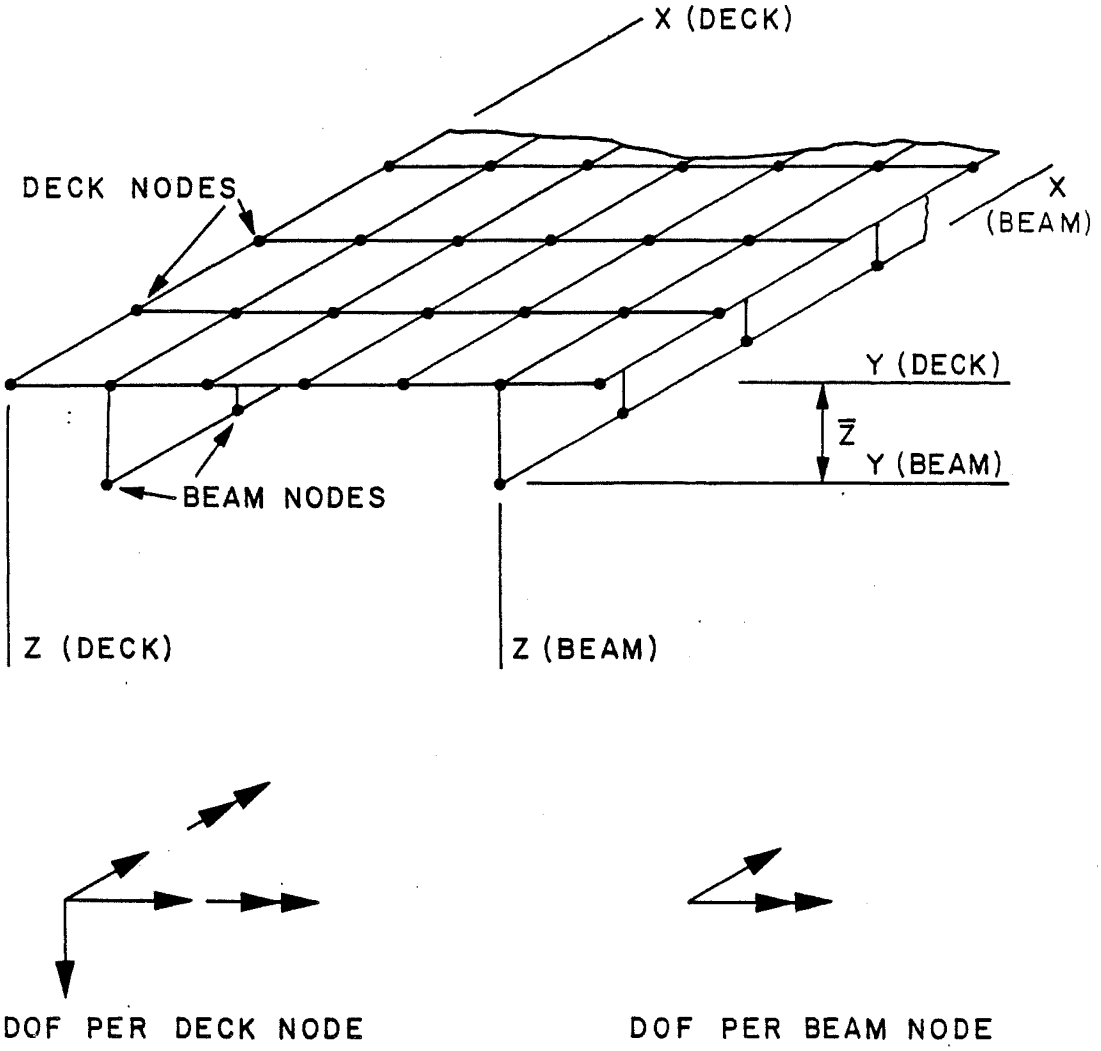

Fig. 13 Bridge Model Using Tumminelli-Kostem Element and Degrees of Freedom

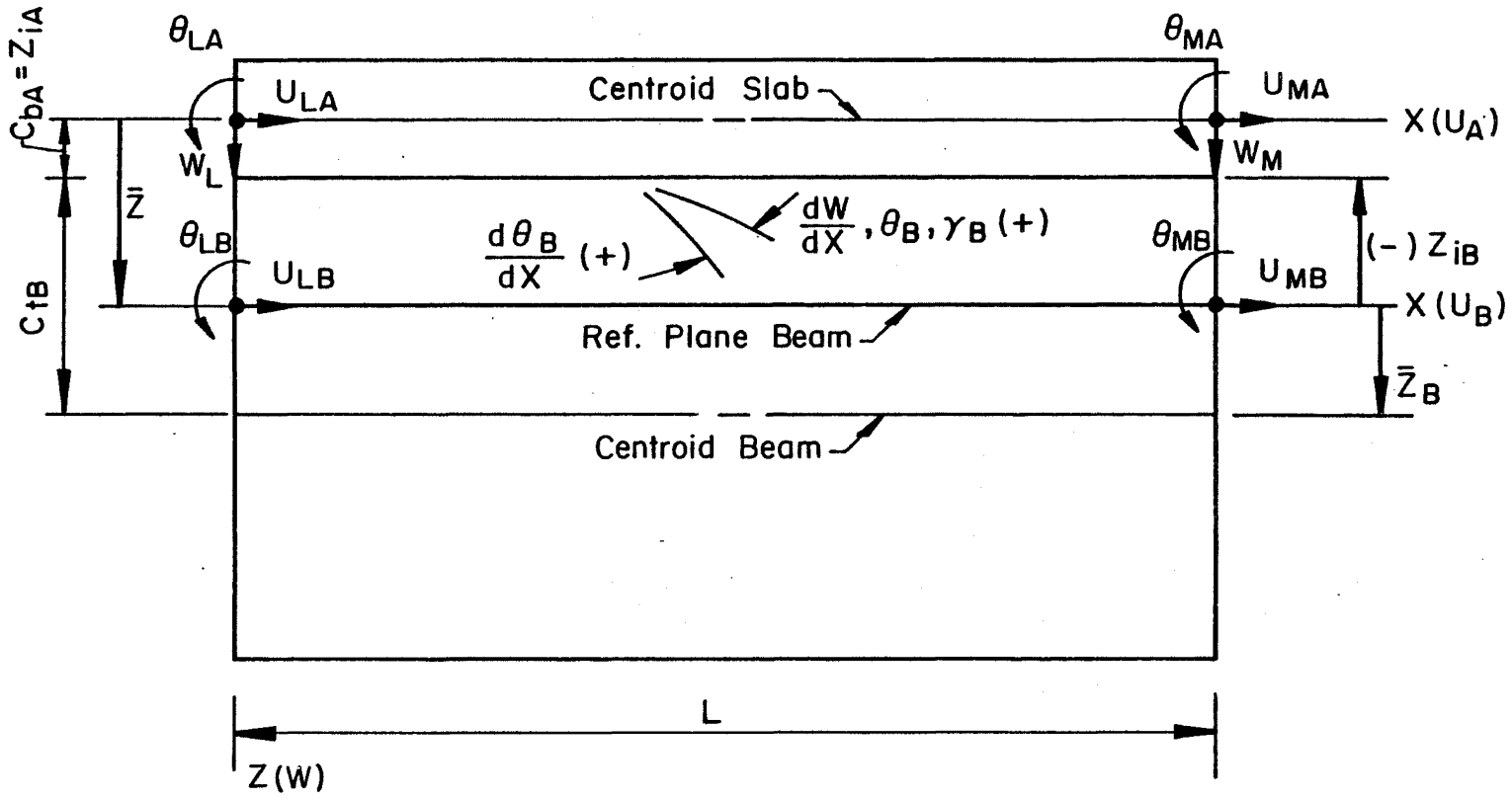

Fig. 14 Composite Element Node Point Deformations and Sign Conventions

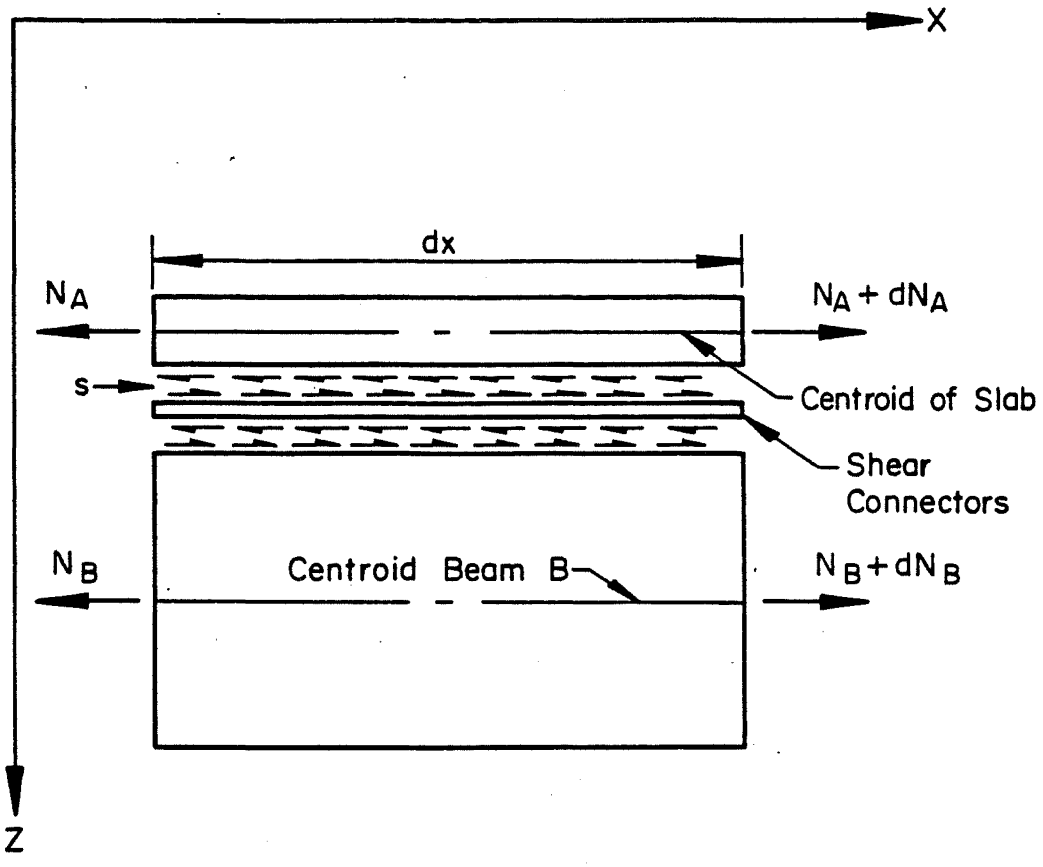

Fig. 15 Composite Element Shear-Flow Equilibrium Diagram

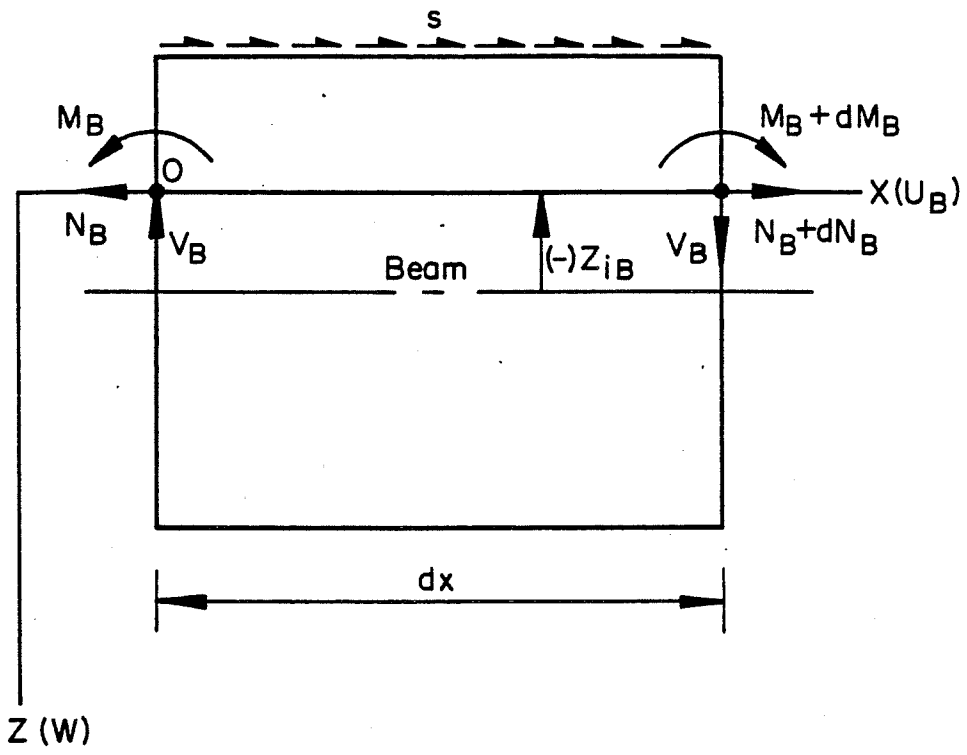

Fig. 16 Beam Internal Force Equilibrium Diagram and Sign Convention

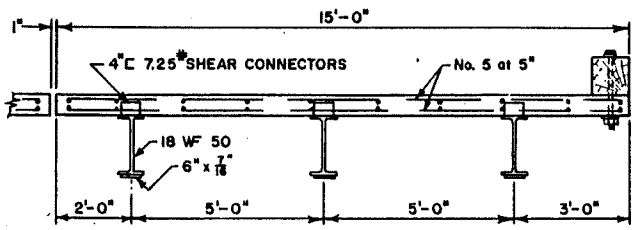

Fig. 17 Cross Section, Example No. 1
(AASHTO Bridge 3B)

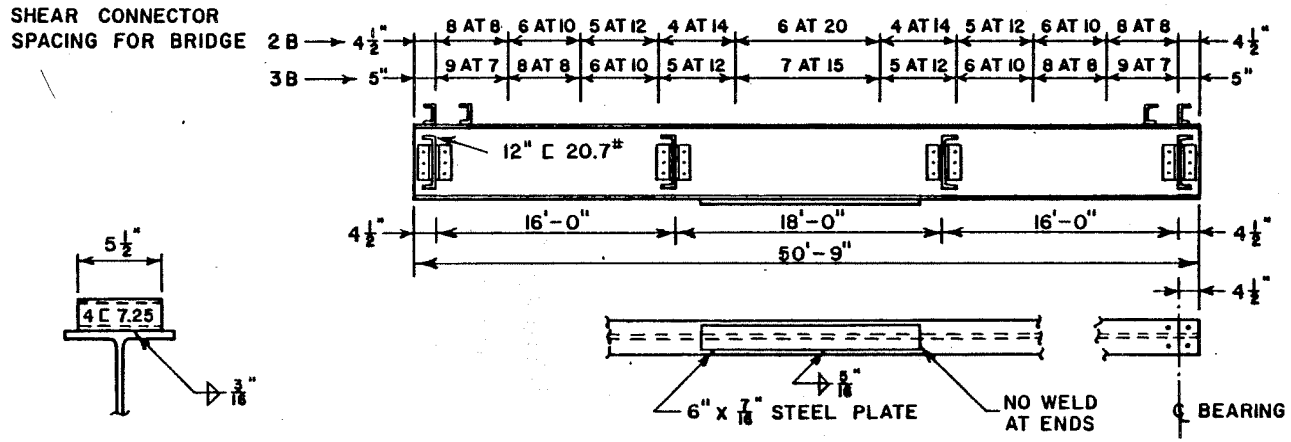

Fig. 18 Beam Elevation, Example No. 1 (AASHTO Bridge 3B)

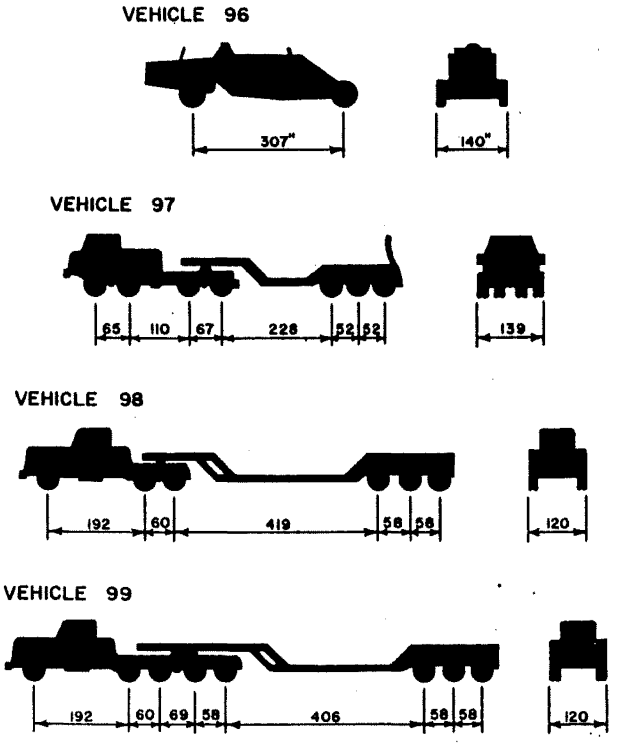

Fig. 19 Overloaded Test Vehicles, Example No. 1
(AASHTO Bridge 3B)

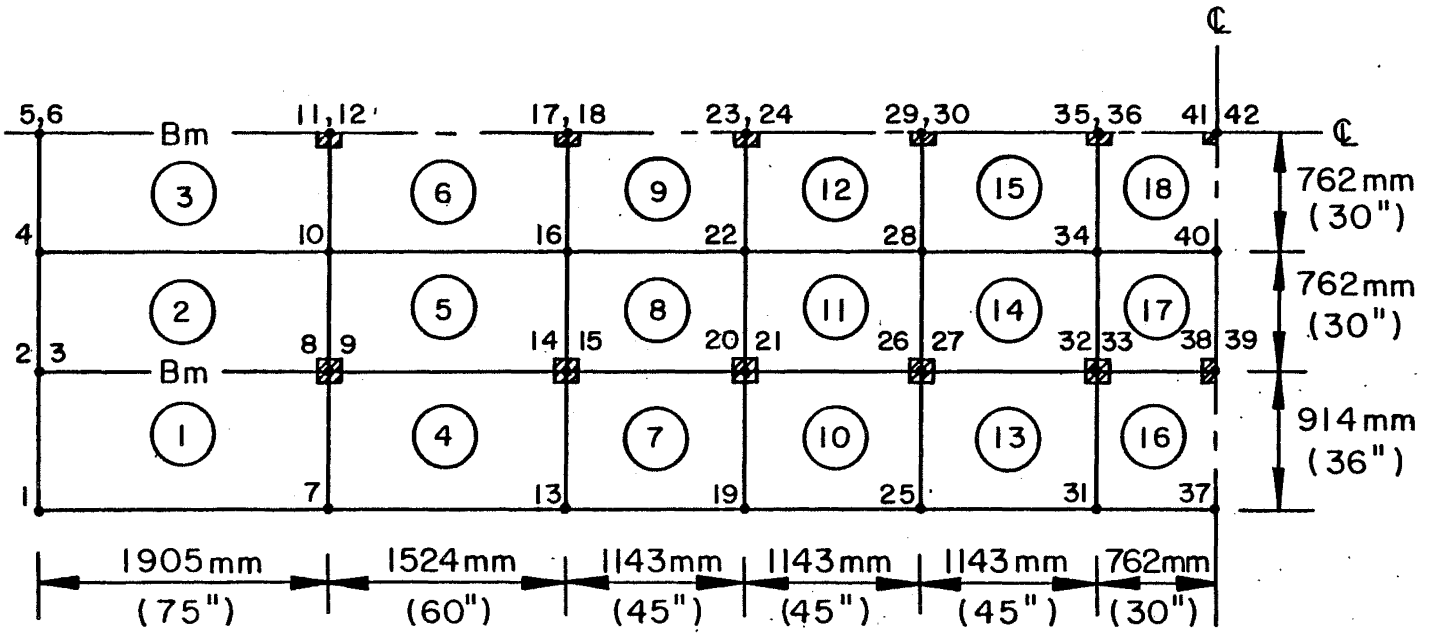

Fig. 20 Example No. 1 (AASHTO, Bridge 3B)
Finite Element Discretization

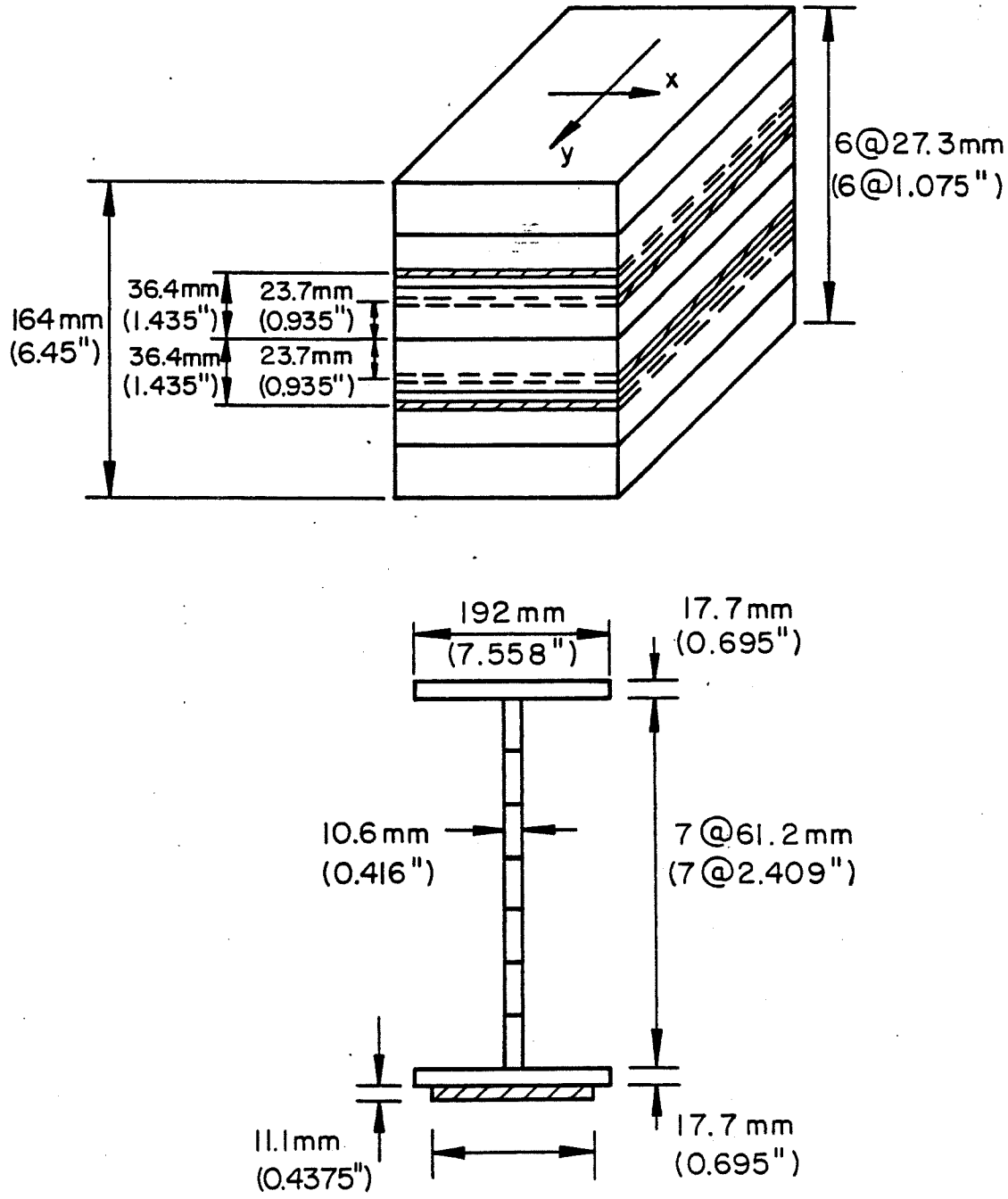

Fig. 21 Example No. 1 (AASHTO Bridge 3B)
Slab and Beam Layering

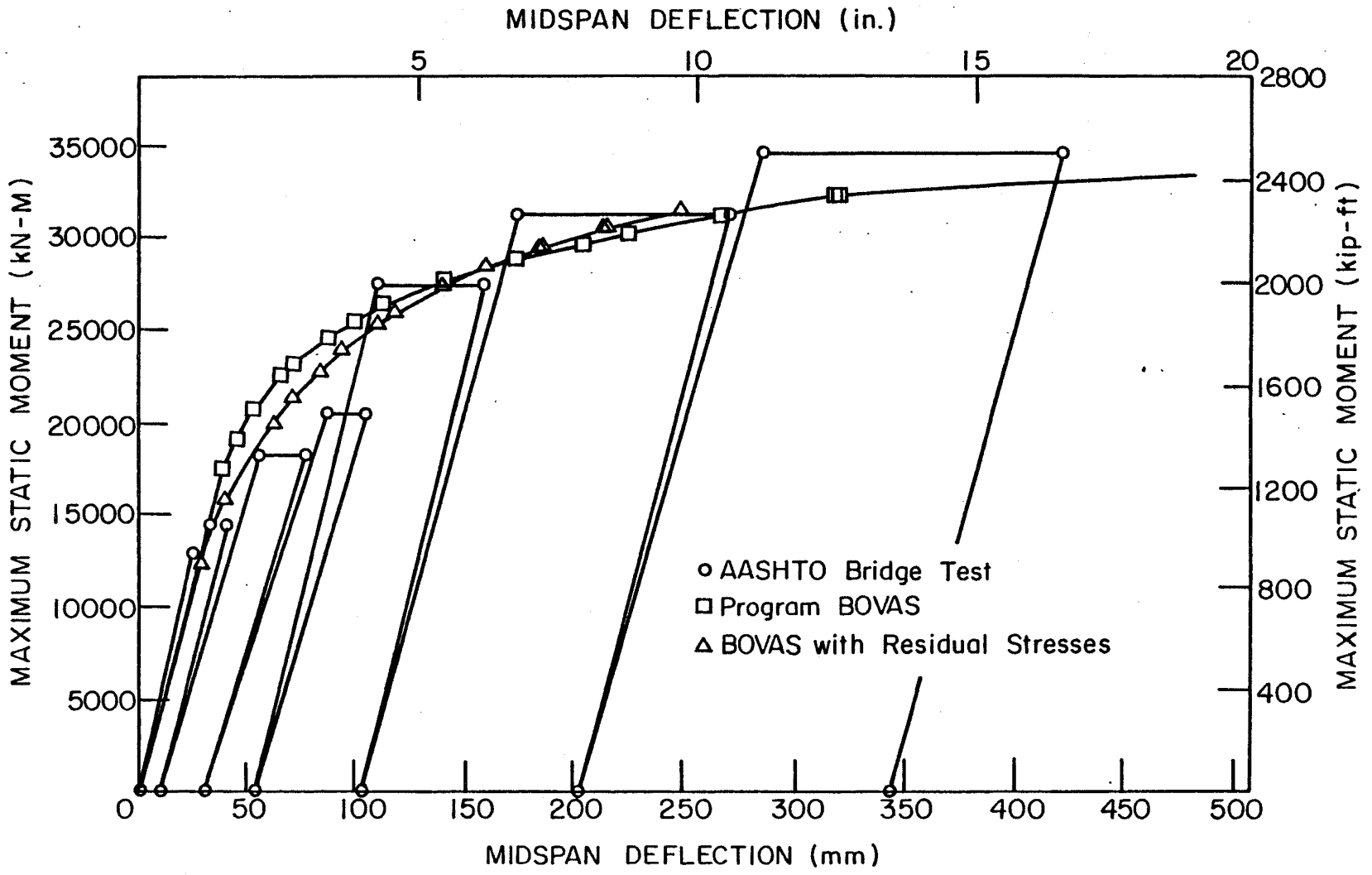

Fig. 22 Example No. 1 (AASHTO, Bridge 3B) - Moment versus Deflection Diagram

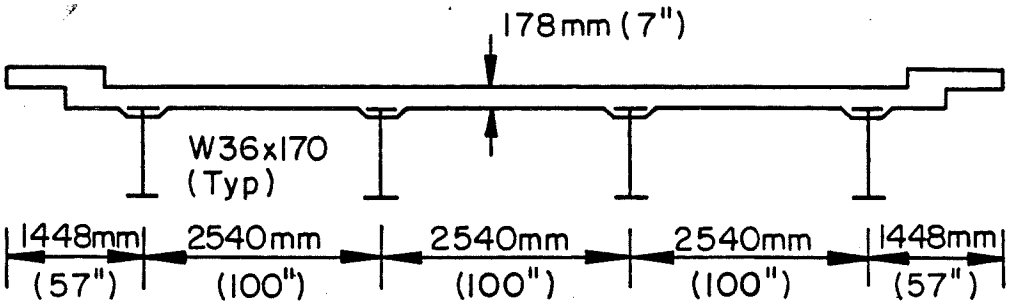

Fig. 23a Example No. 2 Actual Cross Section

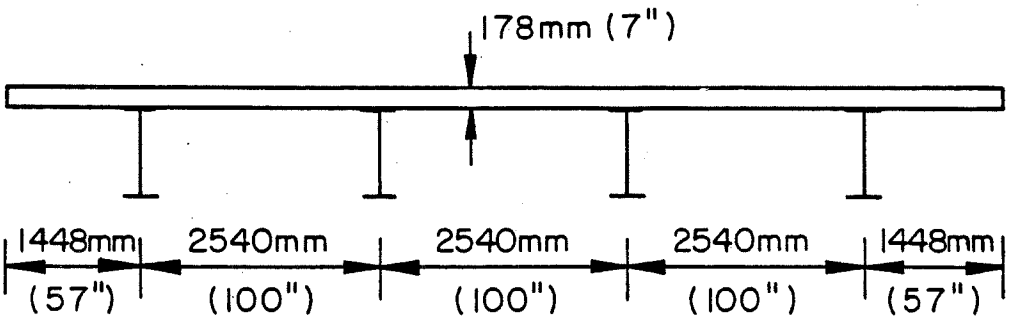

Fig. 23b Example No. 2 Idealized Cross Section

Fig. 23 Test Bridge, University of Tennessee

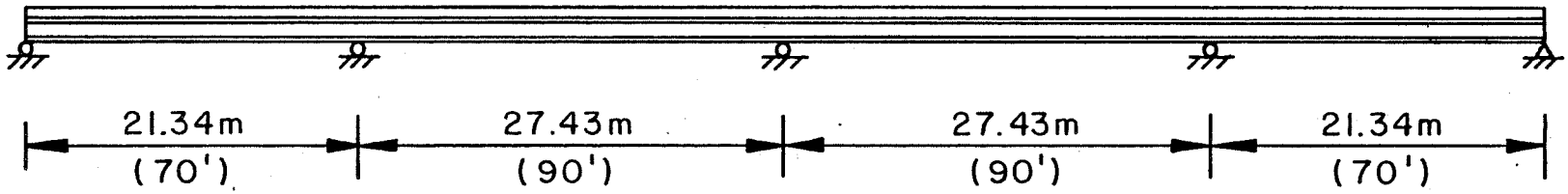

Fig. 24a Example No. 2 Elevation

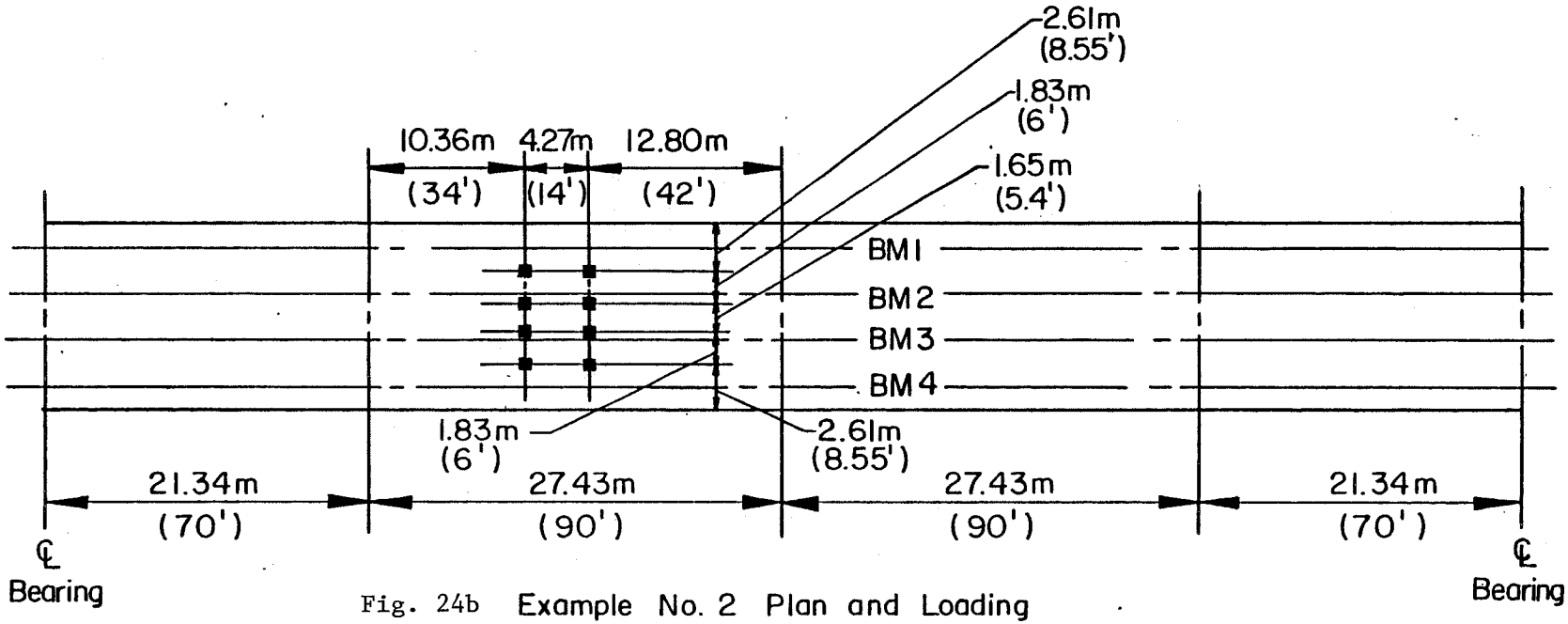

Fig. 24b Example No. 2 Plan and Loading

Fig. 24 Test Bridge, University of Tennessee

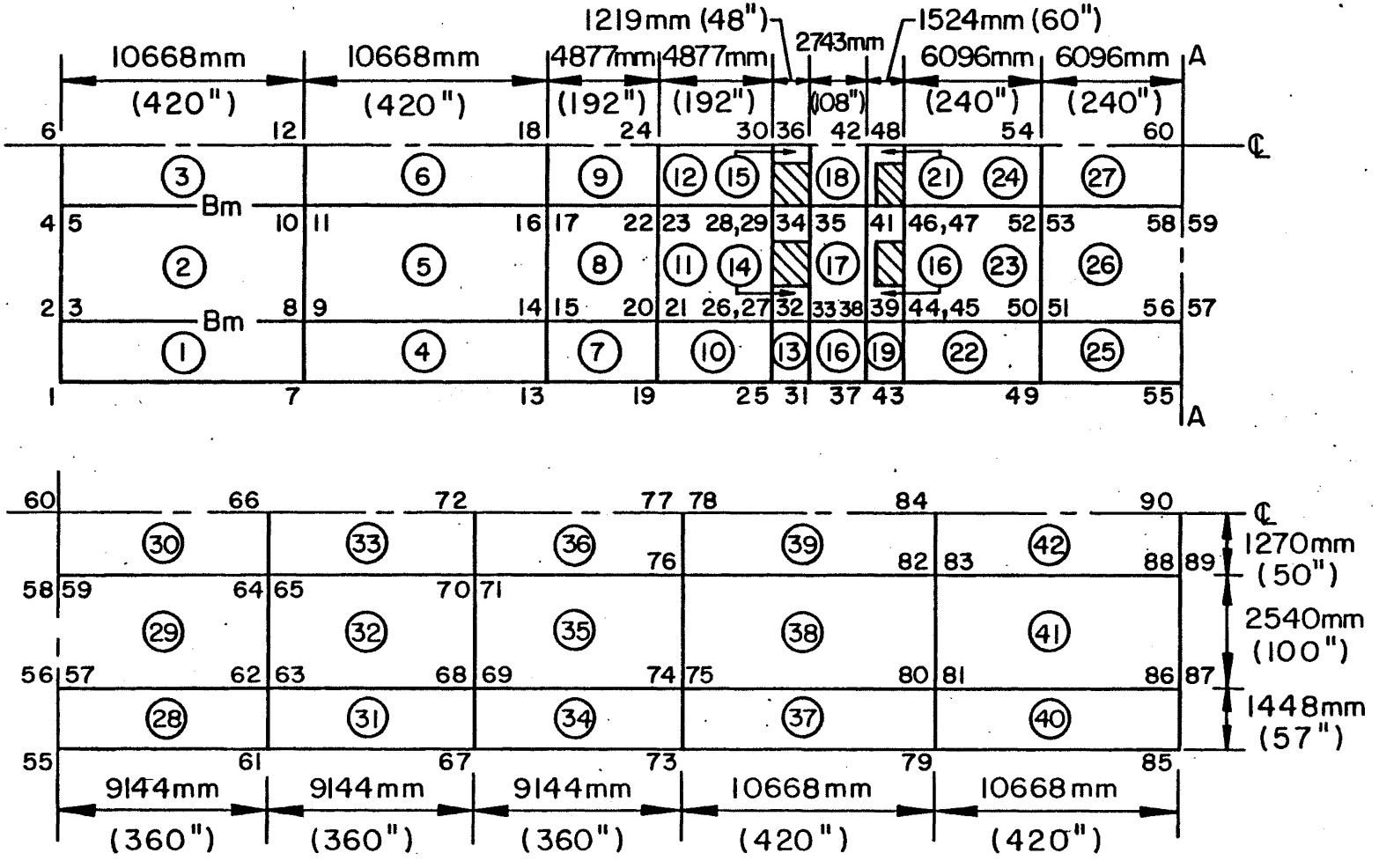

Fig. 25 Example No. 2 (University of Tennessee) - Finite Element Discretization

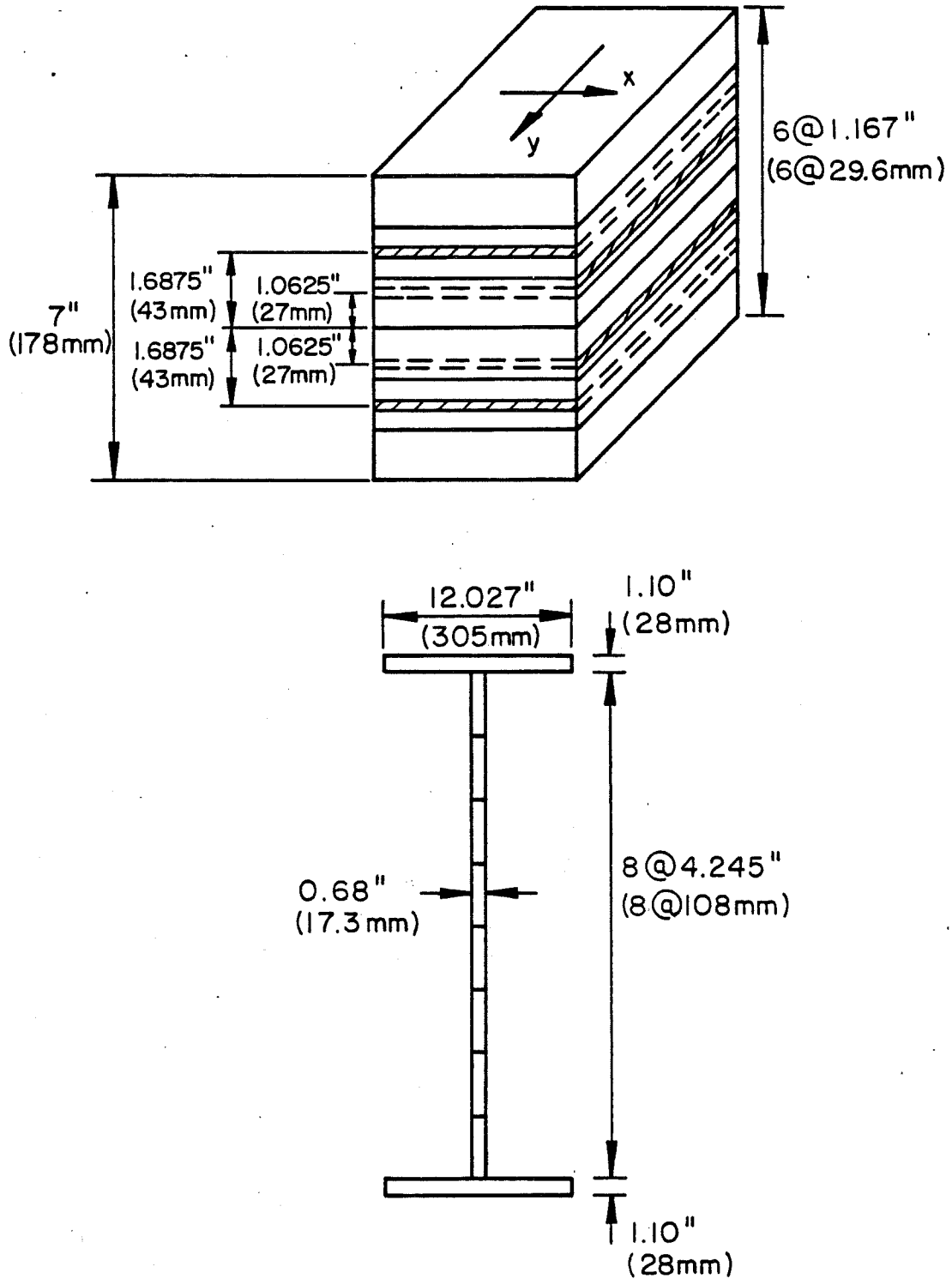

Fig. 26 Example No. 2 (University of Tennessee)
Slab and Beam Layering

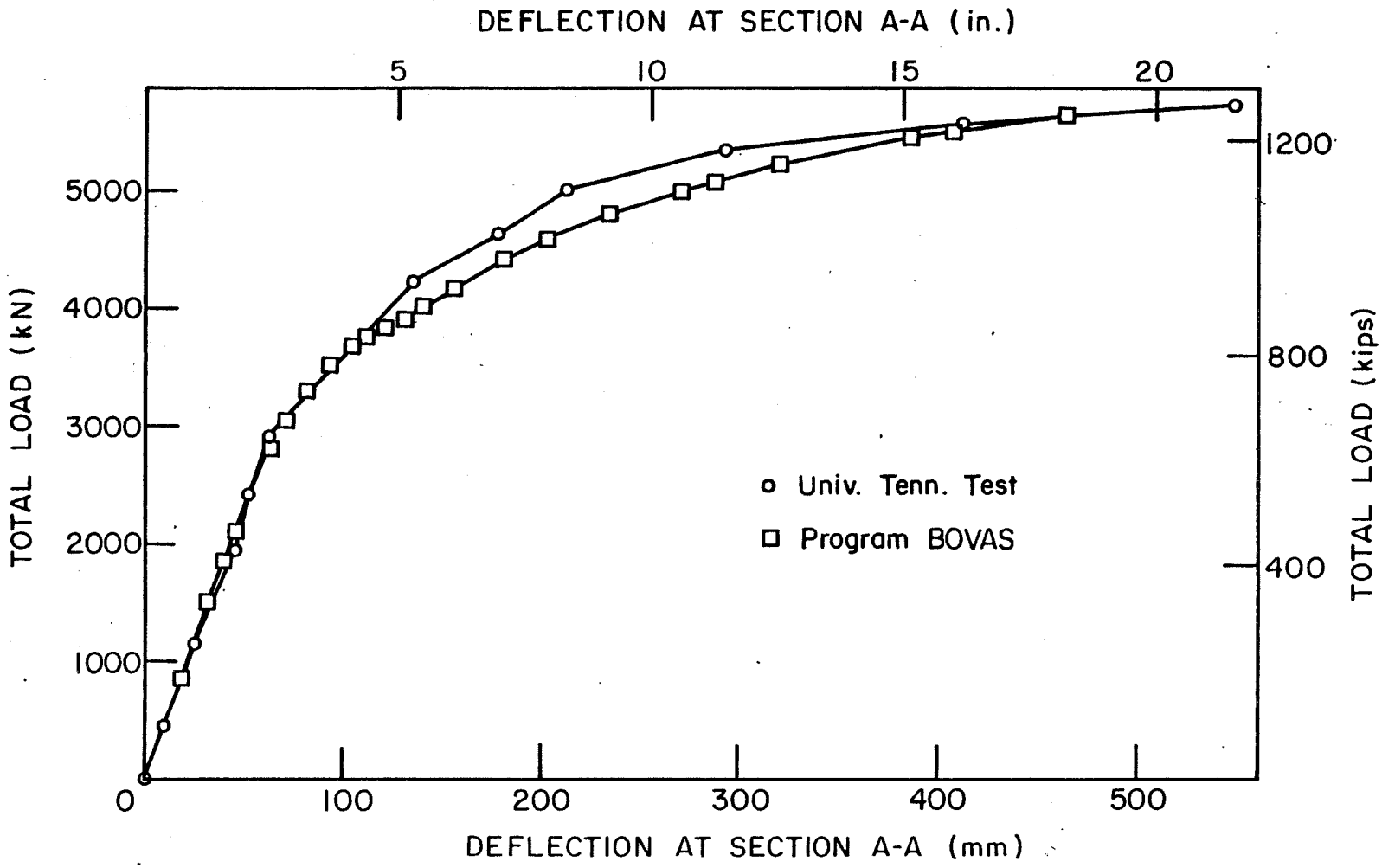

Fig. 27 Example No. 2 (University of Tennessee) - Load versus Deflection Curve

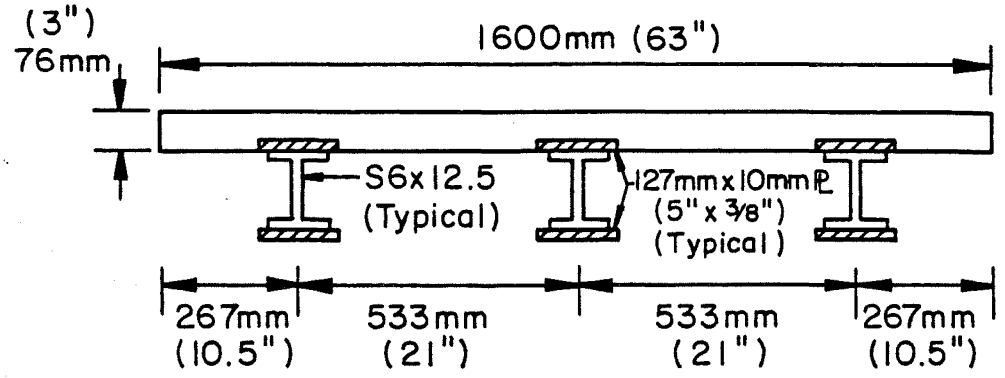

Fig. 28a Example No. 3 (University of Maryland)
Two Span Cross Section

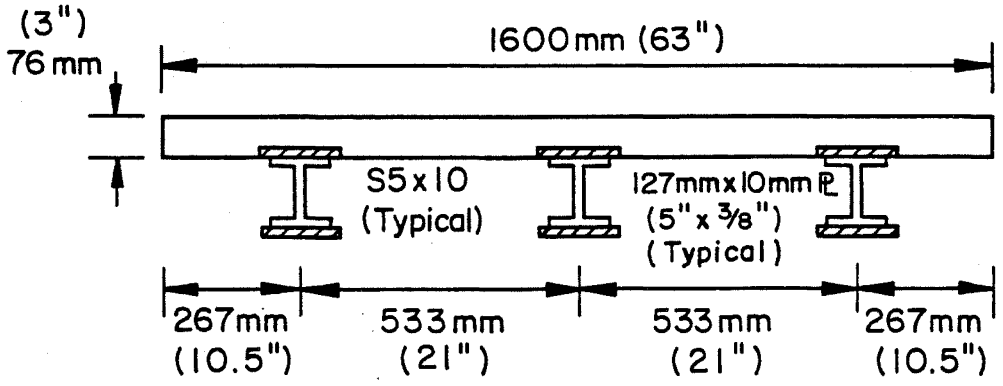

Fig. 28b Example No. 4 (University of Maryland)
Three Span Cross Section

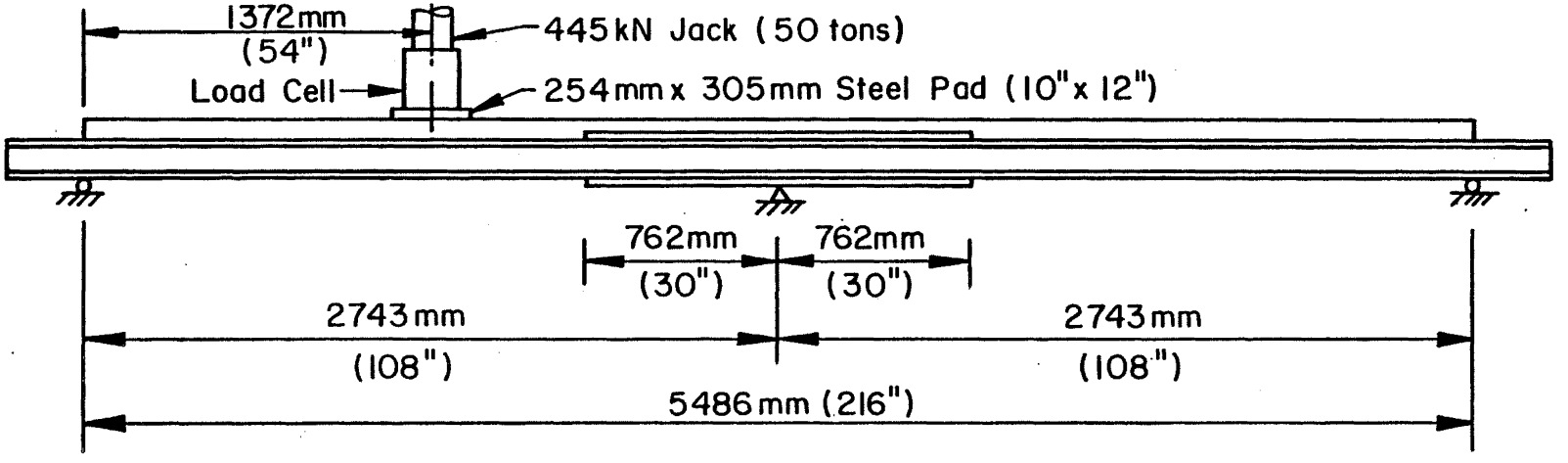

Fig. 29a Example No. 3 (University of Maryland) - Two Span Elevation

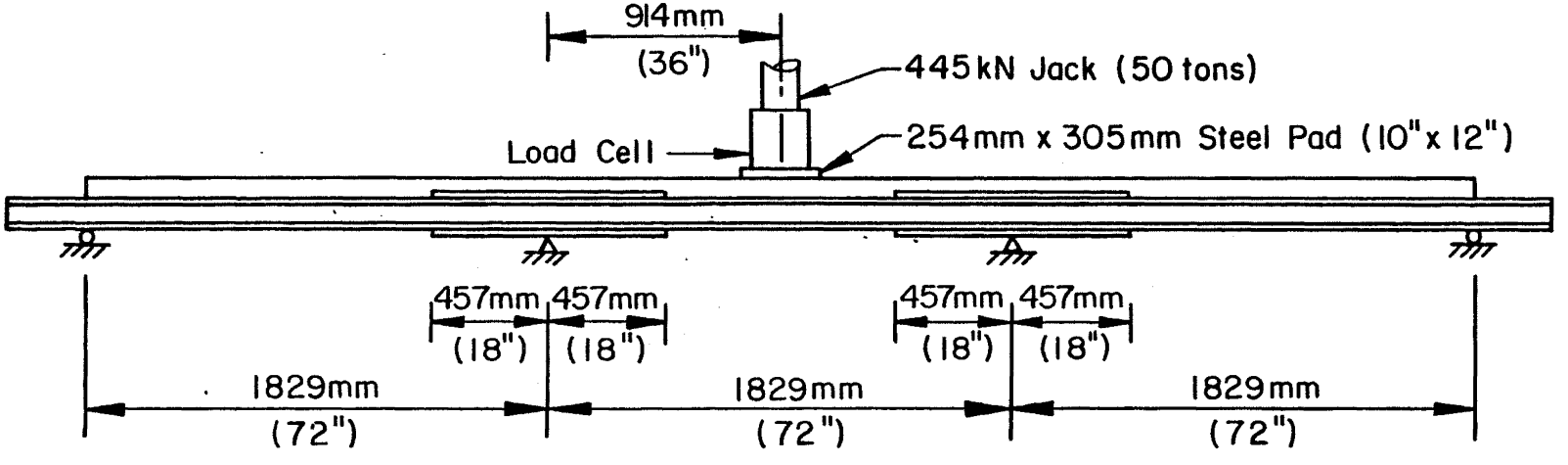

Fig. 29b Example No. 4 (University of Maryland) - Three Span Elevation

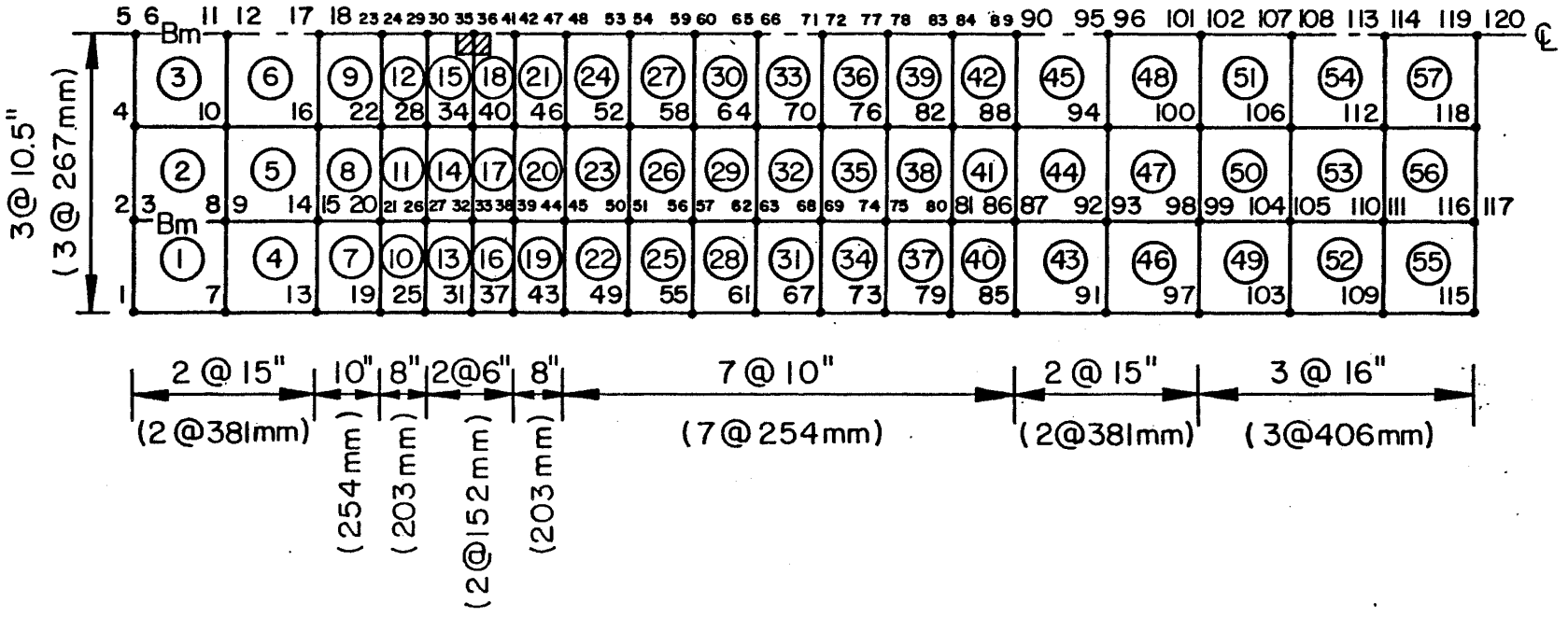

Fig. 30 Example No. 3 (University of Maryland) - Two Span Finite Element Discretization

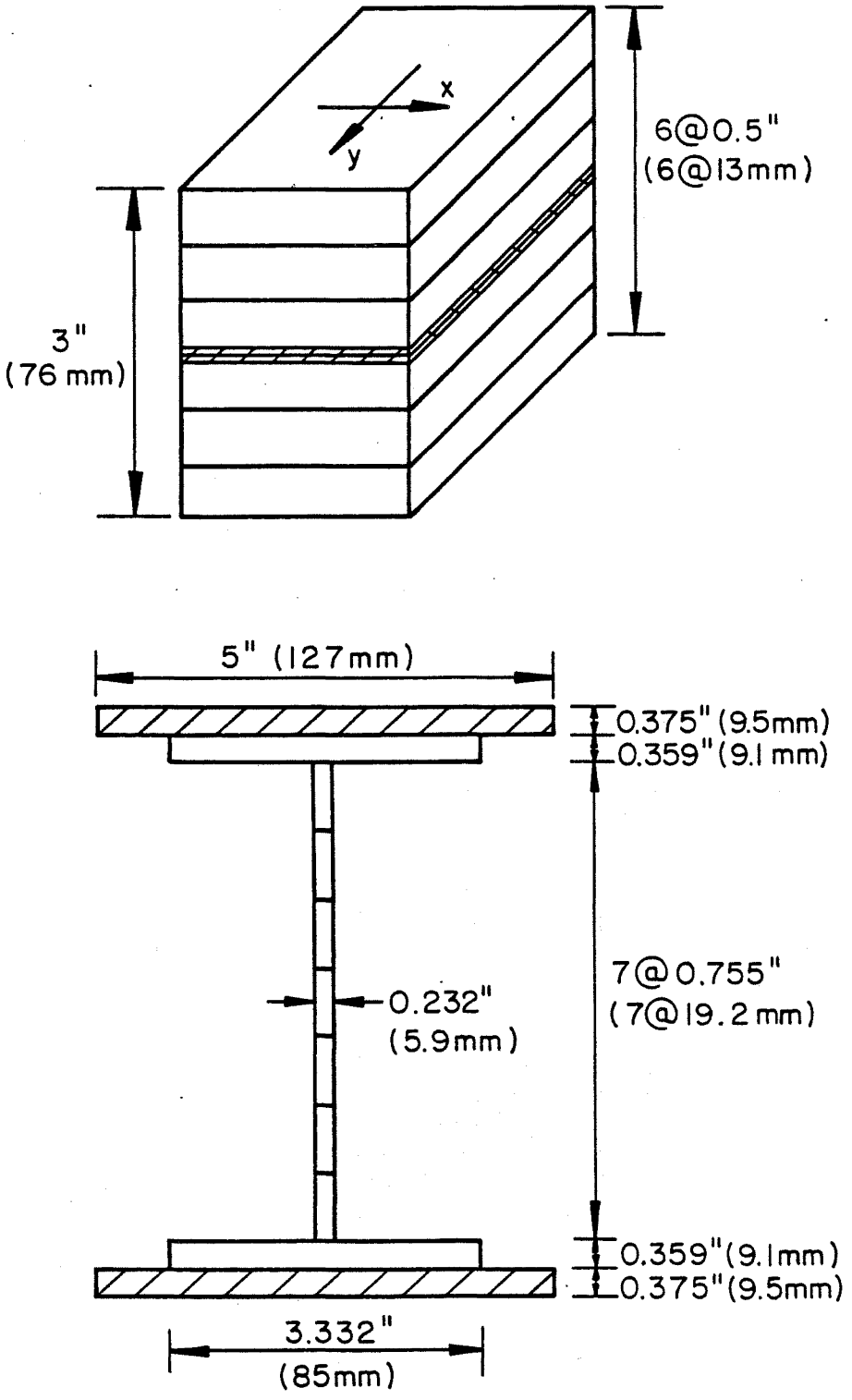

Fig. 31 Example No. 3 (University of Maryland)
Two Span Slab and Beam Layering

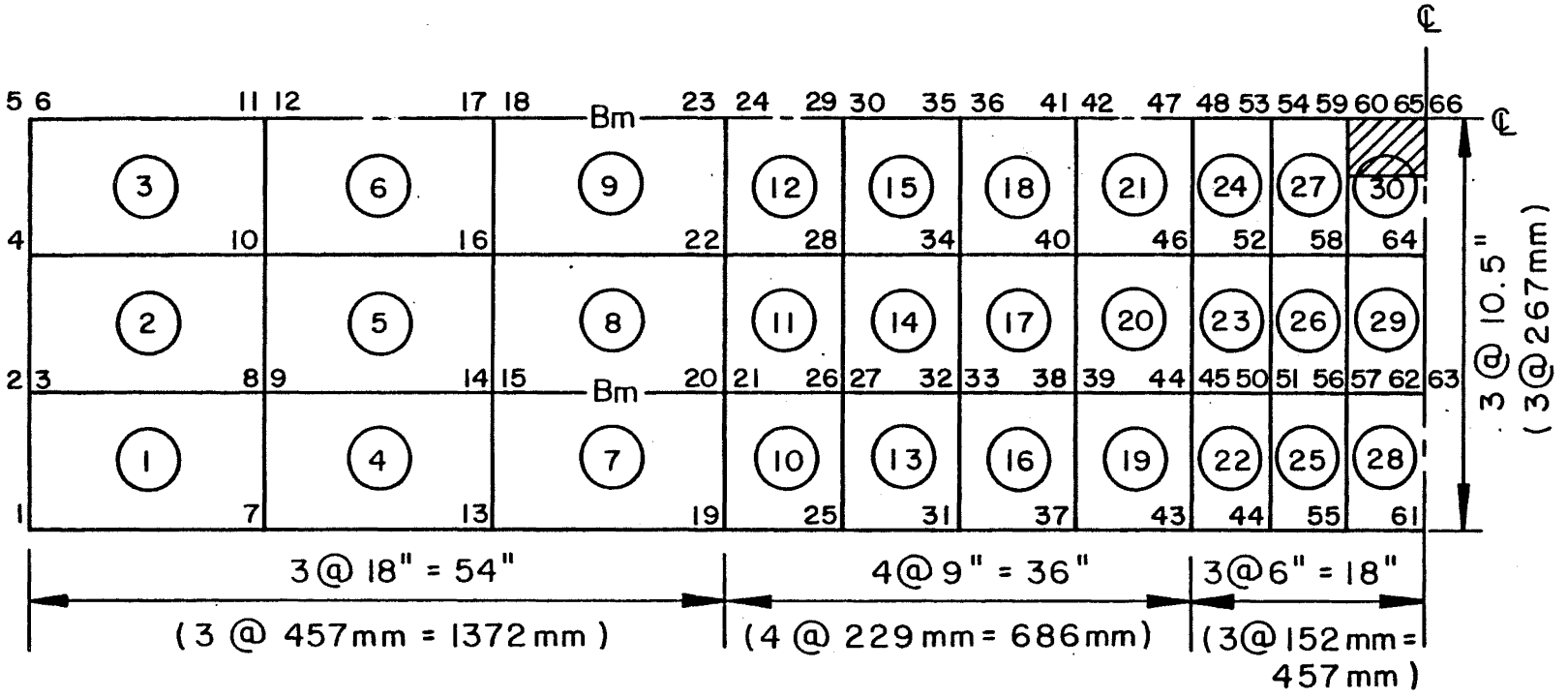

Fig. 32 Example No. 4 (University of Maryland) - Three Span Finite Element Discretization

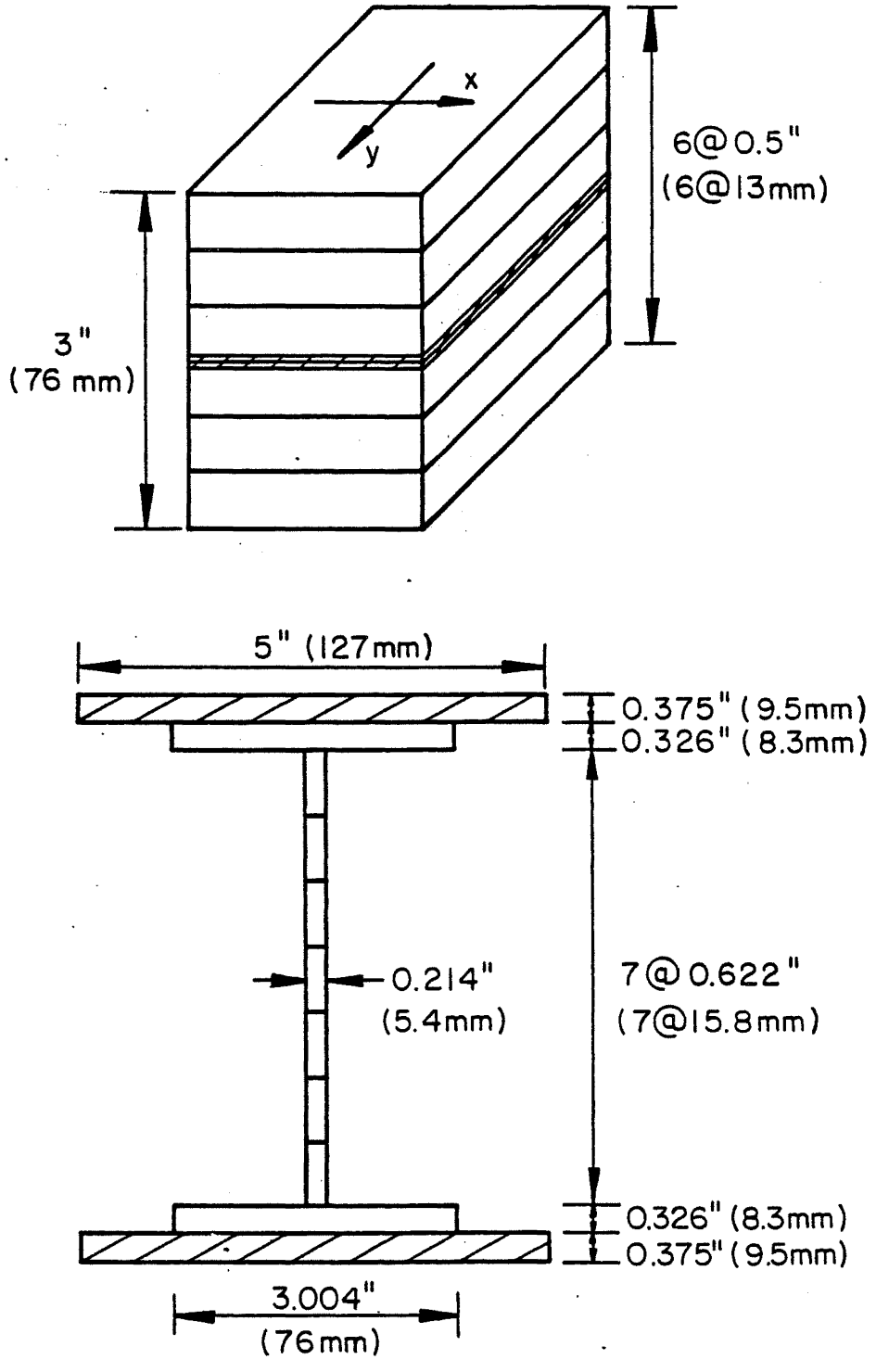

Fig. 33 Example No. 4 (University of Maryland)
Three Span Slab and Beam Layering

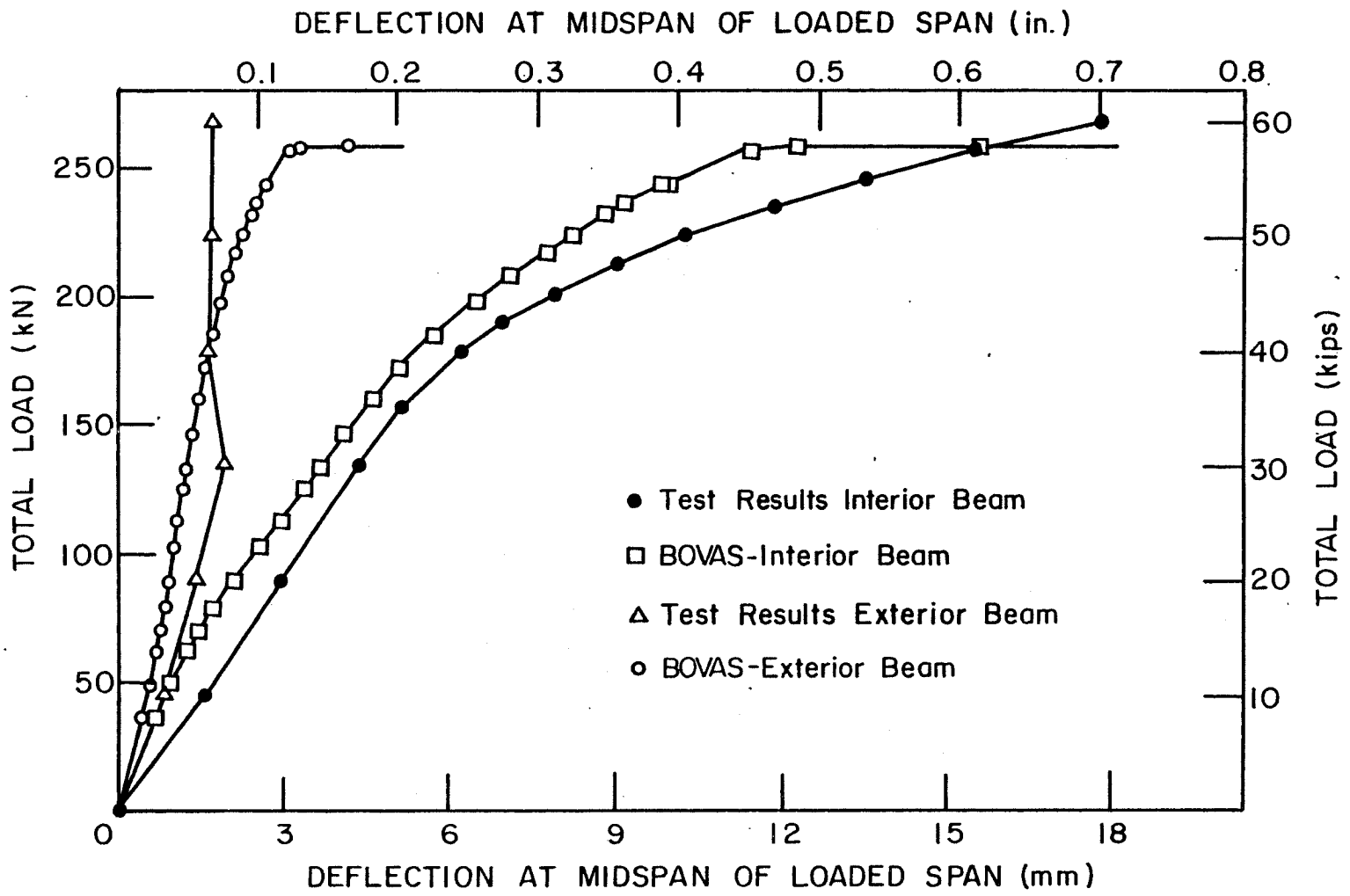

Fig. 34 Example No. 3 (University of Maryland) - Two Span Load versus Deflection Diagram for Interior and Exterior Beams

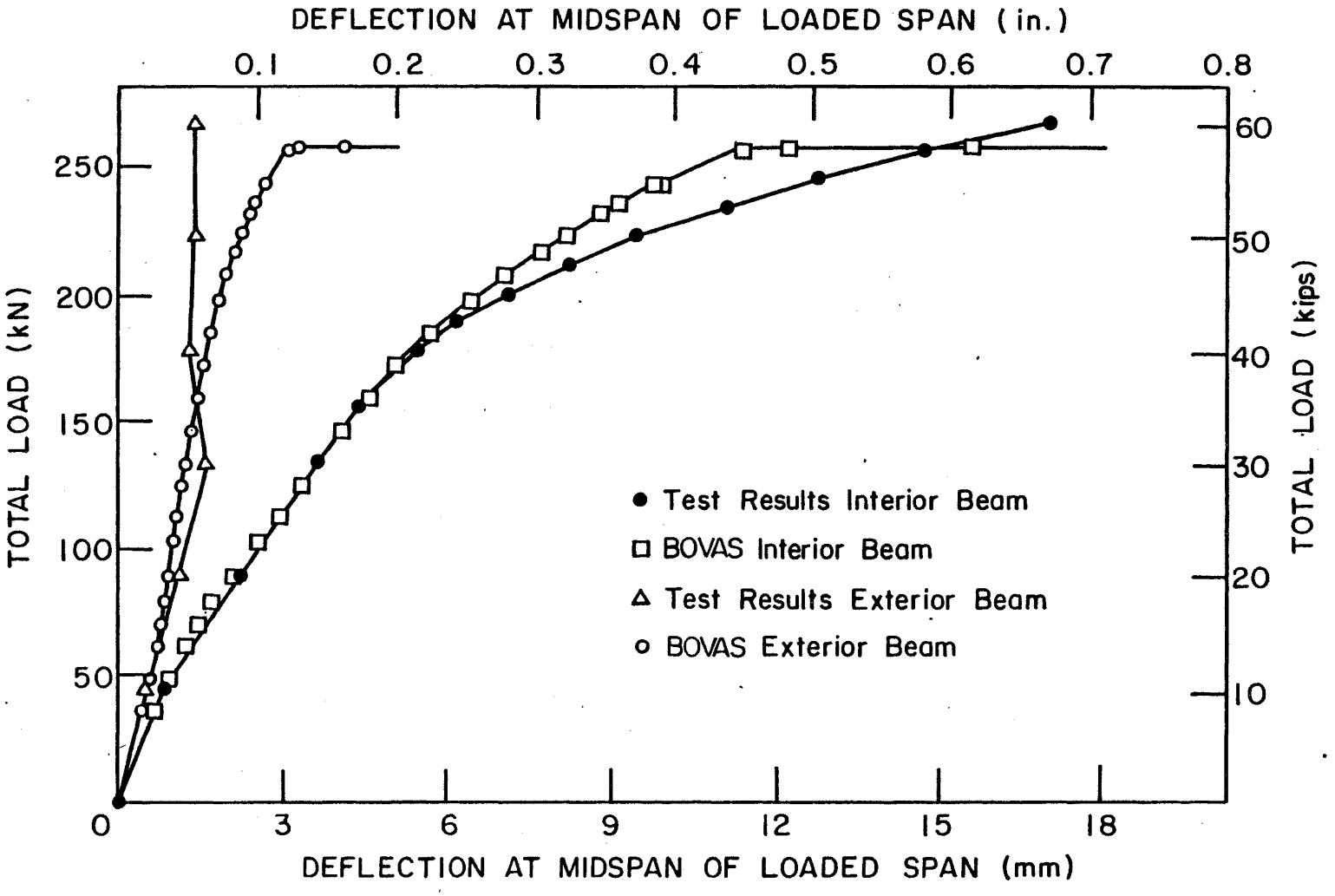

Fig. 35 Example No. 3 (University of Maryland) – Two Span Adjusted Load versus Deflection Diagram for Interior and Exterior Beams

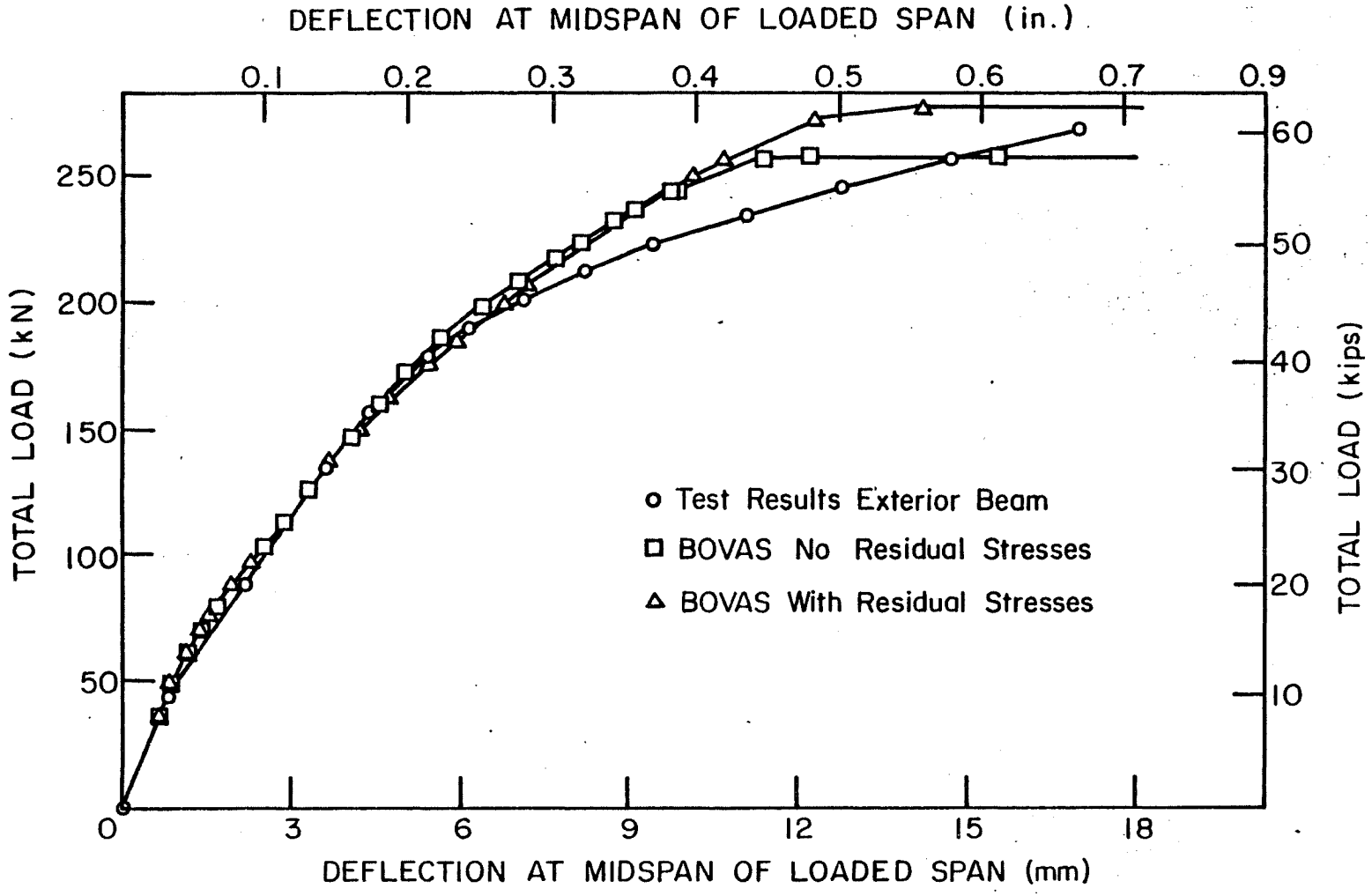

Fig. 36 Example No. 3 (University of Maryland) - Two Span Adjusted Load versus Deflection Diagram for Exterior Beam Including Effect of Residual Stresses

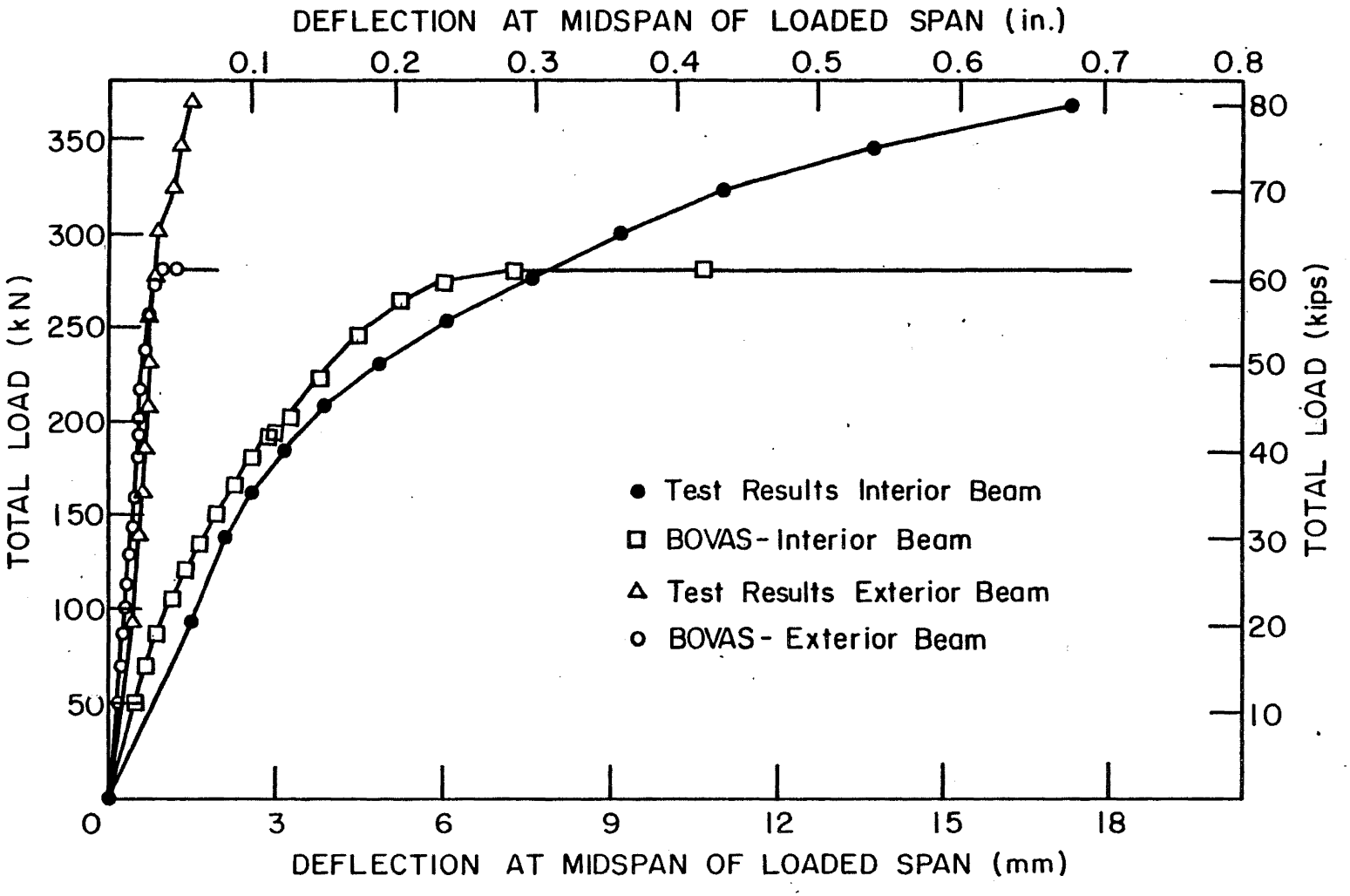

Fig. 37 Example No. 4 (University of Maryland) - Three Span Load versus Deflection Diagram for Interior and Exterior Beams

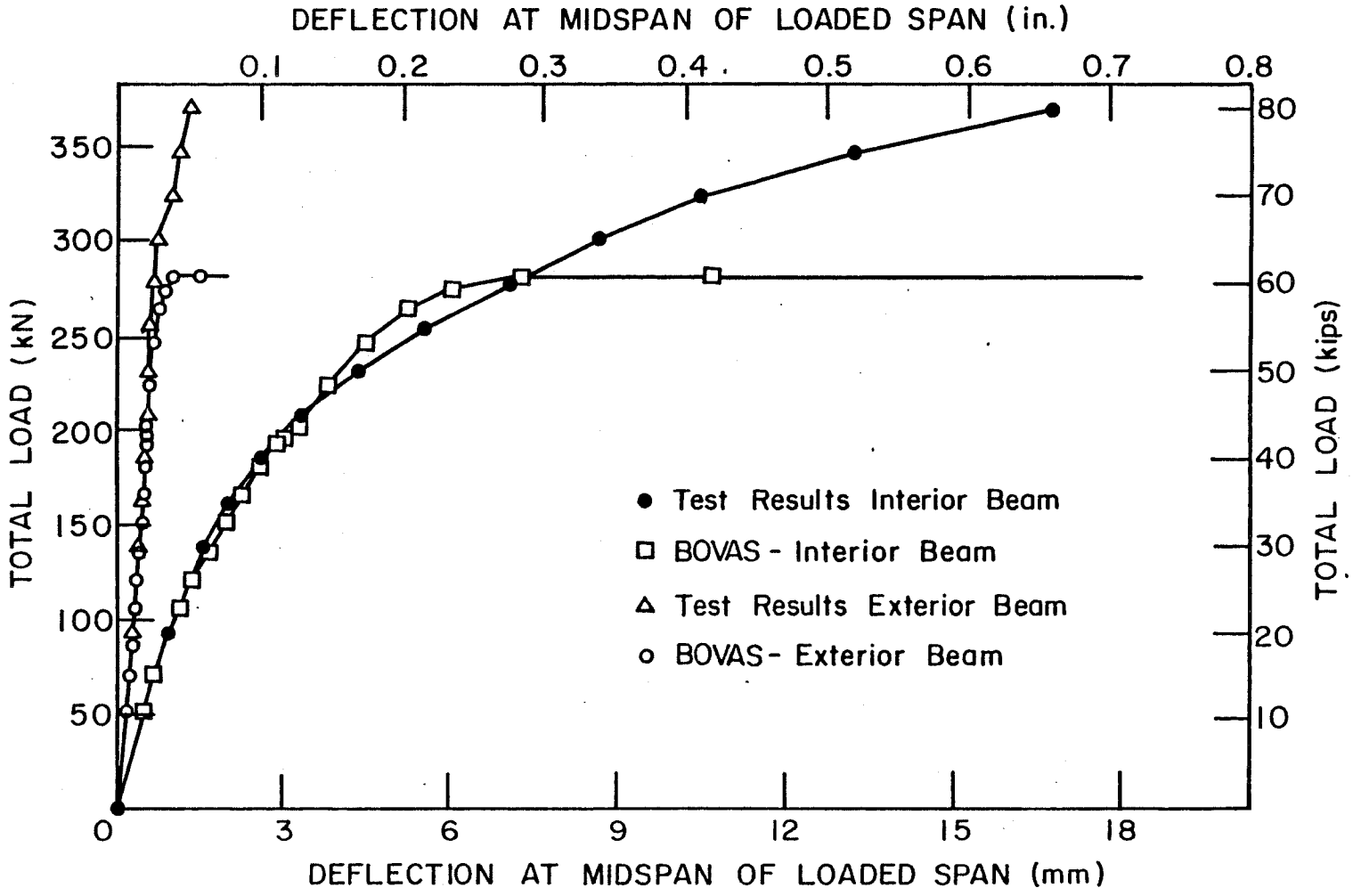

Fig. 38 Example No. 4 (University of Maryland) - Three Span Adjusted Load versus Deflection Diagram for Interior and Exterior Beams

NOMENCLATURE

NOMENCLATURE

A	=	Cross-sectional area
A_i	=	Layer area
A_s	=	Area of steel reinforcement in slab
A_{SB}	=	Effective shear area in beam
C,D	=	Curve parameters
C_E	=	Constant associated with shear connector stiffness, k_{sc}
$D_{11},D_{12},$ $D_{13},D_{22},$ D_{23},D_{33}	=	Components of the rigidity matrices
E	=	Modulus of Elasticity
EA	=	Axial rigidity (ExA)
EI	=	Flexural rigidity (ExI)
ES	=	Modulus of Elasticity x first moment of inertia (ExS)
E_C	=	Initial tangent modulus in uniaxial loading for concrete
E_{d_c}	=	Downward slope of concrete stress-strain curve for compression
E_{d_t}	=	Downward slope of the concrete stress-strain curve for tension
E_i	=	Initial modulus of elasticity for the Ramberg-Osgood stress-strain relationship

$(E)_i$ = Beam element layer stiffness

E_p = Tangent modulus at the peak stress

E_S = Initial modulus of elasticity for steel

E_{1b}, E_{2b} = Tangent moduli for the two principal stress directions

E'_{1b}, E'_{2b} = Tangent moduli for the principal stress directions employed in formulating $[\bar{D}]$

F = Generalized nodal forces

G = Shear modulus

I = Second moment of inertia

I,J,K,L = Nodal points for slab element

I_i = Moment of inertia for layer i about its centroid

J1 = Parameter in beam element formulation

L = Beam element length

M = Moment

N = Axial Force

S = First moment of inertia for beam

U = Axial displacement for beams or in-plane displacement in x-direction for plate

U_Z = In-plane or axial displacement in x-direction at depth z

V = In-plane displacement in y-direction for plate

V_B = Shear in beam

V_Z = In-plane displacement in y-direction for plate at depth z

W = Displacement in z direction

Z_i, Z_{i+1} = Layer boundaries for layer i measured from the reference plane in the vertical direction

$\bar{Z}$ = Vertical distance between reference planes for slab and beam

$\bar{Z}_i$ = Centroid location of layer i measured from reference plane in the vertical direction

$\bar{Z}_{iA}, \bar{Z}_{iB}$ = Vertical distances from reference plane for slab (A) and for beam (B) to the plane of intersecting two element

$\bar{Z}_A, \bar{Z}_B$ = Vertical distances from reference plane for slab (A) and for beam (B) to their respective centroids

a, b = Slab element half lengths

$a_i, \bar{a}_j$ = Coefficients in polynomials for vertical displacement fields, $i = 1,\ldots,12$, $j = 1,\ldots,4$

$b_i, \bar{b}_j, c_j$ = Coefficients in polynomials for in-plane and axial displacement fields, $i = 1,\ldots,8$, $j = 1,\ldots,3$

b_s = Reinforcing bar spacing for slab

C_{tb} = Distance from centroid of beam to top of beam

C_{bA} = Distance from centroid of slab to bottom of slab

d_i = Coefficients in polynomials for rotation field in beam $i = 1,\ldots 3$

f_c' = Representative uniaxial compressive cylinder strength for concrete

f_t = Direct tensile strength for concrete

f_y = Yield strength steel

$k_{uu}, k_{u\phi}, k_{\phi\phi}$ = Slab element submatrices

$k_{Bb}, k_{ss}, k_{\Delta}$ = Beam element submatrices

k_{sc} = Stiffness of uniform medium used to model shear connectors

m,n = Parameters used in Ramberg-Osgood stress-strain relationship

s = Shear flow at interface

t_s = Equivalent thickness of a reinforcing bar layer for the slab

x,y = Local cartesian coordinates

x_n, y_n = Nodal point coordinates

z = Vertical distance from reference plane

α = The stress ratio or the ratio a/b

α_1 = The stress ratio for principal direction 1, σ_2/σ_1

α_2 = The stress ratio for principal direction 2, σ_1/σ_2

β = The ratio b/a

$(\gamma_{xy})_z$ = Shear strain at depth Z

$\dot{\gamma}$ = Shear strain increment

γ_B = Shear strain in beam

ε = Strain in principal stress direction

ε_p = The concrete strain at peak stress

$\varepsilon_{p1}, \varepsilon_{p2}$ = Concrete strains at the peak stress for the two principal stress directions

$\varepsilon_t, \varepsilon_c$ = Peak strains for uniaxially stressed concrete in tension and compression respectively

$\dot{\varepsilon}_x, \dot{\varepsilon}_y, \dot{\gamma}_{xy}$ = Normal and shear strain increments in the x-y coordinate system

$\varepsilon_1, \varepsilon_2$ = Strains in principal stress directions

θ = Angle which defines principal stress directions

θ_x, θ_y = Rotations about x and y axes

θ_A, θ_B = Rotations for slab and beam respectively

ν = Poisson's ratio

ν_1, ν_2 = Poisson's ratio in principal directions

σ = A principal stress

σ_p = The peak stress in a principal direction

σ_{p1}, σ_{p2} = The peak stress for the two principal directions

σ_s = Secant yield strength used in Ramberg-Osgood stress-strain relationship

$\dot{\sigma}_x, \dot{\sigma}_y, \dot{\tau}_{xy}$ = Normal and shear stress increments in x-y coordinate system

$\sigma_x, \sigma_y, \tau_{xy}$ = Normal and shear stresses in x-y coordinate system

σ_1, σ_2 = Stresses in principal directions

$\dot{\tau}$ = Shear stress increment

Matrices

$[B]$, $[B_U][B_\phi]$, $[B_B]_b[B_B]_s$, $[B]_\Delta$ = Strain displacement matrices

$[C]$ = Matrix relating polynomial coefficients to element node displacement using compatibility and constraining equations

$[C1]$, $[C1_u]$, $[C1_\phi]$ = Compatibility matrices = $[P(x,y)]$ evaluated at nodes

$[C2]$ = Matrix of constraining equations

$[CA]$,$[CB]$ = Coefficient-displacement matrices for axial fields in beam and slab

$[CC]$ = Coefficient-displacement matrix for all displacement fields

$[CD]$ = Coefficient-displacement matrix for rotation field

$[CW]$ = Coefficient-displacement matrix for vertical displacement field

$[D]$ = Elasticity matrix based on current state of stress which relates the stress increment to strain increment in x-y coordinate system

$[D_i]$ = Elasticity matrix for layer i

$[D_{uu}]$, $[D_{u\phi}]$, $[D_{\phi\phi}]$ = In-plane, coupling, and bending rigidity matrices respectively

$[\bar{D}]$ = Elasticity matrix in the principal stress space

$\{F\}$ = Vector of generalized nodal forces

$\{f\}$, $\{\Delta(xy)\}$ = Vector of shape functions

$[K]$ = Global stiffness matrix

$[K_1],\ldots [K_6]$ = Component matrices of the slab stiffness matrix

$[k]^e$ = Element stiffness matrix

$[k_{uu}]^e$ = In-plane stiffness matrix for slab element

$[k_{u\phi}]^e$ = Coupling stiffness matrix for slab element

$[k_{\phi\phi}]^e$ = Bending stiffness matrix for slab element

$[k_B]_b^e$ = Axial and bending stiffness matrix for beam element

$[k_B]_s^e$ = Shearing stiffness matrix for beam element

$[k]_\Delta^e$ = Slip stiffness matrix for beam element

$[N]$ = Matrix defining shape functions

$[P(x,y)]$ = Polynomial functions used to describe the displacement field

$[Q], [Q_u], [Q_\phi]$ = A connection matrix relating strains within an element to the constant coefficients of the displacement field

$[S]$ = A coordinate transformation for curvatures

$[T]$ = Use to transform the elasticity relation from the principal to the x-y coordinate system

$\{\alpha\}$ = Vector of polynomial coefficients

$\{\varepsilon\}$ = Vector of strains

$\{\dot{\varepsilon}\}$ = Vector of incremental strains

$[\Gamma]$ = Operator matrix to compute strains from the displacement fields

$\{\delta\}$ = Vector of generalized node displacements

$\{\dot{\delta}\}$ = Vector of incremental generalized node displacements

$\{\sigma\}$ = Vector of stresses

$\{\dot{\sigma}\}$ = Vector of incremental stresses

$\{\bar{\sigma}_i\}$ = Vector of integrated average stress for layers

Notes:

1. The use of subscripts u, ϕ, b, s, and d on matrices indicates that the matrix is derived from the consideration of in-plane deformations (u), bending deformations (ϕ), axial and bending deformations (b), shear deformations (s), and slip (Δ).

2. The use of the subscripts uu, $u\phi$, and $\phi\phi$ on matrices indicates that the matrix is derived from the consideration of in-plane deformations (uu), coupling deformations ($u\phi$), and bending deformations ($\phi\phi$).
3. The use of the subscripts A and B used alone indicates the parameter is associated with either the plate (A) or the beam (B).
4. The use of L or M as a subscript indicates that the quantity is at node L or M.
5. The use of ('), primes, indicates quantities expressed in skew coordinates.
6. The use of superscript, e, on vectors or matrices indicates that the quantities are applicable to the element.
7. The use of 1,2 as subscripts indicates that the quantities are with respect to the directions of principle stress.
8. A ($\cdot$) dot used over any term indicates an incremental quantity.

REFERENCES

REFERENCES

1. Adini, A. and Clough, R. W.
   ANALYSIS OF PLATE BENDING BY THE FINITE ELEMENT METHOD, Report submitted to the National Science Foundation, Grant G7337, University of California, Berkeley, California, 1960.

2. American Society of Civil Engineers
   COMPOSITE STEEL-CONCRETE CONSTRUCTION, Report of the Subcommittee on the State-of-the-Art Survey of the Task Committee on Composite Construction of the Committee on Metals of the Structural Division, Journal of the Structural Division, ASCE, Vol. 100, ST5, May 1974.

3. Armen, H. Pifko and Levine, H. S.
   FINITE ELEMENT ANALYSIS OF STRUCTURES IN PLASTIC RANGE, NASA Contractor Report NASA CR-1649, National Aeronautics and Space Administration, Washington, D.C., 1971.

4. Baldwin, J. W., Jr., Henry, J. R. and Sweeney, C. M.
   STUDY OF COMPOSITE BRIDGE STRINGERS, PHASE II, University of Missouri, Columbia, May 1965.

5. Barnard, P.R.
   RESEARCHES INTO THE COMPLETE STRESS-STRAIN CURVE FOR CONCRETE, Magazine of Concrete Research, Vol. 16, No. 49, December 1964.

6. Bathe, K. J., Wilson, E. L. and Peterson, F. E.
   SAPIV - A STRUCTURAL ANALYSIS PROGRAM FOR STATIC AND DYNAMIC RESPONSE OF LINEAR SYSTEMS, Report EERC 73-11, University of California, Berkeley, June 1973, revised, April 1974.

7. Beedle, L. S. and Tall, L.
   BASIC COLUMN STRENGTH, PROC. ASCE, Vol. 86, No. ST7, July 1960.

8. Butzler, P. W., Colville, J. and Heins, C. P.
   ULTIMATE LOAD TESTS OF CONTINUOUS COMPOSITE-BRIDGE MODELS, Civil Engineering Report No. 61, University of Maryland, College Park, Maryland, June 1976.

9. Butzler, P. W. and Colville, J.
   CONTINUOUS COMPOSITE-BRIDGE MODEL TESTS, Journal of Structural Division, ASCE, Vol. 105, No. ST9, September 1979.

10. Burdette, E. G. and Goodpasture, D. W.
    FINAL REPORT ON FULL SCALE BRIDGE TESTING - AN EVALUATION OF BRIDGE DESIGN CRITERIA, University of Tennessee, 1971.

11. Clough, R. W.
THE FINITE ELEMENT METHOD IN STRUCTURAL MECHANICS, Chapter 7, of Stress Analysis, edited by O. C. Zienkiewicz and G. S. Hollister, John Wiley and Sons, New York, New York, 1965.

12. Dai, P. K., Thiruvengadam, T. R. and Siess, C. P.
INELASTIC ANALYSIS OF COMPOSITE BEAMS, Engineering Extension Series No. 15, Proceedings of the ASCE Specialty Conference on Steel Structures, University of Missouri, Columbia, June 8-12, 1970.

13. Doyle, S. K. and Burdette, E. G.
A COMPARISON OF MEASURED AND COMPUTED LOAD DEFLECTION RELATIONSHIPS FOR FOUR HIGHWAY BRIDGES, The University of Tennessee, March 1972.

14. du Plessis, D. P.
INTERACTION OF FLOORS AND FRAMES IN MULTISTORY BUILDINGS, Ph.D. Dissertation, Lehigh University, Bethlehem, Pennsylvania, 1974.

15. Engineering News Record
BRIDGE CRISES, Engineering News Record, Vol. 198, No. 10, March 10, 1977.

16. Evans, R. H. and Marathe, M. S.
MICROCRACKING AND STRESS-STRAIN CURVES FOR CONCRETE IN TENSION, Materiaux et Constructions, Vol. 1, Janvier - Février 1968.

17. Fu, C. C., Colville, J. and Heins, C. P.
INELASTIC ANALYSIS OF CONTINUOUS COMPOSITE HIGHWAY BRIDGES, Civil Engineering Report No. 62, University of Maryland, College Park, Maryland, June 1976.

18. Gustafson, W. C. and Wright, R. N.
ANALYSIS OF SKEWED COMPOSITE GIRDER BRIDGES, Journal of the Structural Division, ASCE, Vol. 94, ST4, April 1968.

19. Hand, F. R., Pecknold, D. A. and Schnobrich, W. C.
A LAYERED FINITE ELEMENT NONLINEAR ANALYSIS OF REINFORCED CONCRETE PLATES AND SHELLS, Civil Engineering Studies, Structural Research Series No. 389, University of Illinois, Urbana, Illinois, August 1972.

20. Hand, F. R., Pecknold, D. A. and Schnobrich, W. C.
NONLINEAR LAYERED ANALYSIS OF RC PLATES AND SHELLS, Journal of the Structural Division, ASCE, Vol. 99, No. ST7, July 1973.

21. Heins, C. P. and Colville, J.
LOAD FACTOR DESIGN RECOMMENDATIONS FOR STEEL I BEAM COMPOSITE HIGHWAY BRIDGES, Civil Engineering Report No. 63, University of Maryland, College Park, Maryland, September 1976.

22. Highway Research Board
THE AASHO ROAD TEST, Report 2, MATERIALS AND CONSTRUCTION, Special Report 61B, 1962.

23. Highway Research Board
THE AASHO ROAD TEST, Report 4, BRIDGE RESEARCH, Special Report 61D, 1962.

24. Highway Research Board
OVERSIZE-OVERWEIGHT PERMIT OPERATION ON STATE HIGHWAYS, National Cooperative Highway Research Program Report 80, 1969.

25. Hsu, T. T. C., Slate, F. O., Stuman, G. M. and Winter, G.
MICROCRACKING OF PLAIN CONCRETE AND THE SHAPE OF THE STRESS-STRAIN CURVE, Journal of the American Concrete Institute, Vol. 60, No. 2, February 1963.

26. Hughes, B. P. and Chapman, G. P.
THE COMPLETE STRESS-STRAIN CURVE FOR CONCRETE IN DIRECT TENSION, BULLETIN RILEM, No. 30, March 1966.

27. Johnson, R. P.
RESEARCH ON STEEL-CONCRETE COMPOSITE BEAMS, Journal of Structural Division, ASCE, Vol. 96, ST3, March 1970.

28. Johnston, B. G., editor
GUIDE TO STABILITY DESIGN CRITERIA FOR METAL STRUCTURES, 3rd Edition, John Wiley & Sons, New York, New York, 1976.

29. Kulicki, J. M. and Kostem, C. N.
THE INELASTIC ANALYSIS OF REINFORCED AND PRESTRESSED CONCRETE BEAMS, Fritz Engineering Laboratory Report No. 378B.1, Lehigh University, Bethlehem, Pennsylvania, November 1972.

30. Kulicki, J. M. and Kostem, C. N.
USER'S MANUAL FOR PROGRAM BEAM, Fritz Engineering Laboratory Report No. 378B.2, Lehigh University, Bethlehem, Pennsylvania, February 1973.

31. Kulicki, J. M. and Kostem, C. N.
FURTHER STUDIES ON THE NONLINEAR FINITE ELEMENT ANALYSIS OF BEAMS, Fritz Engineering Laboratory Report No. 378A.5, Lehigh University, Bethlehem, Pennsylvania, April 1973.

32. Kulicki, J. M. and Kostem, C. N.
THE INELASTIC ANALYSIS OF PRESTRESSED AND REINFORCED CONCRETE BRIDGE BEAMS BY THE FINITE ELEMENT METHOD, Fritz Engineering Laboratory Report No. 378A.6, Lehigh University, Bethlehem, Pennsylvania, September 1973.

33. Kupfer, H., Hilsdorf, H. K., and Rusch, H.
BEHAVIOR OF CONCRETE UNDER BIAXIAL STRESSES, Journal of the American Concrete Institute, Vol. 66, No. 8, August 1969.

34. Lin, C. S.
NONLINEAR ANALYSIS OF REINFORCED CONCRETE SLABS AND SHELLS, Ph.D. Dissertation, University of California, Berkeley, California, September 1972.

35. Liu, T. C.
STRESS-STRAIN RESPONSE AND FRACTURE OF CONCRETE IN BIAXIAL COMPRESSION, Ph.D. Dissertation, Structural Engineering Department, Cornell University, Ithaca, New York, 1971.

36. Liu, T. C., Nilson, A. H. and Slate, F. O.
BIAXIAL STRESS-STRAIN RELATIONS FOR CONCRETE, Journal of Structural Division, ASCE, Vol. 98, No. ST5, May 1972.

37. Neilissen, L. J. M.
BIAXIAL TESTING OF NORMAL CONCRETE, HERON, Vol. 18, No. 1, 1972, Stevin-Laboratory of the Department of Civil Engineering of the Technological University and Institute TNO for Building Materials and Building Structures, Delft, The Netherlands.

38. Newmark, N. M.
A DISTRIBUTION PROCEDURE FOR THE ANALYSIS OF SLABS CONTINUOUS OVER FLEXIBLE BEAMS, University of Illinois Engineering Experiment Station Bulletin No. 304, University of Illinois, Urbana, 1938.

39. Peterson, W. S., Kostem, C. N. and Kulicki, J. M.
THE INELASTIC ANALYSIS OF REINFORCED CONCRETE SLABS, Fritz Engineering Laboratory Report No. 378B.3, Lehigh University, Bethlehem, Pennsylvania, May 1974.

40. Peterson, W. S., Kostem, C. N. and Kulicki, J. M.
DISCUSSION OF "FULL RANGE ANALYSIS OF ECCENTRICALLY STIFFENED PLATES," by A. W. Wegmuller, Journal of the Structural Division, ASCE, Vol. 100, ST9, September 1974.

41. Peterson, W. S. and Kostem, C. N.
THE INELASTIC ANALYSIS OF BEAM-SLAB HIGHWAY BRIDGE SUPER STRUCTURES, Fritz Engineering Laboratory Report No. 378B.5, Lehigh University, Bethlehem, Pennsylvania, March 1975.

42. Peterson, W. S. and Kostem, C. N.
THE INELASTIC ANALYSIS OF BEAM-SLAB BRIDGES, Fritz Engineering Laboratory Report No. 400.20, Lehigh University, Bethlehem, Pennsylvania, July 1975.

43. Proctor, M. H.
ANALYTICAL AND EXPERIMENTAL STUDY OF LIGHTWEIGHT CONCRETE-STEEL COMPOSITE BEAMS, M.S. Thesis, University of Missouri, Columbia, August 1963.

44. Ramberg, W. and Osgood, W. R.
DESCRIPTION OF STRESS-STRAIN CURVES BY THREE PARAMETERS, NACA, TN 902, July 1943.

45. Siess, C. P., Viest, I. M. and Newmar, N. M.
STUDIES OF SLAB AND BEAM HIGHWAY BRIDGES, PART III - SMALL SCALE TESTS OF SHEAR CONNECTORS AND COMPOSITE T-BEAMS, University of Illinois Engineering Experiment Station Bulletin No. 396, University of Illinois, Urbana, 1952.

46. Smith, G. M. and Young, L. E.
ULTIMATE FLEXURAL ANALYSIS BASED ON STRESS-STRAIN CURVES OF CYLINDERS, Journal of the American Concrete Institute, Vol. 53, No. 6, December 1956.

47. Teraszkiewicz, J. S.
STATIC AND FATIGUE BEHAVIOR OF SIMPLY SUPPORTED AND CONTINUOUS COMPOSITE BEAMS OF STEEL AND CONCRETE, Ph.D. Thesis, Imperial College of Science and Technology, University of London, London, September 1967.

48. Tottenham, H. and Brebbia, C.
FINITE ELEMENT TECHNIQUES IN STRUCTURAL MECHANICS, Southampton University Press, Southampton, England, 1970.

49. Tumminelli, S. C. and Kostem, C. N.
FINITE ELEMENT ANALYSIS FOR THE ELASTIC ANALYSIS OF COMPOSITE BEAMS AND BRIDGES, Fritz Engineering Laboratory Report No. 432.3, Lehigh University, Bethlehem, Pennsylvania, March 1978.

50. Viest, I. M.
REVIEW OF RESEARCH ON COMPOSITE STEEL-CONCRETE BEAMS, Journal of the Structural Division, ASCE, Vol. 86, ST6, June 1960.

51. Wegmuller, A.W. and Kostem, C. N.
ELASTIC-PLASTIC ANALYSIS OF PLEATES, Proceedings of the IASS Symposium on Shell Structures and Climatic Influences, pp. 379-386, Calgary, Canada, July 1972.

52. Wegmuller, A. W. and Kostem, C. N.
FINITE ELEMENT ANALYSIS OF PLATES AND ECCENTRICALLY STIFFENED PLATES, Fritz Engineering Laboratory Report No. 378A.3, Lehigh University, Bethlehem, Pennsylvania, February 1973.

53. Wegmuller, A. W. and Kostem, C. N.
FINITE ELEMENT ANALYSIS OF ELASTIC-PLASTIC PLATES AND ECCENTRICALLY STIFFENED PLATES, Fritz Engineering Laboratory Report No. 378A.4, Lehigh University, Bethlehem, Pennsylvania, February 1973.

54. Whang, B.
ELASTO-PLASTIC ORTHOTROPIC PLATES AND SHELLS, Proceedings of the Symposium on Application of Finite Element Methods in Civil Engineering, Vanderbilt University, Nashville, Tennessee, November 1969.

55. Wu, Y. C.
ANALYSIS OF CONTINUOUS COMPOSITE BEAMS, Ph.D. Dissertation, Lehigh University, Bethlehem, Pennsylvania, December 1970.

56. Yam, L. C. P. and Chapman, J. C.
THE INELASTIC BEHAVIOR OF SIMPLY SUPPORTED COMPOSITE BEAMS OF STEEL AND CONCRETE, Proceedings of the Institution of Civil Engineering, London, December, 1968.

57. Ziekiewicz, O.C.
THE FINITE ELEMENT METHOD IN ENGINEERING SCIENCE, McGraw Hill, New York, New York, 1971.

58. American Association of State Highway and Transportation Officials, STANDARD SPECIFICATIONS FOR HIGHWAY BRIDGES, Washington, D. C., 1974.

APPENDIX A

SLAB ELEMENT STIFFNESS FORMULATION

APPENDIX A

SLAB ELEMENT STIFFNESS FORMULATION

A.1 Introduction

In the basic development of the slab element stiffness matrix, as outlined in Section 3.5 and presented in detail in Appendix A of Reference 41, the following stiffness equations are derived:

$$[k_{uu}]^e_{8\times 8} = [C_u]^{-1^T} \iint_{yx} [Q_u]^T [D_{uu}] [Q_u] \, d_x d_y \, [C_u]^{-1} \tag{A.1}$$

$$[k_{u\phi}]^e_{8\times 12} = [C_u]^{-1^T} \iint_{yx} [Q_u]^T [D_{u\phi}] [S] [Q_\phi] \, d_x d_y \, [C_\phi]^{-1} [T]^{-1} \tag{A.2}$$

$$[k_{\phi\phi}]^e_{12\times 12} = [T]^{-1^T} [C_\phi]^{-1^T} \iint_{yx} [Q_\phi]^T [S]^T [D_{\phi\phi}] [S] [Q_\phi] \, d_x d_y$$

$$[C_\phi]^{-1} [T]^{-1} \tag{A.3}$$

The evaluation of the integrals in Eqs. A.1 to A.3 can be simplified by considering only one element of the rigidity matrices $[D_{uu}]$, $[D_{u\phi}]$, and $[D_{\phi\phi}]$, which are defined by equations 2.13, 2.23, and 3.32, to be nonzero at a time. Equations A.1 to A.3 thus become:

$$[k_{uu}]^e_{8\times 8} = [C_u]^{-1^T} [D_{11}[K_1] + D_{12}[K_2] + D_{13}[K_3] + D_{22}[K_4] +$$

$$D_{23}[K_5] + D_{33}[K_6] \,]_{uu} \, [C_u]^{-1} \tag{A.4}$$

$$[k_{u\phi}]^e_{8\times 12} = [C_u]^{-1^T} [D_{11}[K_1] + D_{12}[K_2] + D_{13}[K_3] + D_{22}[K_4] +$$

$$D_{23}[K_5] + D_{33}[K_6]\ ]_{u\phi}\ [C_\phi]^{-1}\ [T]^{-1} \tag{A.5}$$

$$[k_{\phi\phi}]^e_{12\times12} = [T]^{-1^T}\ [C_\phi]^{-1^T}\ [D_{11}[K_1] + D_{12}[K_2] + D_{13}[K_3] + D_{22}[K_4]$$

$$+ D_{23}[K_5] + D_{33}[K_6]\ ]_{\phi\phi}\ [C_\phi]^{-1}\ [T]^{-1} \tag{A.6}$$

where:

$$[T]^{-1} = \begin{bmatrix}
1 & & & & & & & & & & & \\
0 & b & & & & & & & & & & \\
0 & 0 & a & & & & \text{symmetric} & & & & & \\
0 & 0 & 0 & 1 & & & & & & & & \\
0 & 0 & 0 & 0 & b & & & & & & & \\
0 & 0 & 0 & 0 & 0 & a & & & & & & \\
0 & 0 & 0 & 0 & 0 & 0 & 1 & & & & & \\
0 & 0 & 0 & 0 & 0 & 0 & 0 & b & & & & \\
0 & 0 & 0 & 0 & 0 & 0 & 0 & 0 & a & & & \\
0 & 0 & 0 & 0 & 0 & 0 & 0 & 0 & 0 & 1 & & \\
0 & 0 & 0 & 0 & 0 & 0 & 0 & 0 & 0 & 0 & b & \\
0 & 0 & 0 & 0 & 0 & 0 & 0 & 0 & 0 & 0 & 0 & a
\end{bmatrix} \tag{A.7}$$

$$\begin{bmatrix}
2 & -1 & -1 & 2 & 1 & -1 & 2 & -1 & 1 & 2 & 1 & 1 \\
-3 & 1 & 1 & -3 & -1 & 1 & 3 & -1 & 1 & 3 & 1 & 1 \\
3 & -1 & -1 & -3 & -1 & 1 & 3 & -1 & 1 & -3 & -1 & -1 \\
0 & 0 & 1 & 0 & 0 & 1 & 0 & 0 & -1 & 0 & 0 & -1 \\
-4 & 1 & 1 & 4 & 1 & -1 & 4 & -1 & 1 & -4 & -1 & -1
\end{bmatrix}$$

$$[C_\phi]^{-1} = \frac{1}{8}\begin{bmatrix} 0 & 1 & 0 & 0 & -1 & 0 & 0 & 1 & 0 & 0 & -1 & 0 \\ 1 & 0 & -1 & 1 & 0 & -1 & -1 & 0 & -1 & -1 & 0 & -1 \\ 0 & 0 & 1 & 0 & 0 & -1 & 0 & 0 & -1 & 0 & 0 & 1 \\ 0 & -1 & 0 & 0 & 1 & 0 & 0 & 1 & 0 & 0 & -1 & 0 \\ -1 & 1 & 0 & 1 & 1 & 0 & -1 & 1 & 0 & 1 & 1 & 0 \\ 1 & 0 & -1 & -1 & 0 & 1 & -1 & 0 & -1 & 1 & 0 & -1 \\ 1 & -1 & 0 & -1 & -1 & 0 & -1 & 1 & 0 & 1 & 1 & 0 \end{bmatrix} \qquad \text{(A.8)}$$

$$[C_u]^{-1} = \frac{1}{4}\begin{bmatrix} 1 & 0 & 1 & 0 & 1 & 0 & 1 & 0 \\ -\frac{1}{a} & 0 & -\frac{1}{a} & 0 & \frac{1}{a} & 0 & \frac{1}{a} & 0 \\ \frac{1}{b} & 0 & -\frac{1}{b} & 0 & \frac{1}{b} & 0 & -\frac{1}{b} & 0 \\ -\frac{1}{ab} & 0 & \frac{1}{ab} & 0 & \frac{1}{ab} & 0 & -\frac{1}{ab} & 0 \\ 0 & 1 & 0 & 1 & 0 & 1 & 0 & 1 \\ 0 & -\frac{1}{a} & 0 & -\frac{1}{a} & 0 & \frac{1}{a} & 0 & \frac{1}{a} \\ 0 & \frac{1}{b} & 0 & -\frac{1}{b} & 0 & \frac{1}{b} & 0 & -\frac{1}{b} \\ 0 & -\frac{1}{ab} & 0 & \frac{1}{ab} & 0 & \frac{1}{ab} & 0 & -\frac{1}{ab} \end{bmatrix} \qquad \text{(A.9)}$$

The submatrices pertaining to the inplane stiffness matrix are evaluated by employing Eq. A.4 as follows:

$$(D_{11}[K_1])_{uu} = \iint_{yx} [Q_u]^T \begin{bmatrix} D_{11} & 0 & 0 \\ 0 & 0 & 0 \\ 0 & 0 & 0 \end{bmatrix}_{uu} [Q_u]\, d_x d_y \qquad \text{(A.10a)}$$

$$(D_{12}[K_2])_{uu} = \iint_{yx} [Q_u]^T \begin{bmatrix} 0 & D_{12} & 0 \\ D_{21} & 0 & 0 \\ 0 & 0 & 0 \end{bmatrix}_{uu} [Q_u]\, d_x d_y \qquad \text{(A.10b)}$$

and so on. Explicit expressions for Eqs. A.10 can be developed by utilizing:

$$[Q_u] = \begin{bmatrix} 0 & 1 & 0 & y & 0 & 0 & 0 & 0 \\ 0 & 0 & 0 & 0 & 0 & 0 & 1 & x \\ 0 & 0 & 1 & x & 0 & 1 & 0 & y \end{bmatrix} \qquad \text{(A.11)}$$

The resulting $(D_{ij}[K_n])_{uu}$ matrices are presented in Reference 41. By utilizing:

$$[Q_\phi] = \begin{bmatrix} 0 & 0 & 0 & -2 & 0 & 0 & -6\bar{x} & -2\bar{y} & 0 & 0 & -6\bar{\bar{xy}} & 0 \\ 0 & 0 & 0 & 0 & 0 & -2 & 0 & 0 & -2\bar{x} & -6\bar{y} & 0 & -6\bar{\bar{xy}} \\ 0 & 0 & 0 & 0 & -2 & 0 & 0 & -4\bar{x} & -4\bar{y} & 0 & -6\bar{x}^2 & -6\bar{y}^2 \end{bmatrix} \qquad \text{(A.12)}$$

and

$$[S] = \begin{bmatrix} \frac{1}{a^2} & 0 & 0 \\ 0 & \frac{1}{b^2} & 0 \\ 0 & 0 & \frac{1}{ab} \end{bmatrix} \qquad \text{(A.13)}$$

similar expressions for $(D_{ij}[K_n])_{u\phi}$ and $(D_{ij}[K_n])_{\phi\phi}$ matrices are derived and presented in Reference 41. However, in the previous research the remaining matrix operations of Eqs. A.4 to A.6 are left to be completed by the computer. Since many of the terms in these matrices are equal to zero, such matrix operations performs many unnecessary multiplications and additions. Considerable computation time can be saved by carrying out all matrix operations by hand, so that only direct substitution is required to get the slab element stiffness matrix. Also, in a typical analysis as many as 75 load cycles with three iterations per load cycle may be required, and each slab element stiffness matrix may be recalculated 225 times, and if there are 50 slab elements, this amounts to 11,250 stiffness matrix calculations per job. Thus, a typical reduction in computation time by a factor of 1/100, leads to sigificant saving all around.

A.2 Element Stiffness Matrices

Returning to equation A.4 and evaluating the $(D_{ij}[K_n])_{uu}$ submatrices as given in Ref. 41 yields:

$$(D_{ij}[K_n])_{uu} = \begin{bmatrix} 0 & 0 & 0 & 0 & 0 & 0 & 0 & 0 \\ 0 & D_{11} & D_{13} & 0 & 0 & D_{13} & D_{12} & 0 \\ 0 & D_{13} & D_{33} & 0 & 0 & D_{33} & D_{23} & 0 \\ 0 & 0 & 0 & \frac{D_{11}b^2}{3} + \frac{D_{33}a^2}{3} & 0 & 0 & 0 & \frac{D_{13}b^2}{3} + \frac{D_{23}a^2}{3} \\ 0 & 0 & 0 & 0 & 0 & 0 & 0 & 0 \\ 0 & D_{13} & D_{33} & 0 & 0 & D_{33} & D_{23} & 0 \end{bmatrix}$$

$$\begin{bmatrix} 0 & D_{12} & D_{23} & 0 & 0 & D_{23} & D_{22} & 0 \\ 0 & 0 & 0 & \frac{D_{13}b^2}{3} + \frac{D_{23}a^2}{3} & 0 & 0 & 0 & \frac{D_{22}a^2}{3} + \frac{D_{33}b^2}{3} \end{bmatrix} \quad (A.14)$$

Premultiplying Eq. A.14 by $[C_u]^{-1^T}$ and then postmultiplying the results by $[C_u]^{-1}$ gives an 8 by 8 $[k_{uu}]^e$, inplane element stiffness matrix:

$$k_{uu}(1,1) = \frac{D_{11}\beta}{3} + \frac{D_{33}\alpha}{3} - \frac{D_{13}}{2} \qquad k_{uu}(2,3) = \frac{D_{13}\beta}{6} - \frac{D_{23}\alpha}{3} - \frac{D_{12}}{4} + \frac{D_{33}}{4}$$

$$k_{uu}(1,2) = \frac{D_{13}\beta}{3} + \frac{D_{23}\alpha}{3} - \frac{D_{12}}{4} - \frac{D_{33}}{4} \qquad k_{uu}(2,4) = \frac{D_{33}\beta}{6} - \frac{D_{22}\alpha}{6}$$

$$k_{uu}(1,3) = \frac{D_{11}\beta}{6} - \frac{D_{33}\alpha}{3} \qquad k_{uu}(2,5) = -\frac{D_{13}\beta}{3} + \frac{D_{23}\alpha}{6} + \frac{D_{12}}{4} - \frac{D_{33}}{4}$$

$$k_{uu}(1,4) = \frac{D_{13}\beta}{6} - \frac{D_{23}\alpha}{3} + \frac{D_{12}}{4} - \frac{D_{33}}{4} \qquad k_{uu}(2,6) = -\frac{D_{33}\beta}{3} + \frac{D_{22}\alpha}{6}$$

$$k_{uu}(1,5) = -\frac{D_{11}\beta}{3} + \frac{D_{33}\alpha}{6} \qquad k_{uu}(2,7) = k_{uu}(1,8)$$

$$k_{uu}(1,6) = -\frac{D_{13}\beta}{3} + \frac{D_{23}\alpha}{6} - \frac{D_{12}}{4} + \frac{D_{33}}{4} \qquad k_{uu}(2,8) = -\frac{D_{33}\beta}{6} - \frac{D_{22}\alpha}{6} + \frac{D_{23}}{2}$$

$$k_{uu}(1,7) = -\frac{D_{11}\beta}{6} - \frac{D_{33}\alpha}{6} + \frac{D_{13}}{2} \qquad k_{uu}(3,1) = k_{uu}(1,3)$$

$$k_{uu}(1,8) = -\frac{D_{13}\beta}{6} - \frac{D_{23}\alpha}{6} + \frac{D_{12}}{4} + \frac{D_{33}}{4} \qquad k_{uu}(3,2) = k_{uu}(2,3)$$

$$k_{uu}(2,1) = k_{uu}(1,2) \qquad k_{uu}(3,3) = \frac{D_{11}\beta}{3} + \frac{D_{33}\alpha}{3} + \frac{D_{13}}{2}$$

$$k_{uu}(2,2) = \frac{D_{33}\beta}{3} + \frac{D_{22}\alpha}{3} - \frac{D_{23}}{2} \qquad k_{uu}(3,4) = \frac{D_{13}\beta}{3} + \frac{D_{23}\alpha}{3} + \frac{D_{12}}{4} + \frac{D_{13}}{4}$$

$$k_{uu}(3,5) = -\frac{D_{11}\beta}{6} - \frac{D_{33}\alpha}{6} - \frac{D_{13}}{2} \qquad k_{uu}(5,1) = k_{uu}(1,5)$$

$$k_{uu}(3,6) = -\frac{D_{13}\beta}{6} - \frac{D_{23}\alpha}{6} - \frac{D_{12}}{4} - \frac{D_{33}}{4} \qquad k_{uu}(5,2) = k_{uu}(2,5)$$

$$k_{uu}(3,7) = k_{uu}(1,5) \qquad k_{uu}(5,3) = k_{uu}(3,5)$$

$$k_{uu}(3,8) = k_{uu}(2,5) \qquad k_{uu}(5,4) - k_{uu}(4,5)$$

$$k_{uu}(4,1) = k_{uu}(1,4) \qquad k_{uu}(5,5) = k_{uu}(3,3)$$

$$k_{uu}(4,2) = k_{uu}(2,4) \qquad k_{uu}(5,6) = k_{uu}(3,4)$$

$$k_{uu}(4,3) = k_{uu}(3,4) \qquad k_{uu}(5,7) = k_{uu}(1,3)$$

$$k_{uu}(4,4) = \frac{D_{33}\beta}{3} + \frac{D_{22}\alpha}{3} + \frac{D_{23}}{2} \qquad k_{uu}(5,8) = k_{uu}(2,3)$$

$$k_{uu}(4,5) = k_{uu}(3,6) \qquad k_{uu}(6,1) = k_{uu}(1,6)$$

$$k_{uu}(4,6) = -\frac{D_{33}\beta}{6} - \frac{D_{22}\alpha}{6} - \frac{D_{23}}{2} \qquad k_{uu}(6,2) = k_{uu}(2,6)$$

$$k_{uu}(4,7) = k_{uu}(1,6) \qquad k_{uu}(6,3) = k_{uu}(3,6)$$

$$k_{uu}(4,8) = k_{uu}(2,6) \qquad k_{uu}(6,4) = k_{uu}(4,6)$$

$k_{uu}(6,5) = k_{uu}(5,6)$

$k_{uu}(6,6) = k_{uu}(4,4)$

$k_{uu}(6,7) = k_{uu}(1,4)$

$k_{uu}(6,8) = k_{uu}(2,4)$

$k_{uu}(7,1) = k_{uu}(1,7)$

$k_{uu}(7,2) = k_{uu}(2,7)$

$k_{uu}(7,3) = k_{uu}(3,7)$

$k_{uu}(7,4) = k_{uu}(4,7)$

$k_{uu}(7,5) = k_{uu}(5,7)$

$k_{uu}(7,6) = k_{uu}(6,7)$

$k_{uu}(7,7) = k_{uu}(1,1)$

$k_{uu}(7,8) = k_{uu}(1,2)$

$k_{uu}(8,1) = k_{uu}(1,8)$

$k_{uu}(8,2) = k_{uu}(2,8)$

$k_{uu}(8,3) = k_{uu}(3,8)$

$k_{uu}(8,4) = k_{uu}(4,8)$

$k_{uu}(8,5) = k_{uu}(5,8)$

$k_{uu}(8,6) = k_{uu}(6,8)$

$k_{uu}(8,7) = k_{uu}(7,8)$

$k_{uu}(8,8) = k_{uu}(2,2)$

Combining the appropriate matrix from equation A.5 and Ref. 41 yields the following $(D_{ij}[K_n])_{u\phi}$ matrix:

$$
8\begin{bmatrix}
0 & 0 & 0 & 0 & 0 & 0 & 0 & 0 & 0 & 0 & 0 & 0 \\
0 & 0 & 0 & -D_{11}{}^{\beta} & -D_{13} & -D_{12}{}^{\alpha} & 0 & 0 & 0 & 0 & -D_{13} & -D_{13} \\
0 & 0 & 0 & -D_{13}{}^{\beta} & -D_{33} & -D_{23}{}^{\alpha} & 0 & 0 & 0 & 0 & -D_{33} & -D_{33} \\
0 & 0 & 0 & 0 & 0 & 0 & -D_{13}{}^{b} & -\frac{1}{3}D_{11}{}^{\beta b}-\frac{2}{3}D_{33}{}^{a} & -\frac{2}{3}D_{13}{}^{b}-\frac{1}{3}D_{23}{}^{\alpha a} & -D_{12}{}^{a} & 0 & 0 \\
0 & 0 & 0 & 0 & 0 & 0 & 0 & 0 & 0 & 0 & 0 & 0 \\
0 & 0 & 0 & -D_{13}{}^{\beta} & -D_{33} & -D_{23}{}^{\alpha} & 0 & 0 & 0 & 0 & -D_{33} & -D_{33} \\
0 & 0 & 0 & -D_{12}{}^{\beta} & -D_{23} & -D_{22}{}^{\alpha} & 0 & 0 & 0 & 0 & -D_{23} & -D_{23} \\
0 & 0 & 0 & 0 & 0 & 0 & -D_{12}{}^{b} & -\frac{1}{3}D_{13}{}^{\beta b}-\frac{2}{3}D_{23}{}^{a} & -\frac{2}{3}D_{33}{}^{b}-\frac{1}{3}D_{22}{}^{\alpha a} & -D_{23}{}^{a} & 0 & 0
\end{bmatrix}
\tag{A.16}
$$

By then performing the remaining matrix operation of Eq. A.5 (i.e. $[C_u]^{-1^T}(D_{ij}[K_n])_{u\phi}[C_\phi]^{-1}[T]^{-1}$) the following 8 x 12 $[k_u]^e$ matrix is derived:

$$k_{u\phi}(1,1) = \frac{1}{4}\left(-\frac{D_{13}}{a} + \frac{2D_{33}}{b} - \frac{D_{12}}{b}\right)$$

$$k_{u\phi}(1,2) = \frac{1}{2}\left(-D_{13}\beta + D_{12} - \frac{2D_{23}\alpha}{3}\right)$$

$$k_{u\phi}(1,3) = \frac{1}{2}\left(\frac{2D_{11}\beta}{3} - D_{13} + \frac{D_{33}\alpha}{3}\right)$$

$$k_{u\phi}(1,3) = \frac{1}{4}\left(\frac{3D_{13}}{a} - \frac{2D_{33}}{b} + \frac{D_{12}}{b}\right)$$

$$k_{u\phi}(1,5) = \frac{1}{2}\left(\frac{D_{13}\beta}{3} + \frac{2D_{23}\alpha}{3}\right)$$

$$k_{u\phi}(1,6) = \frac{1}{2}\left(\frac{D_{11}\beta}{3} - D_{13} - \frac{D_{33}\alpha}{3}\right)$$

$$k_{u\phi}(1,7) = \frac{1}{4}\left(\frac{D_{13}}{a} - \frac{2D_{33}}{b} - \frac{D_{12}}{b}\right)$$

$$k_{u\phi}(1,8) = \frac{1}{2}\left(\frac{D_{13}\beta}{3} + D_{12} - \frac{D_{23}\alpha}{3}\right)$$

$$k_{u\phi}(1,9) = \frac{1}{2}\left(-\frac{2D_{11}\beta}{3} - \frac{D_{33}\alpha}{3}\right)$$

$$k_{u\phi}(1,10) = \frac{1}{4}\left(-\frac{3D_{13}}{a} + \frac{2D_{33}}{b} + \frac{D_{12}}{b}\right)$$

$$k_{u\phi}(1,11) = \frac{1}{2}\left(\frac{D_{13}\beta}{3} + \frac{D_{23}\alpha}{3}\right)$$

$$k_{u\phi}(1,12) = \frac{1}{2}\left(-\frac{D_{11}\beta}{3} + \frac{D_{33}\alpha}{3}\right)$$

$$k_{u\phi}(2,1) = \frac{1}{4}\left(-\frac{2D_{33}}{a} + \frac{D_{23}}{b} + \frac{D_{12}}{a}\right)$$

$$k_{u\phi}(2,2) = \frac{1}{2}\left(-\frac{D_{33}\beta}{3} + D_{23} - \frac{2D_{22}\alpha}{3}\right)$$

$$k_{u\phi}(2,3) = \frac{1}{2}\left(\frac{2D_{13}\beta}{3} - D_{12} + \frac{D_{23}\alpha}{3}\right)$$

$$k_{u\phi}(2,4) = \frac{1}{4}\left(\frac{2D_{33}}{a} - \frac{D_{23}}{b} + \frac{D_{12}}{a}\right)$$

$$k_{u\phi}(2,5) = \frac{1}{2}\left(\frac{D_{33}\beta}{3} + \frac{2D_{22}\alpha}{3}\right)$$

$$k_{u\phi}(2,6) = \frac{1}{2}\left(\frac{D_{13}\beta}{3} - D_{12} - \frac{D_{23}\alpha}{3}\right)$$

$$k_{u\phi}(2,7) = \frac{1}{4}\left(\frac{2D_{33}}{a} - \frac{3D_{23}}{b} - \frac{D_{12}}{a}\right)$$

$$k_{u\phi}(2,8) = \frac{1}{2}\left(\frac{D_{33}\beta}{3} + D_{23} - \frac{D_{22}\alpha}{3}\right)$$

$$k_{u\phi}(2,9) = \frac{1}{2}\left(-\frac{2D_{13}\beta}{3} - \frac{D_{23}\alpha}{3}\right)$$

$$k_{u\phi}(2,10) = \frac{1}{4}\left(-\frac{2D_{33}}{a} + \frac{3D_{23}}{b} - \frac{D_{12}}{a}\right)$$

$$k_{u\phi}(2,11) = \frac{1}{2}\left(-\frac{D_{33}\beta}{3} + \frac{D_{22}\alpha}{3}\right)$$

$$k_{u\phi}(2,12) = k_{u\phi}(1,11)$$

$$k_{u\phi}(3,1) = \frac{1}{4}\left(-\frac{3D_{13}}{a} - \frac{2D_{33}}{b} + \frac{D_{12}}{b}\right)$$

$$k_{u\phi}(3,2) = k_{u\phi}(1,5)$$

$$k_{u\phi}(3,3) = \frac{1}{2}\left(\frac{D_{11}{}^{\beta}}{3} + D_{13} - \frac{D_{33}{}^{\alpha}}{3}\right)$$

$$k_{u\phi}(3,4) = \frac{1}{4}\left(\frac{D_{13}}{a} + \frac{2D_{33}}{b} - \frac{D_{12}}{b}\right)$$

$$k_{u\phi}(3,5) = \frac{1}{2}\left(-\frac{D_{13}{}^{\beta}}{3} - D_{12} - \frac{2D_{23}{}^{\alpha}}{3}\right)$$

$$k_{u\phi}(3,6) = \frac{1}{2}\left(\frac{2D_{11}}{3} + D_{13} - \frac{D_{33}}{3}\right)$$

$$k_{u\phi}(3,7) = \frac{1}{4}\left(\frac{3D_{13}}{a} + \frac{2D_{33}}{b} + \frac{D_{12}}{b}\right)$$

$$k_{u\phi}(3,8) = k_{u\phi}(1,11)$$

$$k_{u\phi}(3,9) = k_{u\phi}(1,12)$$

$$k_{u\phi}(3,10) = \frac{1}{4}\left(-\frac{D_{13}}{a} - \frac{2D_{33}}{b} - \frac{D_{12}}{b}\right)$$

$$k_{u\phi}(3,11) = \frac{1}{2}\left(\frac{D_{13}{}^{\beta}}{3} - D_{12} - \frac{D_{23}{}^{\alpha}}{3}\right)$$

$$k_{u\phi}(3,12) = k_{u\phi}(1,9)$$

$$k_{u\phi}(4,1) = \frac{1}{4}\left(-\frac{2D_{33}}{a} - \frac{D_{23}}{b} - \frac{D_{12}}{a}\right)$$

$$k_{u\phi}(4,2) = k_{u\phi}(2,5)$$

$$k_{u\phi}(4,3) = k_{u\phi}(1,8)$$

$$k_{u\phi}(4,4) = \frac{1}{4}\left(\frac{2D_{33}}{a} + \frac{D_{23}}{b} - \frac{D_{12}}{a}\right)$$

$$k_{u\phi}(4,5) = \frac{1}{2}\left(-\frac{D_{33}{}^{\beta}}{3} - D_{23} - \frac{2D_{22}}{3}\right)$$

$$k_{u\phi}(4,6) = \frac{1}{2}\left(\frac{2D_{13}{}^{\beta}}{3} + D_{12} + \frac{D_{23}{}^{\alpha}}{3}\right)$$

$$k_{u\phi}(4,7) = \frac{1}{4}\left(\frac{2D_{33}}{a} + \frac{3D_{23}}{b} - \frac{D_{12}}{a}\right)$$

$$k_{u\phi}(4,8) = k_{u\phi}(2,11)$$

$$k_{u\phi}(4,9) = k_{u\phi}(2,12)$$

$$k_{u\phi}(4,10) = \frac{1}{4}\left(\frac{2D_{33}}{a} - \frac{3D_{23}}{b} + \frac{D_{12}}{a}\right)$$

$$k_{u\phi}(4,11) = \frac{1}{2}\left(\frac{D_{33}{}^{\beta}}{3} - D_{23} - \frac{D_{22}{}^{\alpha}}{3}\right)$$

$$k_{u\phi}(4,12) = k_{u\phi}(2,9)$$

$$k_{u\phi}(5,1) = k_{u\phi}(3,10)$$

$$k_{u\phi}(5,2) = k_{u\phi}(3,11)$$

$$k_{u\phi}(5,3) = k_{u\phi}(3,12)$$

$$k_{u\phi}(5,4) = -k_{u\phi}(3,7)$$

$$k_{u\phi}(5,5) = k_{u\phi}(3,8)$$

$$k_{u\phi}(5,6) = k_{u\phi}(3.9)$$

$$k_{u\phi}(5,7) = -k_{u\phi}(3,4)$$

$$k_{u\phi}(5,8) = k_{u\phi}(3,5)$$

$$k_{u\phi}(5,9) = k_{u\phi}(3,6)$$

$$k_{u\phi}(5,10) = -k_{u\phi}(3,1)$$

$$k_{u\phi}(5,11) = k_{u\phi}(3,2)$$

$$k_{u\phi}(5,12) = k_{u\phi}(3,3)$$

$$k_{u\phi}(6,1) = -k_{u\phi}(4,10)$$

$$k_{u\phi}(6,2) = k_{u\phi}(4,11)$$

$$k_{u\phi}(6,3) = k_{u\phi}(4,12)$$

$$k_{u\phi}(6,4) = -k_{u\phi}(4,7)$$

$$k_{u\phi}(6,5) = k_{u\phi}(4,8)$$

$$k_{u\phi}(6,6) = k_{u\phi}(4,9)$$

$$k_{u\phi}(6,7) = -k_{u\phi}(4,4)$$

$$k_{u\phi}(6,8) = k_{u\phi}(4,5)$$

$$k_{u\phi}(6,9) = k_{u\phi}(4,6)$$

$$k_{u\phi}(6,10) = -k_{u\phi}(4,1)$$

$$k_{u\phi}(6,11) = k_{u\phi}(4,2)$$

$$k_{u\phi}(6,12) = k_{u\phi}(4,3)$$

$$k_{u\phi}(7,1) = -k_{u\phi}(1,10)$$

$$k_{u\phi}(7,2) = k_{u\phi}(1,11)$$

$$k_{u\phi}(7,3) = k_{u\phi}(1,12)$$

$$k_{u\phi}(7,4) = -k_{u\phi}(1,7)$$

$$k_{u\phi}(7,5) = k_{u\phi}(1,8)$$

$$k_{u\phi}(7,6) = k_{u\phi}(1,9)$$

$$k_{u\phi}(7,7) = -k_{u\phi}(1,4)$$

$$k_{u\phi}(7,8) = k_{u\phi}(1,5)$$

$$k_{u\phi}(7,9) = k_{u\phi}(1,6)$$

$$k_{u\phi}(7,10) = -k_{u\phi}(1,1)$$

$$k_{u\phi}(7,11) = k_{u\phi}(1,2)$$

$$k_{u\phi}(7,12) = k_{u\phi}(1,3)$$

$$k_{u\phi}(8,1) = -k_{u\phi}(2,10)$$

$$k_{u\phi}(8,2) = k_{u\phi}(2,11)$$

$$k_{u\phi}(8,3) = k_{u\phi}(2,12)$$

$$k_{u\phi}(8,4) = -k_{u\phi}(2,7)$$

$$k_{u\phi}(8,5) = k_{u\phi}(2,8)$$

$$k_{u\phi}(8,6) = k_{u\phi}(2.9)$$

$$k_{u\phi}(8,7) = -k_{u\phi}(2,4)$$

$$k_{u\phi}(8,8) = k_{u\phi}(2,5)$$

$$k_{u\phi}(8,9) = k_{u\phi}(2,6)$$

$$k_{u\phi}(8,10) = -k_{u\phi}(2,1)$$

$$k_{u\phi}(8,11) = k_{u\phi}(2,2)$$

$$k_{u\phi}(8,12) = k_{u\phi}(2,3)$$

Combining in a similar manner the appropriate submatrices from Eqs. A.6 and Ref. 41 yields the following $(D_{ij}[K_n])_{\phi\phi}$ matrix:

$$
16\begin{bmatrix}
0 & 0 & 0 & 0 & 0 & 0 & 0 & 0 & 0 & 0 & 0 & 0 \\
0 & 0 & 0 & 0 & 0 & 0 & 0 & 0 & 0 & 0 & 0 & 0 \\
0 & 0 & 0 & 0 & 0 & 0 & 0 & 0 & 0 & 0 & 0 & 0 \\
0 & 0 & 0 & \frac{D_{11}^{b}}{a^3} & \frac{D_{13}}{a^2} & \frac{D_{12}}{ab} & 0 & 0 & 0 & 0 & \frac{D_{13}}{a^2} & \frac{D_{13}}{a^2} \\
0 & 0 & 0 & \frac{D_{13}}{a^2} & \frac{D_{33}}{ab} & \frac{D_{23}}{b^2} & 0 & 0 & 0 & 0 & \frac{D_{33}}{ab} & \frac{D_{33}}{ab} \\
0 & 0 & 0 & \frac{D_{12}}{ab} & \frac{D_{23}}{b^2} & \frac{D_{22}^{a}}{b^3} & 0 & 0 & 0 & 0 & \frac{D_{23}}{b^2} & \frac{D_{23}}{b^2} \\
0 & 0 & 0 & 0 & 0 & 0 & \frac{3D_{11}^{b}}{a^3} & \frac{2D_{13}}{a^2} & \frac{D_{12}}{ab} & 0 & 0 & 0 \\
0 & 0 & 0 & 0 & 0 & 0 & \frac{2D_{13}}{a^2} & \frac{D_{11}^{b}}{3a^3}+\frac{4D_{33}}{3ab} & \frac{2D_{13}}{3a^2}+\frac{2D_{23}}{3b^2} & \frac{D_{12}}{ab} & 0 & 0 \\
0 & 0 & 0 & 0 & 0 & 0 & \frac{D_{12}}{ab} & \frac{2D_{13}}{3a^2}+\frac{2D_{23}}{3b^2} & \frac{D_{22}^{a}}{3b^3}+\frac{4D_{33}}{3ab} & \frac{2D_{23}}{b^2} & 0 & 0 \\
0 & 0 & 0 & 0 & 0 & 0 & 0 & \frac{D_{12}}{ab} & \frac{2D_{23}}{b^2} & \frac{3D_{22}^{a}}{b^3} & 0 & 0 \\
0 & 0 & 0 & \frac{D_{13}}{a^2} & \frac{D_{33}}{ab} & \frac{D_{23}}{b^2} & 0 & 0 & 0 & 0 & \frac{D_{11}^{b}}{a^3}+\frac{9D_{33}}{5ab} & \frac{D_{12}}{ab}+\frac{D_{33}}{ab} \\
0 & 0 & 0 & \frac{D_{13}}{a^2} & \frac{D_{33}}{ab} & \frac{D_{23}}{b^2} & 0 & 0 & 0 & 0 & \frac{D_{12}}{ab}+\frac{D_{33}}{ab} & \frac{D_{22}^{a}}{b^3}+\frac{9D_{33}}{5ab}
\end{bmatrix}
\tag{A.18}
$$

By then performing the remaining matrix operations of Eq. A.6 (i.e. $[T]^{-1^T}[C_\phi]^{-1^T}(D_{ij}[K_n])_{\phi\phi}[C_\phi]^{-1}[T]^{-1}$) the following 12 x 12 $[k_{\phi\phi}]^e$ matrix is obtained:

$$k_{\phi\phi}(1,1) = \frac{D_{11}}{a^2\alpha} + \frac{D_{22}}{b^2\beta} + \frac{7D_{33}}{5ab} + \frac{D_{12}}{2ab}$$

$$k_{\phi\phi}(1,2) = -\frac{D_{22}}{b\beta} - \frac{D_{33}}{5a} - \frac{D_{12}}{2a}$$

$$k_{\phi\phi}(1,3) = -\frac{D_{11}}{a\alpha} - \frac{D_{33}}{5b} - \frac{D_{12}}{2b}$$

$$k_{\phi\phi}(1,4) = \frac{D_{11}}{2a^2\alpha} - \frac{D_{22}}{b^2\beta} - \frac{7D_{33}}{5ab} - \frac{D_{12}}{2ab}$$

$$k_{\phi\phi}(1,5) = -\frac{D_{22}}{b\beta} - \frac{D_{33}}{5a}$$

$$k_{\phi\phi}(1,6) = -\frac{D_{11}}{2a\alpha} - \frac{D_{13}}{a} + \frac{D_{33}}{5b} + \frac{D_{12}}{2b}$$

$$k_{\phi\phi}(1,7) = -\frac{D_{11}}{a^2\alpha} + \frac{D_{22}}{2b^2\beta} - \frac{7D_{33}}{5ab} - \frac{D_{12}}{2ab}$$

$$k_{\phi\phi}(1,8) = -\frac{D_{23}}{b} - \frac{D_{22}}{2b\beta} + \frac{D_{33}}{5a} + \frac{D_{12}}{2a}$$

$$k_{\phi\phi}(1,9) = -\frac{D_{11}}{a\alpha} - \frac{D_{33}}{5b}$$

$$k_{\phi\phi}(1,10) = -\frac{D_{11}}{2a^2\alpha} - \frac{D_{22}}{2b^2\beta} + \frac{7D_{33}}{5ab} + \frac{D_{12}}{2ab}$$

$$k_{\phi\phi}(1,11) = \frac{D_{23}}{b} - \frac{D_{22}}{2b\beta} + \frac{D_{33}}{5a}$$

$$k_{\phi\phi}(1,12) = -\frac{D_{11}}{2a\alpha} + \frac{D_{13}}{a} + \frac{D_{33}}{5b}$$

$$k_{\phi\phi}(2,1) = k_{\phi\phi}(1,2)$$

$$k_{\phi\phi}(2,2) = -D_{23} + \frac{4D_{22}}{3\beta} + \frac{8D_{33}}{15\alpha}$$

$$k_{\phi\phi}(2,3) = -\frac{D_{23}}{6\beta} - \frac{D_{13}}{6\alpha} + D_{12}$$

$$k_{\phi\phi}(2,4) = -k_{\phi\phi}(1,5)$$

$$k_{\phi\phi}(2,5) = \frac{2D_{22}}{3\beta} - \frac{2D_{33}}{15\alpha}$$

$$k_{\phi\phi}(2,6) = \frac{D_{23}}{6\beta} + \frac{D_{13}}{6\alpha}$$

$$k_{\phi\phi}(2,7) = \frac{D_{23}}{b} - \frac{D_{22}}{2b\beta} + \frac{D_{33}}{5a} + \frac{D_{12}}{2a}$$

$$k_{\phi\phi}(2,8) = \frac{2D_{22}}{3\beta} - \frac{8D_{33}}{15\alpha}$$

$$k_{\phi\phi}(2,9) = k_{\phi\phi}(2,6)$$

$$k_{\phi\phi}(2,10) = -k_{\phi\phi}(1,11)$$

$$k_{\phi\phi}(2,11) = -D_{23} + \frac{D_{22}}{3\beta} + \frac{2D_{33}}{15\alpha}$$

$$k_{\phi\phi}(2,12) = -k_{\phi\phi}(2,6)$$

$$k_{\phi\phi}(3,1) = k_{\phi\phi}(1,3)$$

$$k_{\phi\phi}(3,2) = k_{\phi\phi}(2,3)$$

$$k_{\phi\phi}(3,3) = \frac{4D_{11}}{3\alpha} - D_{13} + \frac{8D_{33}}{15\beta}$$

$$k_{\phi\phi}(3,4) = -\frac{D_{11}}{2a\alpha} + \frac{D_{22}}{a} + \frac{D_{33}}{5b} + \frac{D_{12}}{2b}$$

$$k_{\phi\phi}(3,5) = k_{\phi\phi}(2,6)$$

$$k_{\phi\phi}(3,6) = \frac{2D_{11}}{3\alpha} - \frac{8D_{33}}{15\beta}$$

$$k_{\phi\phi}(3,7) = -k_{\phi\phi}(1,9)$$

$$k_{\phi\phi}(3,8) = k_{\phi\phi}(2,6)$$

$$k_{\phi\phi}(3,9) = \frac{2D_{11}}{3\alpha} - \frac{2D_{33}}{15\beta}$$

$$k_{\phi\phi}(3,10) = -k_{\phi\phi}(1,12)$$

$$k_{\phi\phi}(3,11) = k_{\phi\phi}(2,12)$$

$$k_{\phi\phi}(3,12) = \frac{D_{11}}{3\alpha} - D_{13} + \frac{2D_{33}}{15\beta}$$

$$k_{\phi\phi}(4,1) = k_{\phi\phi}(1,4)$$

$$k_{\phi\phi}(4,2) = k_{\phi\phi}(2,4)$$

$$k_{\phi\phi}(4,3) = k_{\phi\phi}(3,4)$$

$$k_{\phi\phi}(4,4) = k_{\phi\phi}(1,1)$$

$$k_{\phi\phi}(4,5) = -k_{\phi\phi}(1,2)$$

$$k_{\phi\phi}(4,6) = k_{\phi\phi}(1,3)$$

$$k_{\phi\phi}(4,7) = k_{\phi\phi}(1,10)$$

$$k_{\phi\phi}(4,8) = \frac{D_{23}}{b} + \frac{D_{22}}{2b\beta} - \frac{D_{33}}{5a}$$

$$k_{\phi\phi}(4,9) = -\frac{D_{11}}{2a\alpha} - \frac{D_{13}}{a} + \frac{D_{33}}{5b}$$

$$k_{\phi\phi}(4,10) = k_{\phi\phi}(1,7)$$

$$k_{\phi\phi}(4,11) = -k_{\phi\phi}(2,7)$$

$$k_{\phi\phi}(4,12) = k_{\phi\phi}(1,9)$$

$$k_{\phi\phi}(5,1) = k_{\phi\phi}(1,5)$$

$$k_{\phi\phi}(5,2) = k_{\phi\phi}(2,5)$$

$$k_{\phi\phi}(5,3) = k_{\phi\phi}(3,5)$$

$$k_{\phi\phi}(5,4) = k_{\phi\phi}(4,5)$$

$$k_{\phi\phi}(5,5) = D_{23} + \frac{4D_{22}}{3\beta} + \frac{8D_{33}}{15\alpha}$$

$$k_{\phi\phi}(5,6) = -\frac{D_{23}}{6\beta} - \frac{D_{13}}{6\alpha} - D_{12}$$

$$k_{\phi\phi}(5,7) = -k_{\phi\phi}(4,8)$$

$$k_{\phi\phi}(5,8) = D_{23} + \frac{D_{22}}{3\beta} + \frac{D_{33}}{5\alpha}$$

$$k_{\phi\phi}(5,9) = -k_{\phi\phi}(2,6)$$

$$k_{\phi\phi}(5,10) = -k_{\phi\phi}(1,8)$$

$$k_{\phi\phi}(5,11) = k_{\phi\phi}(2,8)$$

$$k_{\phi\phi}(5,12) = k_{\phi\phi}(2,6)$$

$$k_{\phi\phi}(6,1) = k_{\phi\phi}(1,6)$$

$$k_{\phi\phi}(6,2) = k_{\phi\phi}(2,6)$$

$$k_{\phi\phi}(6,3) = k_{\phi\phi}(3,6)$$

$$k_{\phi\phi}(6,4) = k_{\phi\phi}(4,6)$$

$$k_{\phi\phi}(6,5) = k_{\phi\phi}(5,6)$$

$$k_{\phi\phi}(6,6) = \frac{4D_{11}}{3\alpha} + D_{13} + \frac{5D_{33}}{15\beta}$$

$$k_{\phi\phi}(6,7) = -k_{\phi\phi}(4,7)$$

$$k_{\phi\phi}(6,8) = -k_{\phi\phi}(2,6)$$

$$k_{\phi\phi}(6,9) = \frac{D_{11}}{6\alpha} + D_{13} + \frac{2D_{33}}{15\beta}$$

$$k_{\phi\phi}(6,10) = -k_{\phi\phi}(1,9)$$

$$k_{\phi\phi}(6,11) = k_{\phi\phi}(2,6)$$

$$k_{\phi\phi}(6,12) = k_{\phi\phi}(3,9)$$

$$k_{\phi\phi}(7,1) = k_{\phi\phi}(1,7)$$

$$k_{\phi\phi}(7,2) = k_{\phi\phi}(2,7)$$

$$k_{\phi\phi}(7,3) = k_{\phi\phi}(3,7)$$

$$k_{\phi\phi}(7,4) = k_{\phi\phi}(4,7)$$

$$k_{\phi\phi}(7,5) = k_{\phi\phi}(5,7)$$

$$k_{\phi\phi}(7,6) = k_{\phi\phi}(6,7)$$

$$k_{\phi\phi}(7,7) = k_{\phi\phi}(1,1)$$

$$k_{\phi\phi}(7,8) = k_{\phi\phi}(1,2)$$

$$k_{\phi\phi}(7,9) = -k_{\phi\phi}(1,3)$$

$$k_{\phi\phi}(7,10) = k_{\phi\phi}(1,4)$$

$$k_{\phi\phi}(7,11) = k_{\phi\phi}(1,5)$$

$$k_{\phi\phi}(7,12) = \frac{D_{11}}{2a\alpha} - \frac{D_{13}}{a} - \frac{D_{33}}{5b} - \frac{D_{12}}{2b}$$

$$k_{\phi\phi}(8,1) = k_{\phi\phi}(1,8)$$

$$k_{\phi\phi}(8,2) = k_{\phi\phi}(2,8)$$

$$k_{\phi\phi}(8,3) = k_{\phi\phi}(3,8)$$

$$k_{\phi\phi}(8,4) = k_{\phi\phi}(4,8)$$

$$k_{\phi\phi}(8,5) = k_{\phi\phi}(5,8)$$

$k_{\phi\phi}(8,6) = k_{\phi\phi}(6,8)$

$k_{\phi\phi}(8,7) = k_{\phi\phi}(7,8)$

$k_{\phi\phi}(8,8) = k_{\phi\phi}(5,5)$

$k_{\phi\phi}(8,9) = k_{\phi\phi}(5,6)$

$k_{\phi\phi}(8,10) = k_{\phi\phi}(2,4)$

$k_{\phi\phi}(8,11) = k_{\phi\phi}(2,5)$

$k_{\phi\phi}(8,12) = k_{\phi\phi}(2,6)$

$k_{\phi\phi}(9,1) = k_{\phi\phi}(1,9)$

$k_{\phi\phi}(9,2) = k_{\phi\phi}(2,9)$

$k_{\phi\phi}(9,3) = k_{\phi\phi}(3,9)$

$k_{\phi\phi}(9,4) = k_{\phi\phi}(4,9)$

$k_{\phi\phi}(9,5) = k_{\phi\phi}(5,9)$

$k_{\phi\phi}(9,6) = k_{\phi\phi}(6.9)$

$k_{\phi\phi}(9,7) = k_{\phi\phi}(7,9)$

$k_{\phi\phi}(9,8) = k_{\phi\phi}(8,9)$

$k_{\phi\phi}(9,9) = k_{\phi\phi}(6,6)$

$k_{\phi\phi}(9,10) = -k_{\phi\phi}(1,6)$

$k_{\phi\phi}(9,11) = k_{\phi\phi}(2,6)$

$k_{\phi\phi}(9,12) = k_{\phi\phi}(3,6)$

$k_{\phi\phi}(10,1) = k_{\phi\phi}(1,10)$

$k_{\phi\phi}(10,2) = k_{\phi\phi}(2,10)$

$k_{\phi\phi}(10,3) = k_{\phi\phi}(3,10)$

$k_{\phi\phi}(10,4) = k_{\phi\phi}(4,10)$

$k_{\phi\phi}(10,5) = k_{\phi\phi}(5,10)$

$k_{\phi\phi}(10,6) = k_{\phi\phi}(6,10)$

$k_{\phi\phi}(10,7) = k_{\phi\phi}(7,10)$

$k_{\phi\phi}(10,8) = k_{\phi\phi}(8,10)$

$k_{\phi\phi}(10,9) = k_{\phi\phi}(9,10)$

$k_{\phi\phi}(10,10) = k_{\phi\phi}(1,1)$

$k_{\phi\phi}(10,11) = -k_{\phi\phi}(1,2)$

$k_{\phi\phi}(10,12) = -k_{\phi\phi}(1,3)$

$k_{\phi\phi}(11,1) = k_{\phi\phi}(1,11)$

$k_{\phi\phi}(11,2) = k_{\phi\phi}(2,11)$

$k_{\phi\phi}(11,3) = k_{\phi\phi}(3,11)$

$k_{\phi\phi}(11,4) = k_{\phi\phi}(4,11)$

$k_{\phi\phi}(11,5) = k_{\phi\phi}(5,11)$

$k_{\phi\phi}(11,6) = k_{\phi\phi}(6,11)$

$k_{\phi\phi}(11,7) = k_{\phi\phi}(7,11)$

$k_{\phi\phi}(11,8) = k_{\phi\phi}(8,11)$

$k_{\phi\phi}(11,9) = k_{\phi\phi}(9,11)$

$k_{\phi\phi}(11,10) = k_{\phi\phi}(10,11)$

$k_{\phi\phi}(11,11) = k_{\phi\phi}(2,2)$

$k_{\phi\phi}(11,12) = k_{\phi\phi}(2,3)$

$k_{\phi\phi}(12,1) = k_{\phi\phi}(1,12)$

$k_{\phi\phi}(12,2) = k_{\phi\phi}(2,12)$

$k_{\phi\phi}(12,3) = k_{\phi\phi}(3,12)$

$k_{\phi\phi}(12,4) = k_{\phi\phi}(4,12)$

$k_{\phi\phi}(12,5) = k_{\phi\phi}(5,12)$

$k_{\phi\phi}(12,6) = k_{\phi\phi}(6,12)$

$k_{\phi\phi}(12,7) = k_{\phi\phi}(7,12)$

$k_{\phi\phi}(12,8) = k_{\phi\phi}(8,12)$

$k_{\phi\phi}(12,9) = k_{\phi\phi}(9,12)$

$$k_{\phi\phi}(12,10) = k_{\phi\phi}(10,12) \qquad k_{\phi\phi}(12,12) = k_{\phi\phi}(3,3)$$

$$k_{\phi\phi}(12,11) = k_{\phi\phi}(11,12) \tag{A.19}$$

In the above matrices the D_{ij} terms for each matrix are different and are given by Eqs. 3.32a, 3.32b, and 3.32c, for the in-plane, coupling, and bending matrices respectively.

Once the $[k_{uu}]^e_{8x8}$, $[k_{u\phi}]^e_{8x12}$ and $[k_{\phi\phi}]^e_{12x12}$ matrices are established as above, the total slab element stiffness matrix can be obtained by stacking the component submatrices according to Eq. 3.31. By doing so the 20x20 slab element stiffness matrix becomes fully populated as shown by the symbolic matrix Eq. A.20:

$$\begin{bmatrix}
II & CCC & II & CCC & II & CCC & II & CCC \\
II & CCC & II & CCC & II & CCC & II & CCC \\
OO & BBB & OO & BBB & OO & BBB & OO & BBB \\
OO & BBB & OO & BBB & OO & BBB & OO & BBB \\
OO & BBB & OO & BBB & OO & BBB & OO & BBB \\
II & CCC & II & CCC & II & CCC & II & CCC \\
II & CCC & II & CCC & II & CCC & II & CCC \\
OO & BBB & OO & BBB & OO & BBB & OO & BBB \\
OO & BBB & OO & BBB & OO & BBB & OO & BBB \\
OO & BBB & OO & BBB & OO & BBB & OO & BBB \\
II & CCC & II & CCC & II & CCC & II & CCC \\
II & CCC & II & CCC & II & CCC & II & CCC
\end{bmatrix}$$

$$
\begin{bmatrix}
OO & BBB & OO & BBB & OO & BBB & OO & BBB \\
OO & BBB & OO & BBB & OO & BBB & OO & BBB \\
OO & BBB & OO & BBB & OO & BBB & OO & BBB \\
II & CCC & II & CCC & II & CCC & II & CCC \\
II & CCC & II & CCC & II & CCC & II & CCC \\
OO & BBB & OO & BBB & OO & BBB & OO & BBB \\
OO & BBB & OO & BBB & OO & BBB & OO & BBB \\
OO & BBB & OO & BBB & OO & BBB & OO & BBB
\end{bmatrix} \qquad \text{A.20}
$$

where

I = Inplane stiffness matrix terms, $[k_{uu}]^e$

C = Coupling stiffness matrix terms, $[k_{u\phi}]^e$

O = Transpose of coupling stiffness terms, $[k_{u\phi}]^{e^T}$

B = Bending stiffness matrix terms, $[k_{\phi\phi}]^e$

APPENDIX B

BEAM ELEMENT STIFFNESS FORMULATION

APPENDIX B

BEAM ELEMENT STIFFNESS FORMULATION

B.1 Introduction

The development of the beam element stiffness matrix, which was outlined in Section 3.6, will be expanded and completed in this appendix.

The following equations were arrived at in Section 3.6:

$$[k_B]_b = \int_V [B_B]_b^T [E_B][B_B]_b \, dV \tag{B.1}$$

$$[k_B]_s = \int_V [B_B]_s^T [G_B][B_B]_s \, dV \tag{B.2}$$

$$[k]_d = \int_L [B]_d^T [k_{sc}][B]_d \, dx \tag{B.3}$$

Where

$$[B_B]_b = [0 \; 1 \; 2X][CB] - Z\,[0 \; 1 \; 2X][CD] \tag{B.4}$$

$$[B_B]_s = [0 \; 1 \; 2X \; 3X^2][CW] - [1 \; X \; X^2][CD] \tag{B.5}$$

$$[B]_d = [1 \; x \; x^2 \; -1 \; -X \; -X^2 \; 0 \; -Z_{iA} \; -2Z_{iA}X \; -3Z_{iA}X^2$$

$$Z_{iB} \; Z_{iB}X \; Z_{iB}X^2][CC] \tag{B.6}$$

and where [CB], [CW], [CD], and [CC] matrices are given by equations 3.48 and 3.49.

Treating $[E_B]$ as a scalar multiplier and performing the indicated integration in (B.1) yields:

$k_{Bb}(1,1) = 0$

$k_{Bb}(1,2) = 0$

$k_{Bb}(1,3) = 0$

$k_{Bb}(1,4) = 0$

$k_{Bb}(1,5) = 0$

$k_{Bb}(1,6) = 0$

$k_{Bb}(1,7) = 0$

$k_{Bb}(1,8) = 0$

$k_{Bb}(1,9) = 0$

$k_{Bb}(1,10) = 0$

$k_{Bb}(2,1) = 0$

$k_{Bb}(2,2) = \frac{EA_B}{L}$

$k_{Bb}(2,3) = 0$

$k_{Bb}(2,4) = 0$

$k_{Bb}(2,5) = \frac{ES_B}{L}$

$k_{Bb}(2,6) = 0$

$k_{Bb}(2,7) = -\frac{EA_B}{L}$

$k_{Bb}(2,8) = 0$

$k_{Bb}(2,9) = 0$

$k_{Bb}(2,10) = -\frac{ES_B}{L}$

$k_{Bb}(3,1) = 0$

$k_{Bb}(3,2) = 0$

$k_{Bb}(3,3) = \frac{3}{4} J1^2 L \left(EI_B - EA_B \bar{Z}_B^2 \right)$

$k_{Bb}(3,4) = \frac{J1^2 L^2}{8} \left(- EI_B + EA_B \bar{Z}_B^2 \right)$

$k_{Bb}(3,5) = \frac{J1^2 L^2}{4} \left(- EI_B + EA_B \bar{Z}_B^2 \right)$

$k_{Bb}(3,6) = 0$

$$k_{Bb}(3,7) = 0$$

$$k_{Bb}(3,8) = - k_{Bb}(3,3)$$

$$k_{Bb}(3,9) = k_{Bb}(3,4)$$

$$k_{Bb}(3,10) = k_{Bb}(3,5)$$

$$k_{Bb}(4,1) = 0$$

$$k_{Bb}(4,2) = 0$$

$$k_{Bb}(4,3) = k_{Bb}(3,4)$$

$$k_{Bb}(4,4) = \frac{J1^2L^3}{48}\left(EI_B - EA_B\bar{Z}_B^2\right)$$

$$k_{Bb}(4,5) = \frac{J1^2L^3}{24}\left(EI_B - EA_B\bar{Z}_B^2\right)$$

$$k_{Bb}(4,6) = 0$$

$$k_{Bb}(4,7) = 0$$

$$k_{Bb}(4,8) = - k_{Bb}(4,3)$$

$$k_{Bb}(4,9) = k_{Bb}(4,4)$$

$$k_{Bb}(4,10) = k_{Bb}(4,5)$$

$$k_{Bb}(5,1) = 0$$

$$k_{Bb}(5,2) = k_{Bb}(2,5)$$

$$k_{Bb}(5,3) = k_{Bb}(3,5)$$

$$k_{Bb}(5,4) = k_{Bb}(4,5)$$

$$k_{Bb}(5,5) = \frac{EI_B}{L} + \frac{J1^2L^3}{12}\left(EI_B - EA_B\bar{Z}_B^2\right)$$

$$k_{Bb}(5,6) = 0$$

$$k_{Bb}(5,7) = - k_{Bb}(2,5)$$

$$k_{Bb}(5,8) = - k_{Bb}(3,5)$$

$$k_{Bb}(5,9) = k_{Bb}(4,5)$$

$$k_{Bb}(5,10) = \frac{EI_B}{L} + \frac{J1^2L^3}{12}\left(EI_B - EA_B\bar{Z}_B^2\right)$$

$k_{Bb}(6,1) = 0$

$k_{Bb}(6,2) = 0$

$k_{Bb}(6,3) = 0$

$k_{Bb}(6,4) = 0$

$k_{Bb}(6,5) = 0$

$k_{Bb}(6,6) = 0$

$k_{Bb}(6,7) = 0$

$k_{Bb}(6,8) = 0$

$k_{Bb}(6,9) = 0$

$k_{Bb}(6,10) = 0$

$k_{Bb}(7,1) = 0$

$k_{Bb}(7,2) = k_{Bb}(2,7)$

$k_{Bb}(7,3) = 0$

$k_{Bb}(7,4) = 0$

$k_{Bb}(7,5) = k_{Bb}(5,7)$

$k_{Bb}(7,6) = 0$

$k_{Bb}(7,7) = k_{Bb}(2,2)$

$k_{Bb}(7,8) = 0$

$k_{Bb}(7,9) = 0$

$k_{Bb}(7,10) = k_{Bb}(5,2)$

$k_{Bb}(8,1) = 0$

$k_{Bb}(8,2) = 0$

$k_{Bb}(8,3) = k_{Bb}(3,8)$

$k_{Bb}(8,4) = k_{Bb}(4,8)$

$k_{Bb}(8,5) = k_{Bb}(5,8)$

$k_{Bb}(8,6) = 0$

$k_{Bb}(8,7) = 0$

$k_{Bb}(8,8) = k_{Bb}(3,3)$

$k_{Bb}(8,9) = - k_{Bb}(4,3)$

$k_{Bb}(8,10) = - k_{Bb}(5,3)$

$k_{Bb}(9,1) = 0$

$k_{Bb}(9,2) = 0$

$k_{Bb}(9,3) = k_{Bb}(3,9)$

$k_{Bb}(9,4) = k_{Bb}(4,9)$

$k_{Bb}(9,5) = k_{Bb}(5,9)$

$k_{Bb}(9,6) = 0$

$k_{Bb}(9,7) = 0$

$k_{Bb}(9,8) = k_{Bb}(8,9)$

$k_{Bb}(9,9) = k_{Bb}(4,4)$

$k_{Bb}(9,10) = k_{Bb}(5,4)$

$k_{Bb}(10,1) = 0$

$k_{Bb}(10,2) = k_{Bb}(2,10)$

$k_{Bb}(10,3) = k_{Bb}(3,10)$

$k_{Bb}(10,4) = k_{Bb}(4,10)$

$k_{Bb}(10,5) = k_{Bb}(5,10)$

$k_{Bb}(10,6) = 0$

$k_{Bb}(10,7) = k_{Bb}(7,10)$

$k_{Bb}(10,8) = k_{Bb}(8,10)$

$$k_{Bb}(10,9) = k_{Bb}(9,10)$$

$$k_{Bb}(10,10) = k_{Bb}(5,5) \qquad \text{(B.7)}$$

Where:

$$J1 = \frac{4\ GA_{SB}}{L^2\ GA_{SB} + 8EI_B}$$

EA_B, ES_B, EI_B, and GA_{SB} are given by equations 3.59 a, b, c, d.

Evaluating the integral in eq. B.2 in a similar manner gives the following stiffness matrix:

$k_{Bs}(1,1) = 0$ $\qquad$ $k_{Bs}(1,8) = 0$

$k_{Bs}(1,2) = 0$ $\qquad$ $k_{Bs}(1,9) = 0$

$k_{Bs}(1,3) = 0$ $\qquad$ $k_{Bs}(1,10) = 0$

$k_{Bs}(1,4) = 0$ $\qquad$ $k_{Bs}(2,1) = 0$

$k_{Bs}(1,5) = 0$ $\qquad$ $k_{Bs}(2,2) = 0$

$k_{Bs}(1,6) = 0$ $\qquad$ $k_{Bs}(2,3) = 0$

$k_{Bs}(1,7) = 0$ $\qquad$ $k_{Bs}(2,4) = 0$

$$k_{Bs}(2,5) = 0$$

$$k_{Bs}(2,6) = 0$$

$$k_{Bs}(2,7) = 0$$

$$k_{Bs}(2,8) = 0$$

$$k_{Bs}(2,9) = 0$$

$$k_{Bs}(2,10) = 0$$

$$k_{Bs}(3,1) = 0$$

$$k_{Bs}(3,2) = 0$$

$$k_{Bs}(3,3) = GA_{SB}\left(\frac{6}{5L} - \frac{3J1L}{5} + \frac{3J1^2L^3}{40}\right)$$

$$k_{Bs}(3,4) = GA_{SB}\left(-\frac{1}{10} + \frac{3J1L^2}{40} - \frac{J1^2L^4}{80}\right)$$

$$k_{Bs}(3,5) = GA_{SB}\left(-\frac{1}{2} + \frac{9J1L^2}{40} - \frac{J1^2L^4}{40}\right)$$

$$k_{Bs}(3,6) = 0$$

$$k_{Bs}(3,7) = 0$$

$$k_{Bs}(3,8) = -k_{Bs}(3,3)$$

$$k_{Bs}(3,9) = k_{Bs}(3,4)$$

$$k_{Bs}(3,10) = GA_{SB}\left(\frac{1}{2} + \frac{9J1L^2}{40} - \frac{J1^2L^4}{40}\right)$$

$$k_{Bs}(4,1) = 0$$

$$k_{Bs}(4,2) = 0$$

$$k_{Bs}(4,3) = k_{Bs}(3,4)$$

$$k_{Bs}(4,4) = GA_{SB}\left(\frac{2L}{15} - \frac{J1L^3}{120} + \frac{J1^2L^5}{480}\right)$$

$$k_{Bs}(4,5) = GA_{SB}\left(-\frac{L}{12} - \frac{7J1L^3}{240} + \frac{J1^2L^5}{240}\right)$$

$$k_{Bs}(4,6) = 0$$

$$k_{Bs}(4,7) = 0$$

$$k_{Bs}(4,8) = -k(3,4)$$

$$k_{Bs}(4,9) = GA_{SB}\left(-\frac{L}{30} - \frac{J1L^3}{120} + \frac{J1^2L^5}{480}\right)$$

$$k_{Bs}(4,10) = GA_{SB}\left(\frac{L}{12} - \frac{7J1L^3}{240} + \frac{J1^2L^5}{240}\right)$$

$$k_{Bs}(5,1) = 0$$

$$k_{Bs}(5,2) = 0$$

$$k_{Bs}(5,3) = k_{Bs}(3,5)$$

$$k_{Bs}(5,4) = k_{Bs}(4,5)$$

$$k_{Bs}(5,5) = GA_{SB}\left(\frac{L}{3} - \frac{J1L^3}{12} + \frac{J1^2L^5}{120}\right)$$

$$k_{Bs}(5,6) = 0$$

$$k_{Bs}(5,7) = 0$$

$$k_{Bs}(5,8) = -k_{Bs}(3,5)$$

$$k_{Bs}(5,9) = k_{Bs}(4,10)$$

$$k_{Bs}(5,10) = k_{Bs}(3,5)$$

$k_{Bs}(6,1) = 0$

$k_{Bs}(6,2) = 0$

$k_{Bs}(6,3) = 0$

$k_{Bs}(6,4) = 0$

$k_{Bs}(6,5) = 0$

$k_{Bs}(6,6) = 0$

$k_{Bs}(6,7) = 0$

$k_{Bs}(6,8) = 0$

$k_{Bs}(6,9) = 0$

$k_{Bs}(6,10) = 0$

$k_{Bs}(7,1) = 0$

$k_{Bs}(7,2) = 0$

$k_{Bs}(7,3) = 0$

$k_{Bs}(7,4) = 0$

$k_{Bs}(7,5) = 0$

$k_{Bs}(7,6) = 0$

$k_{Bs}(7,7) = 0$

$k_{Bs}(7,8) = 0$

$k_{Bs}(7,9) = 0$

$k_{Bs}(7,10) = 0$

$k_{Bs}(8,1) = 0$

$k_{Bs}(8,2) = 0$

$k_{Bs}(8,3) = k_{Bs}(3,8)$

$k_{Bs}(8,4) = k_{Bs}(4,8)$

$k_{Bs}(8,5) = k_{Bs}(5,8)$

$k_{Bs}(8,6) = 0$

$$k_{Bs}(8,7) = 0$$

$$k_{Bs}(8,8) = k_{Bs}(3,3)$$

$$k_{Bs}(8,9) = -k_{Bs}(3,4)$$

$$k_{Bs}(8,10) = -k_{Bs}(3,10)$$

$$k_{Bs}(9,1) = 0$$

$$k_{Bs}(9,2) = 0$$

$$k_{Bs}(9,3) = k_{Bs}(3,9)$$

$$k_{Bs}(9,4) = k_{Bs}(4,9)$$

$$k_{Bs}(9,5) = k_{Bs}(5,9)$$

$$k_{Bs}(9,6) = 0$$

$$k_{Bs}(9,7) = 0$$

$$k_{Bs}(9,8) = k_{Bs}(8,9)$$

$$k_{Bs}(9,9) = k_{Bs}(4,4)$$

$$k_{Bs}(9,10) = k_{Bs}(4,5)$$

$$k_{Bs}(10,1) = 0$$

$$k_{Bs}(10,2) = 0$$

$$k_{Bs}(10,3) = k_{Bs}(3,10)$$

$$k_{Bs}(10,4) = k_{Bs}(4,10)$$

$$k_{Bs}(10,5) = k_{Bs}(5,10)$$

$$k_{Bs}(10,6) = 0$$

$$k_{Bs}(10,7) = 0$$

$$k_{Bs}(10,8) = k_{Bs}(8,10)$$

$$k_{Bs}(10,9) = k_{Bs}(9,10)$$

$$k_{Bs}(10,10) = k_{Bs}(5,5) \qquad \text{(B.8)}$$

Performing the indicated integration in eq. B.3, the following $[k]_d$ matrix is obtained:

$$k_d(1,1) = \frac{k_{sc}L}{3}$$

$$k_d(1,2) = -k_d(1,1)$$

$$k_d(1,3) = k_{sc}\left(\frac{C_{bA}}{2} + \frac{J1L^2}{8} C_{tB} \right)$$

$$k_d(1,4) = k_{sc}\left(\frac{Z_{iA}L}{12} - \frac{J1L^3}{48} C_{tB} \right)$$

$$k_d(1,5) = k_{sc}\left(- \frac{Z_{iB}L}{3} - \frac{J1L^3}{24} C_{tB} \right)$$

$$k_d(1,6) = \frac{k_{sc}L}{6}$$

$$k_d(1,7) = -k_d(1,6)$$

$$k_d(1,8) = -k_d(1,3)$$

$$k_d(1,9) = k_{sc}\left(- \frac{Z_{iA}L}{12} - \frac{J1L^3 C_{tB}}{48} \right)$$

$$k_d(1,10) = k_{sc}\left(- \frac{Z_{iB}L}{6} - \frac{J1L^3}{24} C_{tB} \right)$$

$$k_d(2,1) = k_d(1,2)$$

$k_d(2,2) = k_d(1,1)$

$k_d(2,3) = -k_d(1,3)$

$k_d(2,4) = -k_d(1,4)$

$k_d(2,5) = -k_d(1,5)$

$k_d(2,6) = k_d(1,7)$

$k_d(2,7) = k_d(1,6)$

$k_d(2,8) = k_d(1,3)$

$k_d(2,9) = -k_d(1,9)$

$k_d(2,10) = -k_d(1,10)$

$k_d(3,1) = k_d(1,3)$

$k_d(3,2) = -k_d(1,3)$

$k_d(3,3) = k_{sc}M1$

$k_d(3,4) = k_{sc}M2$

$k_d(3,5) = k_{sc}M3$

$k_d(3,6) = k_d(1,3)$

$k_d(3,7) = -k_d(1,3)$

$k_d(3,8) = -k_d(3,3)$

$k_d(3,9) = k_d(3,4)$

$k_d(3,10) = k_d(3,5)$

$k_d(4,1) = k_d(1,4)$

$k_d(4,2) = k_d(2,4)$

$k_d(4,3) = k_d(3,4)$

$k_d(4,4) = k_{sc}M4$

$k_d(4,5) = k_{sc}M5$

$k_d(4,6) = k_d(1,9)$

$k_d(4,7) = -k_d(1,9)$

$k_d(4,8) = -k_d(3,4)$

$k_d(4,9) = k_{sc}M6$

$k_d(4,10) = k_{sc}M7$

$k_d(5,1) = k_d(1,5)$

$k_d(5,2) = k_d(2,5)$

$k_d(5,3) = k_d(3,5)$

$k_d(5,4) = k_d(4,5)$

$k_d(5,5) = k_{sc}M8$

$k_d(5,6) = k_d(1,10)$

$k_d(5,7) = -k_d(1,10)$

$k_d(5,8) = -k_d(3,5)$

$k_d(5,9) = k_d(4,10)$

$k_d(5,10) = k_{sc}M9$

$k_d(6,1) = k_d(1,6)$

$k_d(6,2) = k_d(2,6)$

$k_d(6,3) = k_d(3,6)$

$k_d(6,4) = k_d(4,6)$

$k_d(6,5) = k_d(5,6)$

$k_d(6,6) = k_d(1,1)$

$k_d(6,7) = -k_d(1,1)$

$k_d(6,8) = -k_d(1,3)$

$k_d(6,9) = k_d(1,4)$

$k_d(6,10) = k_d(1,5)$

$k_d(7,1) = k_d(1,7)$

$k_d(7,2) = k_d(2,7)$

$k_d(7,3) = k_d(3,7)$

$k_d(7,4) = k_d(4,7)$

$k_d(7,5) = k_d(5,7)$

$k_d(7,6) = k_d(6,7)$

$k_d(7,7) = k_d(1,1)$

$k_d(7,8) = k_d(1,3)$

$k_d(7,9) = -k_d(1,4)$

$k_d(7,10) = -k_d(1,5)$

$k_d(8,1) = k_d(1,8)$

$k_d(8,2) = k_d(2,8)$

$k_d(8,3) = k_d(3,8)$

$k_d(8,4) = k_d(4,8)$

$k_d(8,5) = k_d(5,8)$

$k_d(8,6) = k_d(6,8)$

$k_d(8,7) = k_d(7,8)$

$k_d(8,8) = k_d(3,3)$

$k_d(8,9) = -k_d(3,4)$

$k_d(8,10) = -k_d(3,5)$

$k_d(9,1) = k_d(1,9)$

$k_d(9,2) = k_d(2,9)$

$k_d(9,3) = k_d(3,9)$

$k_d(9,4) = k_d(4,9)$

$k_d(9,5) = k_d(5,9)$

$k_d(9,6) = k_d(6,9)$

$k_d(9,7) = k_d(7,9)$

$$k_d(9,8) = k_d(8,9) \qquad k_d(10,5) = k_d(5,10)$$

$$k_d(9,9) = k_d(4,4) \qquad k_d(10,6) = k_d(6,10)$$

$$k_d(9,10) = k_d(4,5) \qquad k_d(10,7) = k_d(7,10)$$

$$k_d(10,1) = k_d(1,10) \qquad k_d(10,8) = k_d(8,10)$$

$$k_d(10,2) = k_d(2,10) \qquad k_d(10,9) = k_d(9,10)$$

$$k_d(10,3) = k_d(3,10) \qquad k_d(10,10) = k_d(5,5) \qquad \text{(B.9)}$$

$$k_d(10,4) = k_d(4,10)$$

Where:

$$M1 = \frac{6C_{bA}^2}{5L} + \frac{3J1L}{5} C_{bA}C_{tB} + \frac{3J1^2L^3}{40} C_{tB}^2$$

$$M2 = -\frac{Z_{iA}^2}{10} - \frac{J1L^2}{20} C_{bA}C_{tB} - \frac{J1^2L^4}{80} C_{tB}^2 - \frac{Z_{iA}J1L^2}{40} C_{tB}$$

$$M3 = -\frac{Z_{iA}Z_{iB}}{2} - \frac{J1L^2}{10} C_{bA}C_{tA} - \frac{Z_{iB}J1L^2}{8} C_{tB} - \frac{J1^2L^4}{40} C_{tB}^2$$

$$M4 = \frac{2Z_{iA}^2L}{15} + \frac{Z_{iA}J1L^3}{120} C_{tB} + \frac{J1^2L^5}{480} C_{tB}^2$$

$$M5 = -\frac{Z_{iA}Z_{iB}L}{12} + \frac{Z_{iA}J1L^3}{120}C_{tB} + \frac{Z_{iB}J1L^3}{48}C_{tB} + \frac{J1^2L^5}{240}C_{tB}^2$$

$$M6 = -\frac{Z_{iA}^2L}{30} + \frac{Z_{iA}J1L^3}{120}C_{tB} + \frac{J1^2L^5}{480}C_{tB}^2$$

$$M7 = \frac{Z_{iA}Z_{iB}L}{12} + \frac{Z_{iA}J1L^3}{120}C_{tB} + \frac{Z_{iB}J1L^3}{48}C_{tB} + \frac{J1^2L^5}{240}C_{tB}^2$$

$$M8 = \frac{Z_{iB}^2L}{3} + \frac{Z_{iB}J1L^3}{12}C_{tB} + \frac{J1^2L^5}{120}C_{tB}^2$$

$$M9 = \frac{Z_{iB}^2L}{6} + \frac{Z_{iB}J1L^3}{12}C_{tB} + \frac{J1^2L^5}{120}C_{tB}^2$$

Once the three component matrices, $[k_B]^e_{b_{10x10}}$, $[k_B]^e_{s_{10x10}}$, and $[k]^e_{u_{10x10}}$, are obtained by the above substitutions, the total beam element stiffness matrix is obtained by adding the three matrices together according to eq. B.10.

$$[k]^e_{BEAM} = [k_B]^e_b + [k_B]^e_s + [k]^e_u \qquad (B.10)$$

ACKNOWLEDGEMENTS

This study was conducted in the Department of Civil Engineering and Fritz Engineering Laboratory, under the auspices of the Lehigh University Office of Research, as a part of the research investigation sponsored by the Pennsylvania Department of Transportation and the U.S. Department of Transportation, Federal Highway Administration.

The basic research planning and the administrative coordination in this investigation were in cooperation with the following individuals representing the Pennsylvania Department of Transportation: Mr. B. F. Kotalik, Bridge Engineer, Mr. H. P. Koretzky, Assistant Chief Bridge Engineer, Mr. Wade Gramling and Mr. I. Janauschek, both from the Office of Research and Special Studies. The valuable contributions provided by the individuals named above have been essential in the completion of the phase of the research reported herein.

The authors would like to thank the staff of the Lehigh University Computing Center for their close cooperation in the development of the computer program used in the reported research. Mrs. Michele Kostem's contribution throughout the development and the typing of the report are gratefully acknowledged.